OLIVINE CRYSTALLIZATION DEPTHS WITHIN KĪLAUEA'S LOWER EAST RIFT ZONE: THE USE OF REHOMOGENIZED MELT INCLUSIONS TO INTERPRET MAGMA TRANSPORT, STORAGE, AND ENERGETIC FOUNTAINING

by

ROBIN MICHELE TUOHY

A THESIS

Presented to the Department of Geological Sciences
and the Graduate School of the University of Oregon
in partial fulfillment of the requirements
for the degree of
Master of Science

December 2013

THESIS APPROVAL PAGE

Student: Robin Michele Tuohy

Title: Olivine Crystallization Depths within Kīlauea's Lower East Rift Zone: The Use of Rehomogenized Melt Inclusions to Interpret Magma Transport, Storage, and Energetic Fountaining

This thesis has been accepted and approved in partial fulfillment of the requirements for the Master of Science degree in the Department of Geological Sciences by:

Dr. Paul J. Wallace	Chair
Dr. Kathy Cashman	Member
Dr. James Watkins	Member
Dr. Eugene Humphreys	Member

and

Kimberly Andrews Espy	Vice President for Research & Innovation/Dean of the Graduate School

Original approval signatures are on file with the University of Oregon Graduate School.

Degree awarded December 2013

THESIS ABSTRACT

Robin Michele Tuohy

Master of Science

Department of Geological Sciences

December 2013

Title: Olivine Crystallization Depths within Kīlauea's Lower East Rift Zone: The Use of Rehomogenized Melt Inclusions to Interpret Magma Transport, Storage, and Energetic Fountaining

H_2O and CO_2 concentrations in olivine-hosted melt inclusions, assuming vapor saturation at the time of trapping, can be used to estimate crystallization depths for the olivine host. Estimating the true CO_2 in melt inclusions is difficult, as much is lost to shrinkage bubbles, which form upon post-entrapment cooling and crystallization. Reheating olivine to temperatures above the melt inclusion trapping temperature and then quenching rapidly can restore CO_2 to the glass because the CO_2 in the bubble redissolves at high temperature. Previous work has established that olivine crystallization for the1959 Kīlauea Iki eruption took place in the shallow summit reservoir, but crystallization depths have not been established for the rift extension of the eruption, at Kapoho. The new data presented here suggest that the most primitive Kīlauea Iki component bypassed the summit reservoir for the east rift zone prior to the start of the eruption and was later erupted at Kapoho.

CURRICULUM VITAE

NAME OF AUTHOR: Robin Michele Tuohy

GRADUATE AND UNDERGRADUATE SCHOOLS ATTENDED

University of Oregon, Eugene, OR
Colorado State University, Fort Collins, CO

DEGREES AWARDED:

Master of Science, Geological Sciences, 2013, University of Oregon
Bachelor of Science, Geology, 2010, Colorado State University

AREAS OF SPECIAL INTEREST:

Volcanology
Geochemistry
Igneous Petrology
Hawaii Geology

PROFESSIONAL EXPERIENCE:

Graduate Teaching Fellow, Geological Sciences, Eugene, OR, 2011-2013

United States Geological Survey/Hawaii Volcano Observatory Gas Geochemistry Volunteer, Hawaii Volcanoes National Park, January – April 2011

Teaching Assistant, Mineraology and Optical Mineralogy, Colorado State University, 2009

GRANTS, AWARDS, AND HONORS:

Johnston Scholarship, University of Oregon, Department of Geological Sciences, 2013

ExxonMobil Geoscience Grant, 2013

United States Geological Survey Jack Kleinman Grant for Volcano Research, 2012

Johnston Scholarship, University of Oregon, Department of Geological Sciences, 2011

United States Geological Survey/National Association of Geoscience Teachers Cooperative Field Training Program nominee, 2010

Association of Women Geoscientists Outstanding Student Award, 2010

Chevron USA, Inc. Undergraduate Student Scholarship, 2009

ACKNOWLEDGMENTS

There are many people who deserve my thanks for their involvement, big or small, in this project. Like so many things, the completion of a master's project is a collaborative effort, and I would not have been able to complete my master's without the support of many people.

First, I need to thank my adviser, Paul Wallace, for giving me the freedom and encouragement to work on a topic I am passionate about. We were able to develop a project together that not only satisfied my interest in Hawaii, but also test new waters in melt inclusion analytical techniques. I would like to thank my entire committee, Kathy Cashman, Jim Watkins, and Gene Humphreys for your thoughtful comments. I need to acknowledge all of the students, past and present, which have been involved in the melt inclusion lab. We learned a lot from each other. I also need to thank Dana Johnston and Stephanie Weaver for allowing me to invade the experimental lab, and provide helpful direction and feedback when I was in the initial stages of this project. I have to thank Michael C. Rowe for picking his brain and demonstrating how to rehomogenize melt inclusions. I have to thank the many people at the Hawaii Volcano Observatory who have assisted me in various ways: Jim Kauahikaua, Steve Brantley, Taeko Jane Takahashi, and Frank Trusdell. I need to give a special thanks to Don Swanson who has been a great collaborator on this project, and I was able to learn so much from him during our two weeks completing fieldwork together. Finally, I have to thank Sanford Trucking Company, and the Lyman family, for allowing me access and collect from the 1955 and 1960 eruptive sites.

The funding for this project came from a variety of sources. This project was partially supported by the University of Oregon. I would like to thank the United States Geological Survey, as well as the family of Jack Kleinman, for selecting me for the 2011 USGS Jack Kleinman Grant, as it was used to support two weeks of fieldwork in Hawaii. I would also like to thank ExxonMobil, for selecting me for the 2013 ExxonMobil Geoscience Grant. I would not have been able to complete all of the analytical work required without their generous contribution.

Personally, I would like to acknowledge the people who have always supported me, no matter where my life and interest in geology have taken me: my husband, Thomas Flowe, and my parents, James and Kathleen Tuohy. I would also like to thank the friends I have made while at University of Oregon, we have a shared perspective on the struggles of a graduate program, and you have always provided a shoulder to lean on: N.A. Famoso, J.K. Marks, M. Myers, and H. Dietterich. I am fortunate to have crossed paths with you.

TABLE OF CONTENTS

Chapter Page

LIST OF FIGURES

LIST OF TABLES

CHAPTER I

INTRODUCTION

Hawaiian Melt Inclusions

Melt inclusions provide a window into magmatic systems at depth and record the melt and volatile composition at their time of trapping (Metrich and Wallace, 2008). Melt inclusion (MIs) studies at Hawaiian volcanoes have been used to investigate a variety of problems, from shallow magmatic processes during individual eruptions (Anderson and Brown, 1993; Wallace and Anderson, 1998; Edmonds et al., 2013) to studies of mantle plume geochemistry and mantle heterogeneities (Hauri, 2002). The results of these studies have helped us to better understand the eruption of high lava fountains and details of Kīlauea's magma plumbing system. At other oceanic islands such as La Réunion, olivine-hosted melt inclusions have also been used to constrain the size and shape of the magma plumbing system (Bureau et al., 1998a; Bureau et al., 1998b) and to understand individual eruptions (Vigouroux et al., 2009).

Melt inclusions that are rapidly quenched are ideal for studying magmatic systems because the inclusions undergo less post entrapment crystallization than those found in lava flows and rapid quenching allows for the preservation of the glass. The primary volatiles recorded in melt inclusions from Hawaiian eruptions are CO_2 and H_2O, but also include S, Cl, and F. The CO_2 and H_2O concentrations in melt inclusions can be used to infer olivine crystallization pressures within the magma plumbing system and thus can be used to estimate magma storage depths (Anderson and Brown, 1993; Riker, 2005). The CO_2 concentration in particular is important for determining olivine crystallization depths.

The Shrinkage Bubble Problem

Although melt inclusions have been used for estimating magmatic conditions at the time of trapping, determining the total volatile content of melt inclusions is complicated by the formation of shrinkage bubbles during post-entrapment cooling and crystallization. Low solubility volatiles, like CO_2, partition into these bubbles, depleting the concentration in the melt. As a result, the CO_2 measured in the glass by Fourier Transform Infrared Spectrometry (FTIR) or ion microprobe (SIMS) can greatly underestimate the amount of CO_2 that was present at the time of trapping. This makes it preferable to either select bubble-free melt inclusions (which may not always be available) or to restore the melt inclusions' true CO_2 content by an alternative method (Anderson and Brown, 1993; Riker, 2005). Shrinkage bubbles have been found to contain between 50-80 % of the melt inclusion's original CO_2 by both experimental reheating on a high temperature stage (Cervantes et al., 2002) and measuring the glass density of vapor bubbles using Raman spectroscopy (Moore et al, in prep).

Figure 1 illustrates how a shrinkage bubble may be formed following melt inclusion trapping. When a melt inclusion is initially trapped, it is bubble free (Figure 1a). A shrinkage bubble is formed during post-entrapment cooling and crystallization because the melt in the inclusion contracts more than its crystalline host does. Crystallization of olivine along the inclusion-host interface adds to this effect because of the negative volume change on crystallization (Figure 1b). This shrinkage causes a drop in pressure in the inclusion that leads to nucleation and growth of a vapor bubble. Following eruption, the shrinkage bubble will continue to expand with continued cooling, as the melt

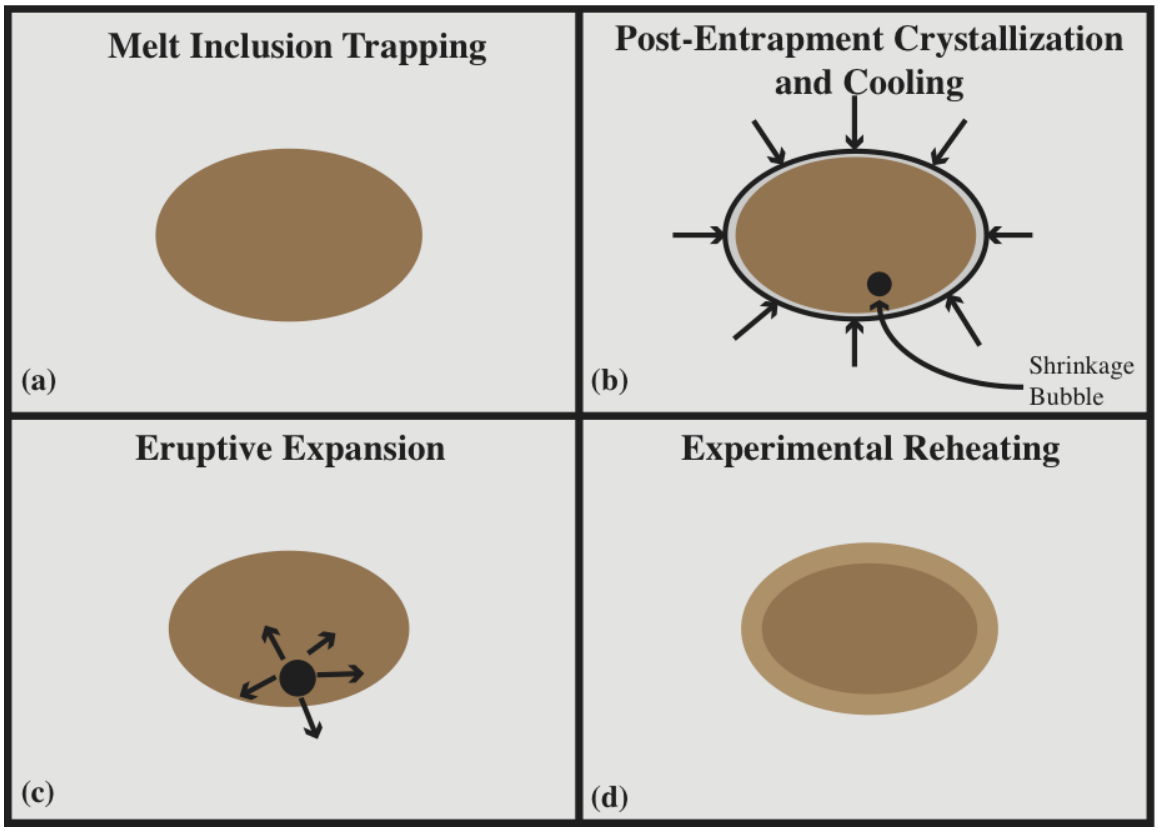

Figure 1. Schematic diagram of shrinkage bubble formation inside trapped melt inclusions. (a) A melt inclusion is trapped, without any primary bubbles. (b) Melt inclusion undergoes post-entrapment crystallization and cooling. The melt inclusion contracts, and experiences a pressure drop. This creates a void space for volatiles to form a shrinkage bubble. (c) The melt inclusion expands following eruption. Since individual host crystals can experience different thermal histories, the amount of post-eruptive expansion will vary. (d) A melt inclusion that has been experimentally reheated is drawn. The melt inclusion walls have a lighter colored, wavy texture, indicating olivine dissolution. The initial bubble has dissolved away, indicating the trapped gas has returned to the glass.

continues to contract more than the olivine host (Figure 1c). Studies that have used the size of shrinkage bubbles to restore their CO_2 (Anderson and Brown, 1993) run into the problem of estimating how much syn-eruptive expansion took place. If one assumes that the final bubble volume represents the pre-eruptive bubble volume, this results in an overestimate of the amount of CO_2 trapped in the bubble. Anderson and Brown (1993), in

their study of Kīlauea Iki, made the simplifying assumption that all of the shrinkage bubbles had the same pre-eruptive bubble volume of 0.5% (corresponding to approximately 55ºC of pre-eruptive cooling) and that varying amounts of post-eruptive expansion resulted in a range of final bubble sizes in the quenched inclusions. Anderson and Brown (1993) then computed the mass of CO_2 in the 0.5 vol. % bubble based on the dissolved concentrations of H_2O and CO_2 that were measured in the glass. Anderson and Brown (1993) noted that their estimates of CO_2 for Kīlauea Iki melt inclusions could be anywhere between 50-150% off. Riker (2005) calculated restored CO_2 concentrations for melt inclusions from the 1859 eruption of Mauna Loa by using the difference between the trapping and pre-eruption temperatures for individual inclusions to estimate the bubble volume just prior to eruption. Recent work by Sides et al. (2013) on the Kīlauea Iki eruption, estimate that up to 85% of CO_2 can be lost to shrinkage bubbles in melt inclusions that experienced up to 30% post entrapment crystallization. CO_2 in the glass correlates negatively with the amount of post entrapment crystallization in the melt inclusion. Sides et al. (2013) also noted that volcanic systems where magma mixing is common can experience a great degree of CO_2 loss to the shrinkage bubble when hot, primitive magma mixes with stored magma and extensive cooling takes place.

Experimentally reheating melt inclusions can redissolve the shrinkage bubble, returning most of the CO_2 to the glass (Fig. 1). These 'true' CO_2 contents of melt inclusions can be converted to trapping pressures of olivine, and by extension, the olivines' crystallization depth. Olivine crystallization depths can be used to constrain the depths of magma storage and transport at Kīlauea volcano, enabling geophysical validation of current magma plumbing system models. Through this study I have also

been able to compare this experimental method with other methods for estimating the true melt inclusion CO_2, which is lost the shrinkage bubble, which is applicable to any melt inclusion study, or volcanic system.

Background on Kīlauea Volcano and Eruptions Studied

Kīlauea's Magma Plumbing System

The nature of Kīlauea's magma storage and plumbing system has been widely debated. While the size, shape, and depth of Kīlauea's summit magma chamber are reasonably well outlined (Ryan, 1988), transport and storage processes in the East Rift Zone are still not well understood. Most models for Hawaiian rift zone eruptions requires a link between the summit and the shallow rift (Eaton and Murata, 1960; Tilling and Dvorak, 1993). The summit magma chamber is located at 2-3 km depth and may represent the depth of neutral buoyancy for magma. Magma from the summit magma chamber is thought to be injected into the rift zone 2-4 kilometers below the surface, and once in the rift, magma may be erupted or stored until a later eruption. Additionally, Ryan (1988)'s schematic cut-away of Kīlauea's magma plumbing system, which is based on seven years of seismic data, suggests there is a deep portion of the rift at 6-8 km depth. This deep portion of the rift is aseismic, and that fact has led numerous workers to conclude that not much activity occurs in the aseismic zone happening here, leading to the conclusion that most of the interaction between the summit and deep rift takes place at shallow levels where seismicity originates. However, if the deep rift is aseismic because it is warm, that doesn't mean that magma is not injected into the deep rift, it only means that we don't really have the ability to tell if magma transport occurs in this zone.

Alternative models have been proposed in which dike injection occurs directly into the shallow rift zone from the mantle (Garcia et al., 2000) or from along the décollement that marks the boundary between the volcanic pile and ocean floor (Clague and Denlinger, 1994). These alternatives are based on the primitive character of some lavas erupted on the submarine lower East Rift Zone (ERZ) (Clague et al., 1995). However, observations from the long-lived Pu'u 'O'o eruption confirm the link between the summit and shallow rift zone, because rift zone tilt and inflation-deflation cycles closely follow those of the summit magma chamber. Submarine eruptions occur on Kīlauea lower's East Rift Zone in the absence of any deformation or seismicity associated with the shallow summit system, and therefore some deep rift transport of magma seems to be required to supply these eruptions (Ryan et al., 1981, Ryan et al., 1988). In addition to Eaton and Murata's (1960) original model, Clague and Denlinger (1994) and Clague et al. (1995) suggest that olivine cumulate bodies drive the south flank instability of Kīlauea, and that these dunite cumulate bodies are the result of accumulated olivine that settles at the base of the summit reservoir, and then flows out away from the summit. Material from these bodies may be entrained in rift zone lavas during high magma flux events (Vinet and Higgins, 2010). The locations and abundance of such cumulates in the rift zones are poorly understood. Finally, though the seaward movement of Kīlauea's south flank has been recognized for a long time (Swanson, 1976), it has not been integrated into any of these magma transport and storage models, but will likely be in the future (Poland et al., 2012).

Kīlauea Iki and Kapoho

The Kīlauea Iki eruption has received a great deal of attention from the scientific community for several reasons. It was one of the first eruptions to be monitored by a modern Hawaiian Volcano Observatory (HVO), and a detailed chronologic narrative of the eruption (Richter et al., 1970) documents this spectacular eruption. The Kīlauea Iki eruption occurred just outside of the main summit caldera to the northeast in the pre-existing Kīlauea Iki crater (Figure 2a). Helz (1987) states the eruption was unusual because it erupted the highest lava fountains recorded in the summit region, was picritic (with an estimated 20 wt. % olivine), contained glasses that were MgO-rich (indicating high eruptive temperatures), and contained several different populations of olivine (deformed, megacrystic, reversely zoned, sulfide-inclusion bearing). Kīlauea Iki also erupted two distinctive magma compositions that had never been seen before at Kīlauea's summit (Wright and Fiske, 1971), and these are referred to as the S-1 and S-2 components. The arrival of the more primitive S-1 component was signaled in August 1959 when a deep earthquake (~55 km depth) was recorded below the summit (Eaton et al., 1987; Helz, 1987). Helz (1987) suggested that this hot, volatile-rich magma, erupted via a seldom-used pathway east of the main summit, and intercepted stored, differentiated magma. The hot, volatile-rich component is known as S-1 and the stored magma it intercepted is known as S-2. The buoyancy of the S-1 component propelled it upward

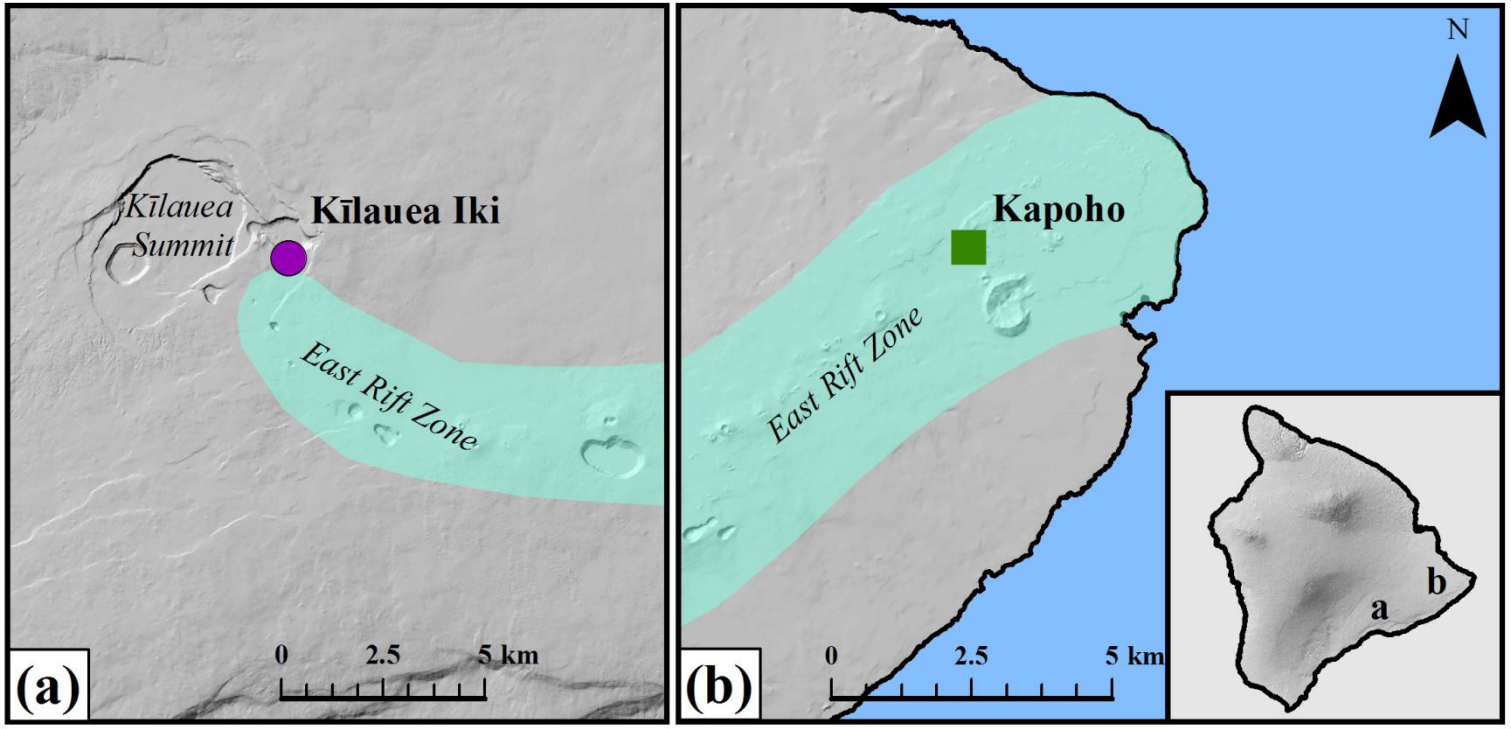

Figure 2. (a) Map of Kilauea volcano, showing the location of Kilauea Iki Crater and the field collection site of S-1 tephra (circle). (b) Map of Kilauea's lower East Rift Zone, northeast of Kilauea's summit region. Collection of tephra was focused on Pu'u Laimana (square), nearby Kapoho Cone (to the south) is unrelated to 1960 eruption.

through the stored magma, causing the initial eruption to be dominated by the S-1 material, followed by mixing of the S-1 and S-2 magmas in the reservoir. The high ascent velocities of S-1 allowed it to entrain olivine cumulates present in the magma chamber. Much of the this stored cumulate was erupted during later phases of the Kīlauea Iki eruption when the S-1 and the S-2 magmas were thoroughly mixed, which is thought to be responsible for the picritic nature of Kīlauea Iki lavas. Clague et al. (1991) suggested the S-1 component was likely the result of a smaller degree of partial melting than is typical for Kīlauean magmas. Melt inclusion work by Anderson and Brown (1993) supported Helz's (1987) model because their results indicated that most of the olivine in the Kīlauea Iki eruption formed at pressures less than 1 kbar, corresponding to crystallization depths of 3-5 km beneath the summit region. Drainback occurred repeatedly during the Kīlauea Iki eruption when degassed magma in the lava lake drained back down the vent. Melt inclusions from multiple phases of the eruption were used by Wallace and Anderson (1998) to show that the degree of recycling of drainback magma increased throughout the eruption, and the mixing of juvenile, volatile-rich material with previously degassed magma yielded a complex range of H_2O and CO_2 values. Overall, melt inclusion H_2O and CO_2 decreased over the course of the eruption and this agrees with recent work by Sides et al. (2013), which found this same trend.

The reason that the S-1 magma component bypassed the summit reservoir is not clear. The bypass may have taken place deep below the volcano, as suggested by Wright and Klein (2006), who reported that prior to the Kīlauea Iki eruption, deep earthquake swarms associated with mantle melting and supply to Kīlauea were located to the north of their normal location below the central summit conduit. Based on this they suggested

tthat another deep, near-vertical conduit system existed in that region below Kīlauea Iki that brought the S-1 component to the surface. This agrees with geochemical interpretations that Kīlauea Iki S-1 magma represents a smaller degree of partial melting, and was also sampling a geochemically heterogeneous plume (Clague et al., 1991). However, the area NE of Halema'uma'u has been used in previous eruptions, such as 1868, and was not a new pathway at the time of the Kīlauea Iki eruption. It may represent a reactivation of the east rift zone near the summit, which now makes a turn to the south before striking to the NE (D.A Swanson, written communication). Summit tilt from the eruption favors an interpretation involving the rise of S-1 magma below the main conduit and then moving quickly to the NE as it moved into the shallow summit system.

The 1960 eruption of Kīlauea at Kapoho, located over 50 km away from Kīlauea's summit (Figure 2b), is the rift extension of the 1959 Kīlauea Iki eruption (Richter et al., 1970). A complex mixture of multiple components (1952, 1959, 1961, 1967-1968) of stored magmas and crystals were erupted at Kapoho (Wright and Helz, 1996). Early Kapoho lavas were differentiated, and this was interpreted to be stored magmas that were expelled from the rift zone (Richter et al., 1970, Wright and Fiske, 1971; Wright and Helz, 1996). Over the course of the Kapoho eruption, the eruptive temperature increased over a period of 10 days, and the lavas became more summit-like (Wright and Fiske, 1971). Kīlauea Iki's hotter, S-1 component erupted late in the 1960 Kapoho eruption and was one of four magma components identified in the material erupted from Kapoho during 1960 (Wright and Helz, 1996). Periods of high fountaining up to 425 m were also documented at Kapoho (Richter et al., 1970). Kapoho lava is classified as olivine phyric, bordering on picritic in some units.

CHAPTER II

FIELD AREA AND SAMPLE DESCRIPTIONS

Fieldwork was conducted in June 2012 with the assistance of Don Swanson from the Hawaiian Volcano Observatory. Sampling efforts were focused in two regions: Kīlauea Iki Crater and near Pu'u Laimana in Kapoho, on Kīlauea's lower East Rift Zone. Full sample descriptions are located in Table 1 of Appendix A. Field collection maps are also located in Appendix A. Relative stratigraphy of the tephra collected from Kapoho are illustrated in Appendix B**.** Kīlauea Iki tephra samples were collected southwest of Kīlauea Iki caldera off the Devastation Trail at a collapse pit that had previously been excavated by Don Swanson and Bruce Houghton (University of Hawaii-Manoa) and are exclusively from Phase 1 of the eruption (also known as Iki 22). Sample numbers indicate the chronological order in which the samples were collected. Collection of 1960 Kapoho tephra was focused in a cinder quarry near Kapoho Cone (unrelated), approximately 47 km away from Kīlauea's summit on the lower East Rift Zone. A total of 8 samples were collected from the 1960 eruption, focused on point sources for the eruption (Pu'u Laimana and Vent E) as well as the tephra plain and chaotic rafted terrain described by Hazlett (1993).

CHAPTER III

METHODS

Sample Preparation

Tephra was dried in air or in a warming oven, gently crushed in a metal crucible, and sieved at 1 phi intervals from 3 to > -1 phi (or 0.25 mm to 2+ mm) to separate olivine from its matrix glass. Following sieving, olivine crystals were selected by picking from a specific size fraction of tephra under a binocular microscope. For some olivine crystals, adhering matrix glass was removed using HBF_4. However, during this study it was determined that this acid treatment left olivine crystals too fragile for the reheating process and subsequent sample preparation and therefore it was not used for a majority of olivine in this study.

Melt Inclusion Rehomogenization

Rehomogenization techniques were adapted from Rowe et al. (2003) and were used to redissolve CO_2-rich vapor bubbles in Kīlauea melt inclusions. Olivine crystals were selected from the 1-2 mm+ size fraction because they were generally the most robust during the reheating process. For each experiment, approximately 20-30 olivine crystals were wrapped in a platinum foil 'taco' and suspended with platinum wire on aluminum rods within a 1 atm-Deltec furnace at the University of Oregon. The platinum foil taco was held outside the furnace's hot zone while the furnace was brought to temperature from 800° C to 1400 °C, and the oxygen fugacity was maintained at the fayallite-magnetite-quartz (FMQ) buffer with a hydrogen and CO_2 gas mixture. The

target furnace temperature was initially chosen based on an estimate of the formation temperature of the olivine host using the Helz and Thornber (1987) melt-MgO thermometer. Using published data specifically for the Kapoho eruption (Wright and Helz, 1996), this temperature was calculated to be approximately 1240°C. Several experiments were conducted at this temperature, and appeared to be unsuccessful in dissolving shrinkage bubbles upon visual inspection of the reheated melt inclusions. Following these unsuccessful experiments, I followed work by Cervantes et al. (2002) on reheating of melt inclusions from a Mauna Loa picrite using a high temperature heating stage, in which it was found that temperatures as high at 1420°C were necessary to redissolve shrinkage bubbles. The oxygen fugacity for Hawaiian magmas is slightly higher than FMQ (Rhodes and Vollinger, 2005) but use of FMQ was reducing enough so that the olivine crystals did not oxidize during reheating. When the desired temperature and buffer were reached, the samples were lowered into the furnace hot zone. The samples were held at temperature for no more than 15 minutes. Running electrical current through the wire cut the platinum wire, and the samples were drop-quenched into a cool water-filled bulb at the base of the furnace. The olivine crystals were then removed from the platinum foil and specific crystals selected for analysis. Some experiments were conducted at 1300°C in order to assess the effect of temperature on rehomogenization and potential loss of H by diffusion through the olivine host.

Melt Inclusion Glass Analysis

FTIR

The H_2O and CO_2 contents of melt inclusions were determined by FTIR spectroscopy with a Thermo-Nicolet Nexus 670 FTIR spectrometer interfaced with a Continuum IR microscope at the University of Oregon. To prepare samples for analysis on the FTIR, melt inclusions in olivine-hosts were intersected and doubly polished using grit paper and diamond paste on a lapidary wheel. Melt inclusions were polished with both 6- and 1-micron diamond paste. The wafers (~ 30-100 microns in thickness) containing melt inclusions were then placed on a NaCl window and analyzed via FTIR. Three replicate transmission spectra for each glass were collected between 1000-6000 cm^{-1}. Total H_2O contents were measured from the peak absorbance at 3550 cm^{-1}, and CO_3^{2-} was measured using the carbonate doublet between 1430-1515 cm^{-1}. Three replicate thickness measurements for each wafer were made using reflectance spectra (Wysocsanki and Tani, 2006). For very thick wafers (>150 microns), the reflectance spectra do not contain interference fringes and therefore a micrometer was used to determine thickness.

H_2O and CO_2 peak absorbance for each melt inclusion were used to calculate the volatile concentrations of the glass using the Beer-Lambert Law equation, which also requires the molecular weight of the species, the density of the glass, the molar absorptivity of the species, and the sample thickness. Standard error of H_2O and CO_2 was determined by use of the Gaussian error propagation equation. In the Beer-Lambert Law equation used to calculate the volatile concentrations of melt inclusions the error in

the calculation of H_2O and CO_2 comes from the uncertainty in thickness measurements and the variation in IR absorbance based on replicate measurements.

Electron Microprobe

Melt inclusion wafers were mounted in epoxy resin and analyzed for major elements on the electron microprobe (CAMECA SX-100) at the University of Oregon. The major elements Si, Mg, Al, Fe, Ca, Na, K, and Mn were analyzed with a 10 nA sample current, 10 micron diameter beam, and 15 kV accelerating voltage. A higher current (50 nA) was used to increase sensitivity for Ti, S, Cl, P, and F. Time dependent intensity corrections were used for Si, Al, Na, and K. Melt inclusions were typically analyzed in three spots. Olivine hosts were also analyzed for their major element composition (Mg, Fe, Al, Mn, Si) to determine their forsterite content under the same operating conditions described above. Three spots on the host were measured in the vicinity of the inclusion(s) of interest. Tephra groundmass glass was analyzed from Kapoho samples Kap8 and Kap6. The operating conditions for the tephra glass used a 30 nA beam current for all elements. S, Cl, and F were not analyzed in the tephra glasses.

CHAPTER IV

RESULTS

Melt Inclusion Textures

Naturally quenched melt inclusions in the samples studied exhibit a variety of colors, shapes, and textures. Naturally quenched and reheated melt inclusions from each eruptive suite are pictured in Figure 3. Naturally quenched melt inclusions from Kīlauea tend to be round to ellipsoidal in shape, medium to dark brown in color, and typically contain one shrinkage bubble and sometimes an accessory phase like Cr-spinel or magnetite. Figure 3a shows a naturally glassy inclusion from Kīlauea Iki that has a wavy, irregularly textured interface between the melt inclusion and the host. This texture is much more common in reheated melt inclusions (3d, f). Reheated melt inclusions tend to retain their round to ellipsoidal shape, but sometimes no longer contain a shrinkage bubble (3b,f) or have a relatively small bubble(s). Figure 3d shows a reheated melt inclusion from Kapoho with an unusual texture, a 'halo' around its shrinkage bubble. This may indicate that the CO_2 did not have enough time to diffuse into the glass completely, or perhaps represents the former size of the original bubble. Because a large number of olivine were heated in each experiment, I was not able to do a before and after examination of individual melt inclusions. However, examining and analyzing naturally quenched inclusions from the same samples allows for a good survey of the natural textures before heating.

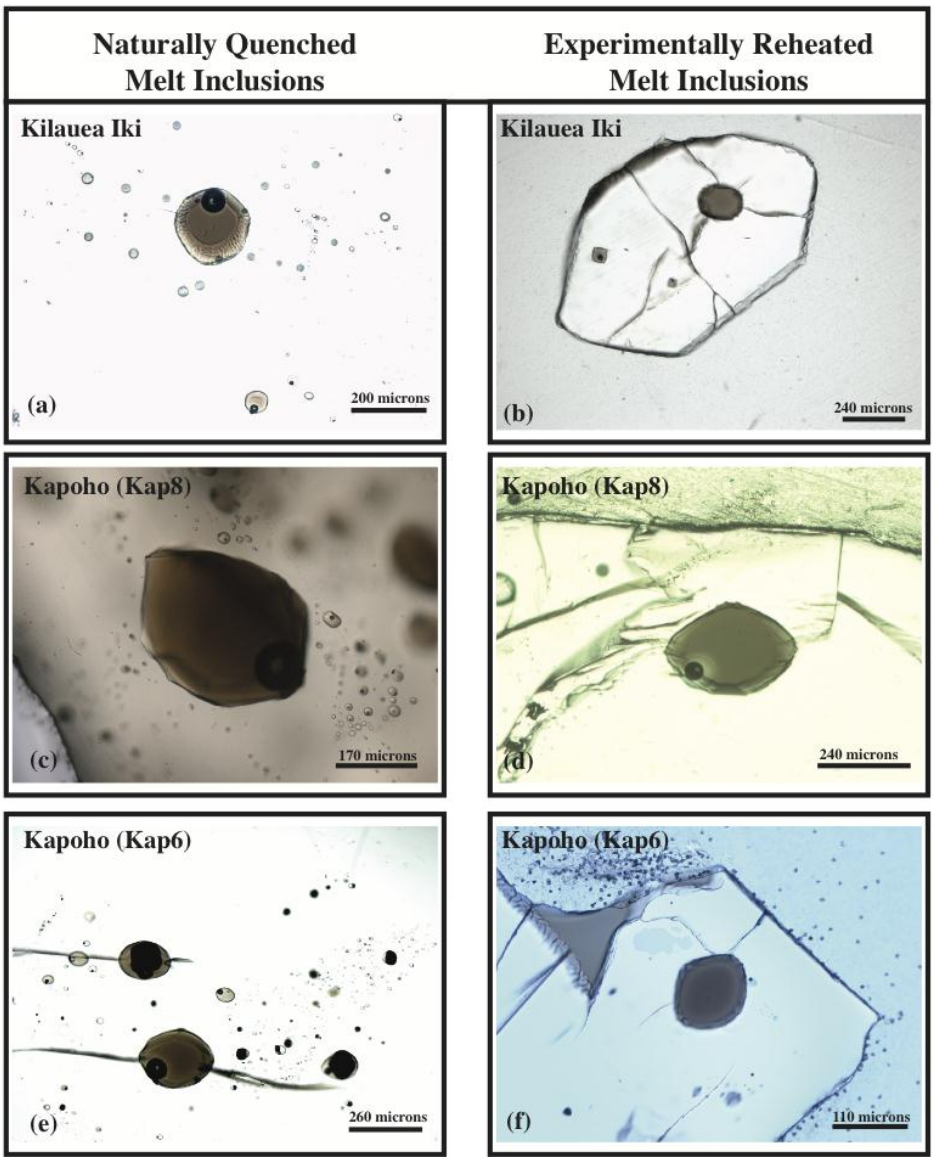

Figure 3. Photo mosaic of naturally quenched and reheated melt inclusions analyzed in this study. Melt inclusions naturally have a variety of textures and experimentally reheating melt inclusions creates an array of additional textures. These are not before and after photos. (a-b) Kilauea Iki melt inclusions. The naturally quenched melt inclusion has wavy walls and a large bubble. The reheated melt inclusion has a subellipsoidal shape and lacks a shrinkage bubble (c-d) Kap8 melt inclusions. The naturally quenched melt inclusion is dark brown, ellipsoidal and contains a large shrinkage bubble. The reheated melt inclusion has a 'halo' around its shrinkage bubble, which may indicate that the bubble did not completely dissolve, or the CO_2 did not have enough time to diffuse into the glass (e-f) Kap6 melt inclusions. The naturally quenched melt inclusion is pictured with other melt inclusions that were trapped with an accessory phase, like Cr-spinel. The reheated melt inclusion contains no bubble and has wavy walls.

Melt Inclusion and Olivine Compositions

Post Entrapment Crystallization and Fe-Diffusive Loss

As a first step in interpreting the analytical data for both the naturally quenched and reheated melt inclusions, I assessed whether the composition of the glass in each inclusion was in equilibrium with its olivine host. Melt inclusions commonly have a lower Mg/Fe ratio than they should if they were in equilibrium with the host as a result of post-entrapment crystallization (Danyushevsky et al., 2002). Conversely, reheated melt inclusions can have too high an Mg/Fe ratio if they were overheated above their trapping temperature (Cervantes et al., 2002). Plotting the forsterite content of the olivine host versus the melt inclusion Mg#, is a way that this can be visualized. In Figure. 4, the Mg# of both naturally quenched and reheated melt inclusions has been plotted against its olivine host for Kīlauea Iki (Fig. 4a) and Kapoho (Fig. 4b).

Figure 4 (next page). Mg# (Mg/[Mg+Fe^{2+}]) of naturally quenched and reheated melt inclusions is plotted against the Fo# (Mg# for olivine) of the olivine host, which is a pictorial way of showing how much post entrapment crystallization or olivine dissolution has taken place to produce the raw compositions of the melt inclusions. Increasing distance below the olivine-melt equilibrium line indicates increasing amounts of post entrapment crystallization. Increasing distance above the olivine-melt equilibrium line indicates increasing amounts of olivine dissolution owed to overheating. The olivine-melt equilibrium line was calculated by correcting the naturally quenched melt inclusions for post entrapment crystallization and Fe diffusive loss in Petrolog3.1. (a) Kilauea Iki naturally quenched melt inclusions plot between 7-15% post entrapment crystallization and 22-29% olivine dissolution for reheated 1400°C melt inclusions (b) Kapoho naturally quenched melt inclusions plot between 3-14% post entrapment crystallization and 3-20% olivine dissolution in 1400°C and 3-12% for 1300°C reheated melt inclusions.

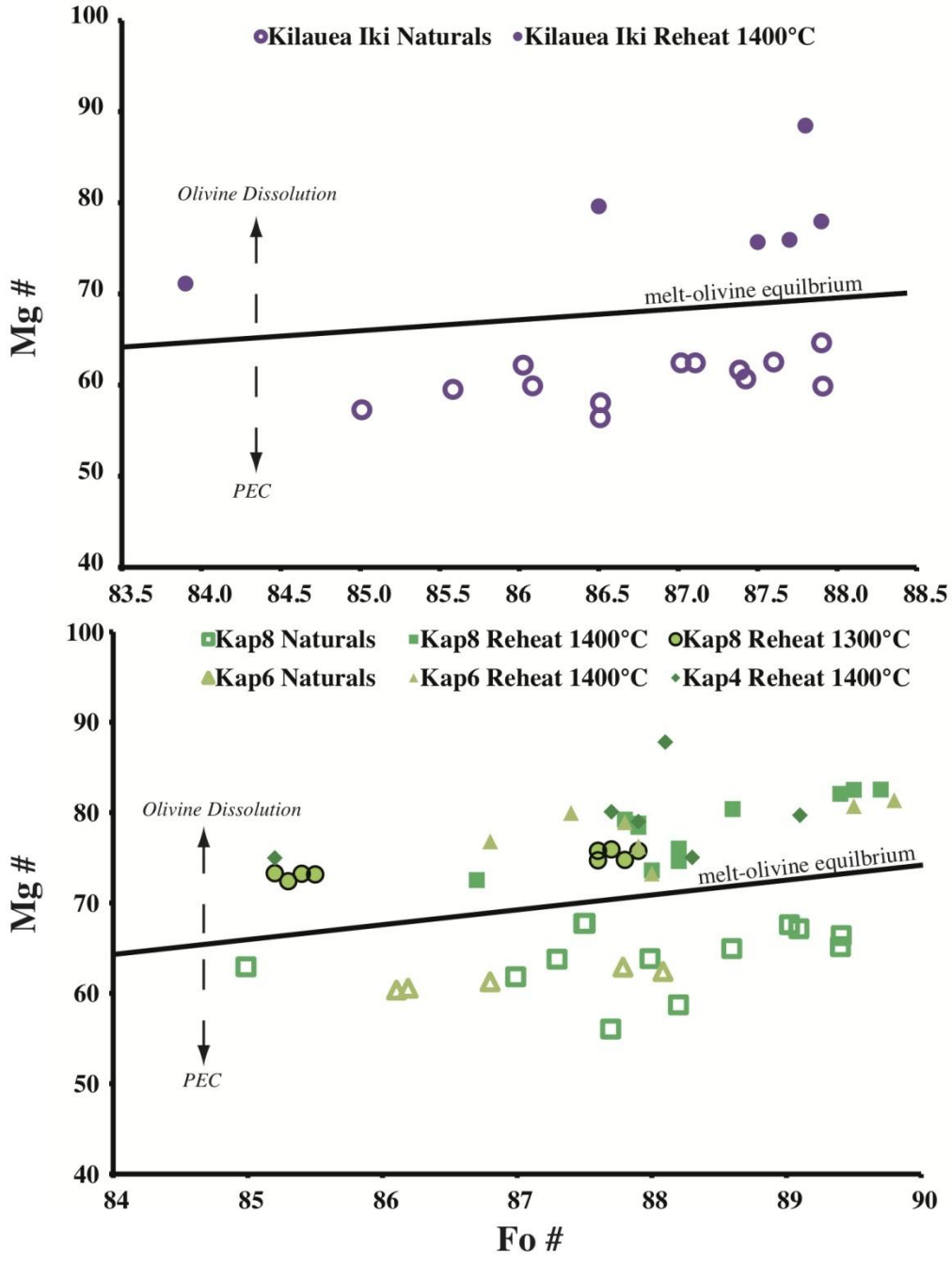
Kilauea Iki Naturals
Kilauea Iki Reheat 1400°C
Olivine Dissolution
melt-olivine equilbrium
PEC
Mg #
Kap8 Naturals
Kap8 Reheat 1400°C
Kap8 Reheat 1300°C
Kap6 Naturals
Kap6 Reheat 1400°C
Kap4 Reheat 1400°C
Olivine Dissolution
melt-olivine equilbrium
PEC
Mg #
Fo #

Note that the plot for Kapoho contains melt inclusions for both 1300°C and 1400°C experiments. The melt-olivine equilibrium line is calculated using a K_d value of 0.30 and assuming an oxidation state at the FMQ buffer (FeO/FeO^T=0.85). Naturally quenched melt inclusions plot below the melt-olivine equilibrium line, with increasing distance from the equilibrium lineindicating greater amounts of post-entrapment crystallization and diffusive Fe loss. Fe diffusive loss occurs when Fe in the melt inclusion diffuses out of the inclusion into the olivine host. Reheated melt inclusions plot above the equilibrium line because the Mg# of a melt inclusion will increase when olivine is dissolved off the inclusion walls, diluting the original trapped composition of the inclusion. Increasing distance above the equilibrium line indicates greater amounts of olivine dissolution. Note that in the cases where olivines were heated to only 1300°C, their melt inclusions lie closer to the melt-olivine equilibrium line.

Proper correction of melt inclusion compositions for the effects of post-entrapment crystallization must take into account the effects of Fe-diffusive loss. The diffusion of Fe can result in Fe rich rims around the melt inclusion when analyzed by electron microprobe traverses across the olivine (Danyushevsky et al., 2002). The effects of Fe loss can be corrected by first plotting the melt inclusions on an MgO versus FeO^T plot with the bulk rock and matrix glass compositions of the host lava. A line of best fit can be drawn, based on the FeO^T composition of bulk rock and matrix glass, so that an appropriate FeO^T can be selected for a given MgO content. Figure 5 shows that all naturally quenched melt inclusions from Kīlauea Iki (Figure 5a) and Kapoho (Figure 5b) have undergone some Fe loss by diffusion, as they fall below the trend line for the bulk rock and matrix glass data. Reheated melt inclusions show various relationships with the

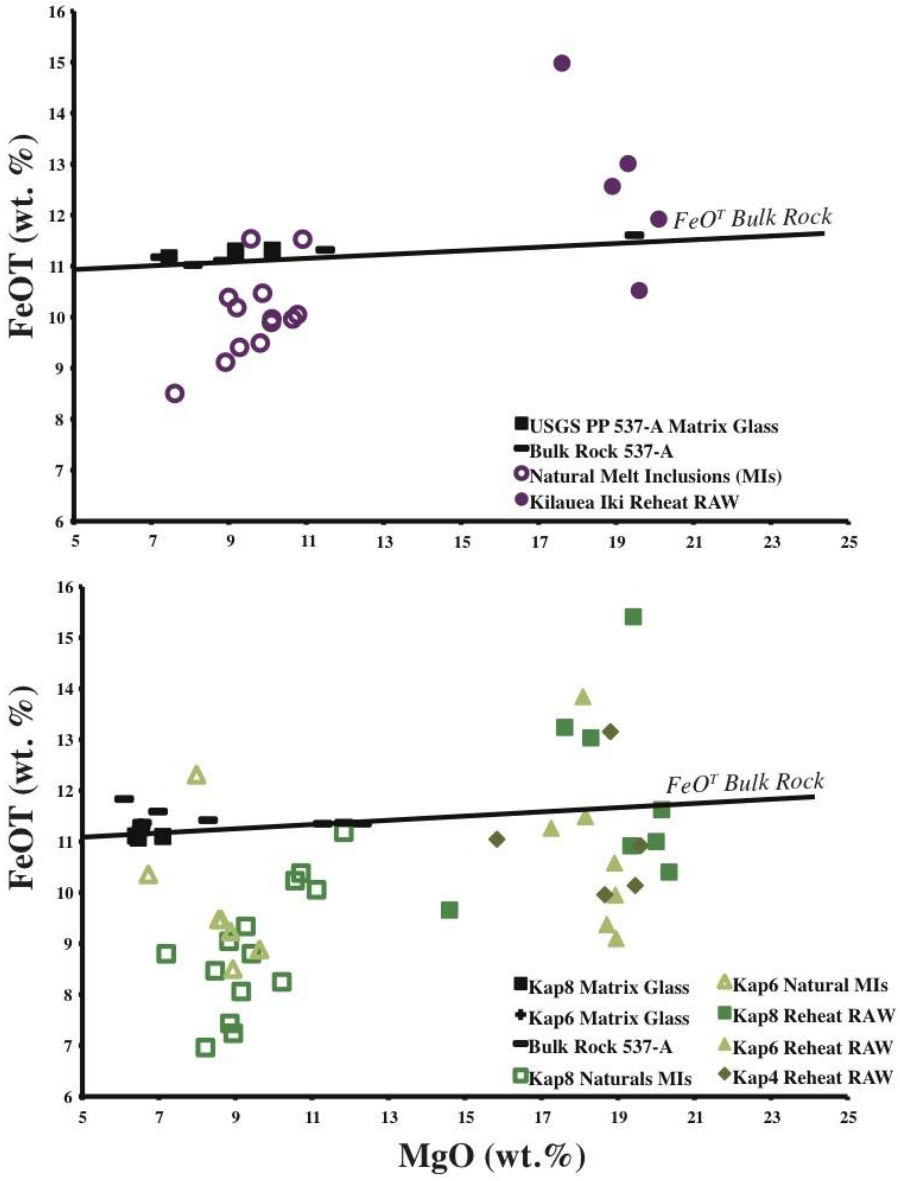

Figure 5. Melt inclusion MgO (wt.%) is plotted against FeOT (wt.%) with their matrix glass and bulk rock for Kīlauea Iki (a) and Kapoho (b). A best fit line is drawn through the bulk rock and matrix glass data. Raw melt inclusion compositions are plotted for naturally quenched, 1300°C, and 1400°C reheated melt inclusions. Naturally quenched melt inclusions from all suites fall below this line, suggesting that the melt inclusions loss Fe by diffusion. These melt inclusions can be corrected by selecting an appropriate Fe from the best fit line for a given MgO content of the melt inclusion. Reheated melt inclusions plot farther to the right of the natural inclusions, as they have greater amounts of MgO from olivine dissolution during overheating. Reheated melt inclusions plot below the line, like the natural melt inclusions, suggesting these melt inclusions regained the Fe lost to the olivine host during overheating, or above the best fit line, which may be the result of dissolving a Fe-rich accessory phase during reheating.

equilibrium line in this diagram and can be grouped into three categories: 1) melt inclusions plotting below the line lost Fe either naturally or during the reheating process 2) melt inclusions plotting on the trend line either did not lose Fe or were able to recover their lost Fe from the zone of olivine immediately adjacent to the inclusion-host interface which remelted during the experiment and 3) reheated melt inclusions plot above the trend line. This third scenario may indicate that magnetite or Cr spinel that was trapped with the melt inclusion could have been partially or completely dissolved during reheating. For both Kīlauea Iki and Kapoho reheated suites, there are melt inclusions that exhibit any of these three relationships. There also does not appear to be a correlation with more melt inclusions from the 1400°C experiments dissolving more spinel ormagnetite, sending them above the line, than the inclusions reheated to 1300°C, refer to plot for Kapoho (Figure 5b).

The post-entrapment crystallization correction involves progressively adding olivine back into the melt composition until it is in equilibrium with its host. All corrections were done using Petrolog3.1 (Danushevsky and Plechov, 2011). The melt inclusions in this study were also corrected for Fe diffusive loss at the same time. For all suites of data, the target FeO^T was between 11.2-11.3 wt.%. Not accounting for Fe loss by diffusion in post-entrapment crystallization corrections can cause an underestimation of the total amount of post-entrapment crystallization that has taken place. For example, Kīlauea Iki naturally quenched melt inclusions, if not corrected for Fe loss, yield an average PEC between 5-10%, whereas after correction for Fe loss, the average PEC increased to ~15%. This is an important correction to make when considering how the difference in PEC corrections can influence the restoration of volatiles like H_2O and CO_2.

The average amount of post-entrapment crystallization for the naturally glass inclusions, including the effects of Fe loss, is 14.3 +/- 3.5 % for Kīlauea Iki and 13.2 +/- 6.9 % for Kapoho.

Reheated melt inclusion compositions were corrected in the same way naturally quenched inclusions are in Petrolog3.1, but instead of incrementally adding olivine back to the melt composition until the melt inclusion is in equilibrium with its host, the olivine is incrementally removed from the raw composition of the glass. The average olivine dissolution for Kīlauea Iki melt inclusions reheated to 1400°C is 24.7% +/- 2.8%. Kapoho melt inclusions reheated to 1400°C have an average of 17.0 +/- 6% dissolution, and those reheated to 1300°C show less dissolution, with an average of 7.1% +/- 3.6%. Some Kapoho melt inclusions from 1300°C experiments showed no dissolution of olivine off the walls of the inclusion (Kap8-R-1300-9). Melt inclusions with more forsteritic olivine hosts also appeared to dissolve less olivine from the inclusion walls compared to more differentiated olivine. For example, Kap8-R-1400-32, with a Fo89.4 host was diluted by about 14% while Kap8-R-1400-18, with a Fo87.9 host was diluted by about 23%. These melt inclusions were selected from the same reheating experiment at 1400°C. The raw and corrected melt inclusion compositions, with their olivine host compositions, are given in Appendix C. Tephra Glass compositions measured at the University of Oregon are also reported in Appendix C.

Volatiles

Naturally Quenched Melt Inclusions

The Petrolog3.1 method used to correct the melt inclusions for effects of post-entrapment crystallization and diffusive Fe loss does not include volatiles. Therefore I used the ratio of K_2O in the corrected melt inclusion composition to K_2O in the raw melt inclusion composition to correct the volatile contents of the melt inclusions measured by FTIR. The concentration of K_2O, like volatiles H_2O and CO_2, is driven up by post entrapment crystallization of olivine, so it can therefore be used to correct the concentrations of volatiles in melt inclusions by calculating a correction factor. The $K_2O_{corrected}/K_2O_{raw}$ ratio for naturally quenched melt inclusions should be less than 1, with increasing amounts of PEC making this number smaller. Table 1 includes the corrected average volatile contents, correction/dissolution factors, and olivine host compositions for each suite of melt inclusions, both naturally quenched and reheated. The standard error for naturally quenched melt inclusions is about 5 % for H_2O and 11% for CO_2 by calculating H_2O and CO_2 concentrations in the Beer-Lambert Law equation and using a form of the Gaussian error propagation formula to estimate the error (the error is dependent on variance in replicate peak absorbance measurements and replicate glass thickness measuremeants. The volatile concentrations of melt inclusions, along with their uncertainties, are reported in Appendix D.

Table 1. Eruptive Suite Averages (Ranges) for Kīlauea Iki and Kapoho Melt Inclusions

Eruptive Suite	Naturally Quenched	Reheat 1300˚C	Reheat 1400˚C
Kilauea Iki			
H_2O (*wt.%*)	0.41 (*0.05-0.64*)	n/a	0.16 (*0.07-0.38*)
CO_2 (*ppm*)	126 (*b.d.l-424*)	n/a	250.4 (*b.d.l-588.46*)
Correction Factor	0.87 (*0.85-0.90*)	n/a	n/a
Dissolution Factor	n/a	n/a	1.34 (*1.30-1.39*)
Olivine host composition (Fo#)	86.6 (*83.6-87.9*)	n/a	86.9 (*83.9-87.9*)

Eruptive Suite	Naturally Quenched	Reheat 1300˚C	Reheat 1400˚C
Kap8			
H_2O (*wt.%*)	0.32 (*0.10-0.62*)	0.41 (*0.14-0.83*)	0.17 (*0.07-0.35*)
CO_2 (*ppm*)	139.4 (*76-288.2*)	153.6 (*22.4-322.1*)	486.4 (*93-1863.6*)
Correction Factor	0.86 (*0.80-0.95*)	n/a	n/a
Dissolution Factor	n/a	1.07 (*1.04-1.12*)	1.22 (*1.02-1.28*)
Olivine host composition (Fo#)	88.1 (*86.2-89.7*)	86.7 (*85.2-88.2*)	88.7 (*86.7-89.8*)
Kap6			
H_2O (*wt.%*)	0.73 (*0.32-1.12*)	n/a	0.27 (*0.13-0.54*)
CO_2 (*ppm*)	158.7 (*75-250.6*)	n/a	225.4 (*108.6-436.3*)
Correction Factor	0.88 (*0.82-0.95*)	n/a	n/a
Dissolution Factor	n/a	n/a	1.17 (*1.08-1.26*)
Olivine host composition (Fo#)	84.9 (*81.4-88.1*)	n/a	88.1 (*86.8-89.8*)
Kap4			
H_2O (*wt.%*)	n/a	n/a	0.24 (*0.09-0.58*)
CO_2 (*ppm*)	n/a	n/a	426.4 (*232.8-711.68*)
Correction Factor	n/a	n/a	n/a
Dissolution Factor	n/a	n/a	1.21 (*1.12-1.30*)
Olivine host composition (Fo#)	n/a	n/a	88.1 (*85.2-89.1*)

Kīlauea Iki

Kīlauea Iki naturally quenched melt inclusions have 0.05-0.55 wt. % H_2O and CO_2 values from below the detection limit (50 ppm) to 400 ppm. The Kīlauea Iki naturally quenched melt inclusions in this study have been plotted with Anderson and Brown's (1993) Iki-22 melt inclusions, as they are both from Phase 1 of the Kīlauea Iki eruption (Figure 6a). The range of Anderson and Brown's (1993) data is 0.25- 0.95 wt. % H_2O and ≤350 ppm CO_2.

Kapoho

Naturally quenched melt inclusions from Kapoho (considering both Kap8 and Kap6 together) have <0.1-0.8 wt. % H_2O and <100-275 ppm CO_2. H_2O values higher than 0.7 wt. % are present in Kap8 inclusions only (Figure 6b). H_2O and CO_2 contents for Kapoho overlap with values for Kīlauea Iki naturally quenched melt inclusions.

Reheated Melt Inclusions

The major element compositions of reheated melt inclusions were corrected using Petrolog3.1, and then, as with the naturally quenched melt inclusions, the ratio of K_2O in the corrected melt inclusion compositions to the K_2O of the raw melt inclusion compositions was used to correct the volatile contents. Because reheated melt inclusions experience considerable olivine dissolution during the experimental reheating, ratio $K_2O_{corrected}/K_2O_{raw}$ ratio is greater than 1, with increasing amounts of olivine dissolution increasing this value.

Kīlauea Iki

Reheated melt inclusions from Kīlauea Iki range from 0.05-0.40 wt. % H_2O and below detection to 600 ppm CO_2, compared to the range for naturally quenched inclusions of 0.05-0.55 wt.% H_2O and below detection to 450 ppm CO_2 (Figure 6a). When reheated melt inclusions are compared to their naturally quenched counterparts, it appears that hydrogen diffusive loss occurred during the experiments, because many reheated inclusions fall in the 0.1 t o 0.2 wt.% range, lower than all the naturally

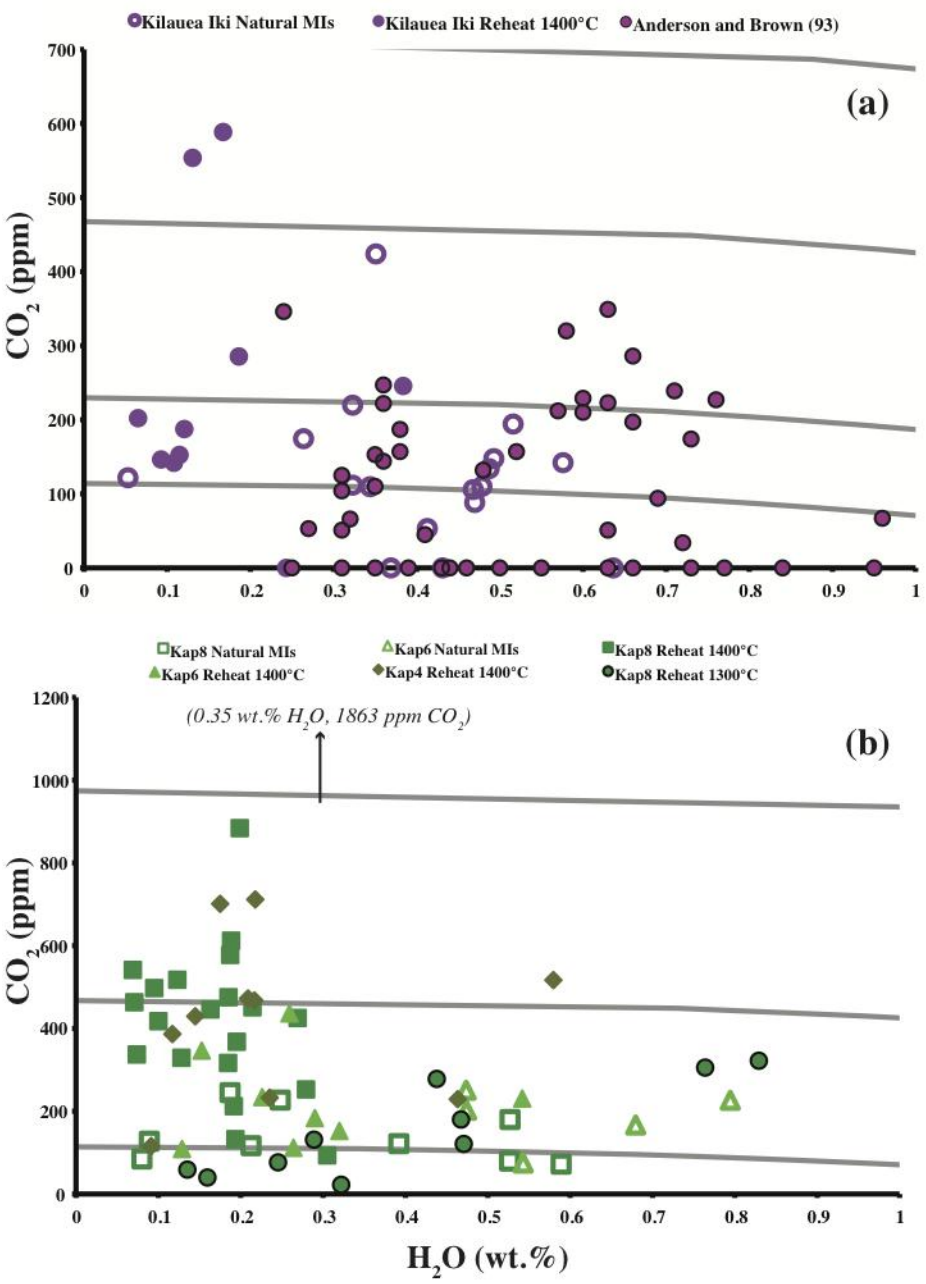

Figure 6. Melt inclusion H_2O is plotted versus CO_2 for naturally quenched and reheated melt inclusions from Kīlauea Iki (a) and Kapoho (b). Plots include corrected data only. Naturally quenched melt inclusions are open symbols and reheated melt inclusions are filled symbols for this study. Isobars (lines of constant pressure) appear in grey and range from 250-1500 bars for Kīlauea Iki and 250-2000 bars for Kapoho.

quenched inclusions. Reheated Kīlauea Iki melt inclusions have higher CO_2 than the naturally quenched ones, suggesting the reheated inclusions gained CO_2 from the shrinkage bubbles during the experiments. Two reheated melt inclusions plot in the range of 500-600 ppm CO_2, which is higher than the maximum restored CO_2 (based on estimating the bubble contribution) in melt inclusions from Anderson and Brown's (1993) study. Overall, there appears to be significant overlap in CO_2 values between the reheated inclusions in this study and the calculated values from Anderson and Brown (1993). However, Anderson and Brown's (1993) data is shifted more towards higher H_2O values than the data in this study, because their methodology did not involve reheating, and thus their inclusions were not affected by hydrogen diffusive loss.

Kapoho

The H_2O and CO_2 concentrations of reheated Kapoho melt inclusions show less overlap with the naturally quenched inclusions than is seen for the Kīlauea Iki data (Figure.6b). When all naturally quenched suites of Kapoho are considered together, the melt inclusions have ~0.1 to 0.8 wt.% H_2O and ~100-250 ppm CO_2. Reheated melt inclusions (1400°C) from all Kapoho samples appear to have also experienced hydrogen diffusive loss during reheating, with ~0.1 to 0.3 wt. % H_2O. The reheated Kapoho melt inclusions have a wide range of CO_2 values, from 100 to 900 ppm CO_2, with one inclusion containing 1863 ppm CO_2. Results for the various Kapoho samples are as follows: Kap8 melt inclusions, taken from tephra erupted from the Tephra Plain deposit downwind from Pu'u Laimana (Cone Complex) range from 0.07-0.35 wt. % H_2O and $\leq$900 ppm CO_2, with one inclusion containing 1863 ppm CO_2. Kap6 melt inclusions,

taken from a glomerocryst-rich tephra sample from Vent E, range from 0.15-0.55 wt. % H_2O and 100-450 ppm CO_2. Kap4 melt inclusions, taken from tephra just above the basal spatter rampart of Cone Complex/Pu'u Laimana, range from 0.1-0.6 wt. % H_2O and 100-700 ppm CO_2. Kap8 melt inclusions that were reheated to 1300° C have a wide range of water contents, but fewer very low values compared to reheated Kīlauea Iki inclusions, and therefore may not have experienced as much hydrogen diffusive loss. However, the inclusions heated to 1300°C have lower CO_2 (below detection-350 ppm CO_2 than the inclusions heated to 1400°C. The inclusions reheated to 1300°C inclusions appear to overlap H_2O and CO_2 with most of the naturally quenched Kapoho melt inclusions. The correction factors for some Kap8 reheated inclusions from the 1300°C experiment indicate that some melt inclusions did not dissolve any olivine from the inclusion walls, and therefore may not have been at a temperature high enough to redissolve all the CO_2 from the shrinkage bubble. The effectiveness of the reheating experiments at 1400ºC and 1300ºC can be visualized in Figure 7. The frequency histogram illustrates that amongst Kapoho melt inclusions, the naturally quenched melt inclusions and reheated to 1300ºC melt inclusions show a similar frequency distribution. When the naturally quenched melt inclusions from both Kīlauea Iki and Kapoho are compared to the 1400ºC reheated melt inclusions, there is a different distribution, with more melt inclusions falling between 200-600 ppm CO_2 for both Kīlauea Iki and Kapoho, and some reheated Kapoho melt inclusions that have even higher CO_2.

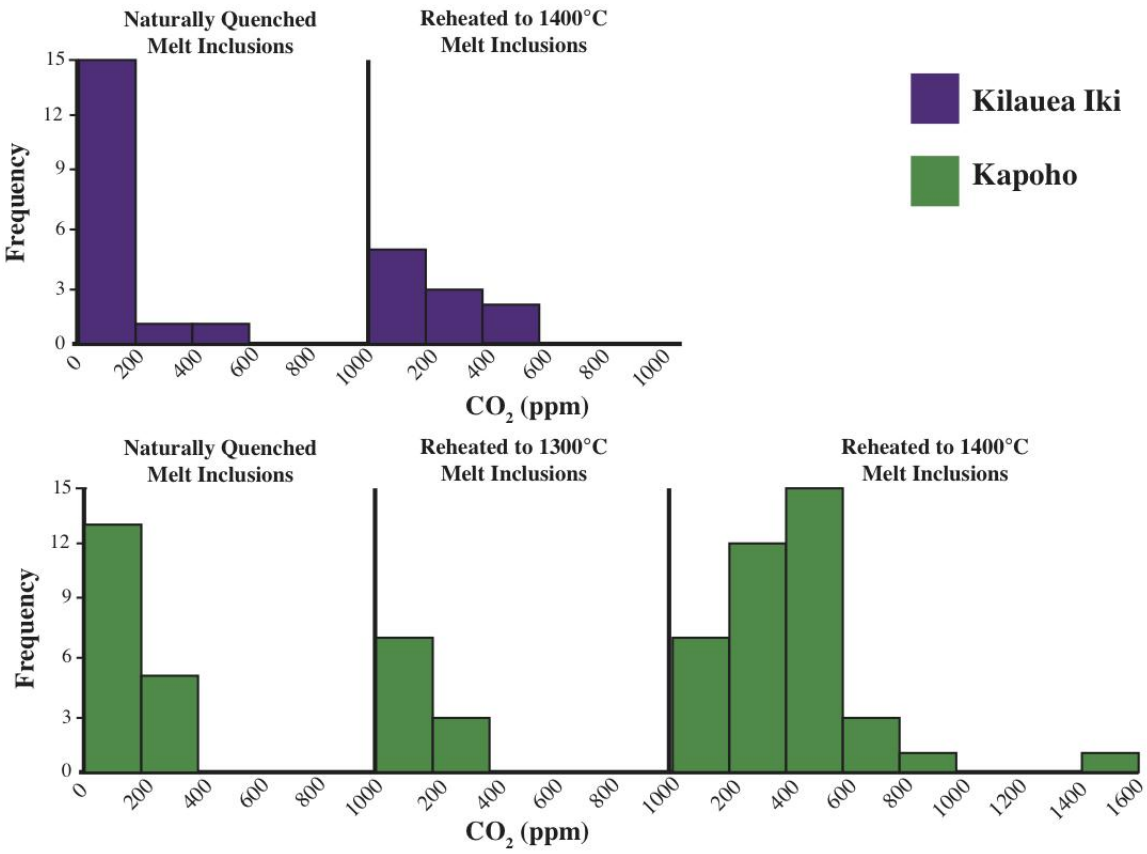

Figure 7. Histograms comparing the amount of CO_2 in naturally quenched melt inclusions to the amount recovered by experimentally reheating melt inclusions above their trapping temperature. (Top Row) Naturally quenched Kīlauea Iki melt inclusions estimated most CO_2 between b.d.l-200 ppm, where the data is distributed throughout b.d.l-600 ppm CO_2 in the reheated melt inclusions, although most still fall between b.d.l.-200 ppm. (Middle Row) Kapoho melt inclusions from all eruptive suites are included. The naturally quenched melt inclusions and 1300°C reheated melt inclusions overlap, with most inclusions estimating b.d.l-400 ppm CO_2. The 1400°C reheated, of which there is the most data available, show a larger range of CO_2, with most data following between 200-600 ppm CO_2, but several inclusions above 600 ppm.

Olivine Crystallization Depth Calculations

Vapor saturation pressures were calculated for all corrected inclusions using a solubility model for H_2O and CO_2 in silicate melts at a temperature of 1200°C (VolatileCalc; Newman and Lowenstern, 2002). There is strong evidence that Kīlauea melts are vapor saturated at crustal pressures (e.g., Gerlach,1986), and therefore the

resulting vapor saturation pressures should be equivalent to trapping pressures and can be used to calculate the crystallization depth of the olivine hosts. We used the depth-density relationship of Ryan (1987) to calculate the crystallization depths from the vapor saturation pressures. This relationship suggests that the bulk density of the crust at shallow levels on the volcano is lower than the density of basalt due to the presence of fluid/vapor filled cracks. As the depth on the volcano increases, so does the density of the crust until it reaches basalt densities at around 4.5 km.

CHAPTER V

DISCUSSION

Hydrogen Loss by Diffusion

Reheating olivine-hosted melt inclusions was successful in redissolving CO_2-rich shrinkage bubbles. However, the high temperatures necessary to redissolve the bubbles resulted in hydrogen diffusive loss from the melt inclusions (Figure 8a). This has been experimentally demonstrated in several previous studies (Hauri, 2002, Gaetani et al., 2012), where the diffusivity of hydrogen in olivine is strongly temperature dependent (Bucholz et al., 2013) and H_2O of natural or hydrated melt inclusions can be driven off completely given a long enough duration (Massare et al., 2002, Gaetani et al., 2012). Work by Bucholz et al. (2013) demonstrated this temperature dependence of hydrogen diffusivity in melt inclusions with initially high H_2O by choosing temperatures of 1100°C and 1250°C, and heating them for the same duration (1 hour). The melt inclusions reheated to 1250°C showed more extensive hydrogen loss. Danyushevsky et al. (2002) also noted that hydrogen loss by diffusion was common to rehomogenization experiments

---

Figure 8 (next page). Hydrogen diffusive loss occurs in both naturally quenched and reheated melt inclusions from 1300°C and 1400°C experiments. Melt inclusion average diameter (a proxy for volume) is plotted against the inclusion's H_2O content. (a) Reheated melt inclusions appear to have lost hydrogen by diffusion, with more inclusions plotting between 0.05-0.25 wt.% H_2O. The low H_2O of some inclusions appears in all suites. Hydrogen diffusivity is temperature dependent, therefore the 1400°C reheated melt inclusions experienced greater H diffusive loss than 1300°C. (b) Naturally quenched melt inclusions appear to show hydrogen diffusive loss. Smaller melt inclusions appear to have lost more H_2O than larger melt inclusions, due to the higher surface area to volume ratio.

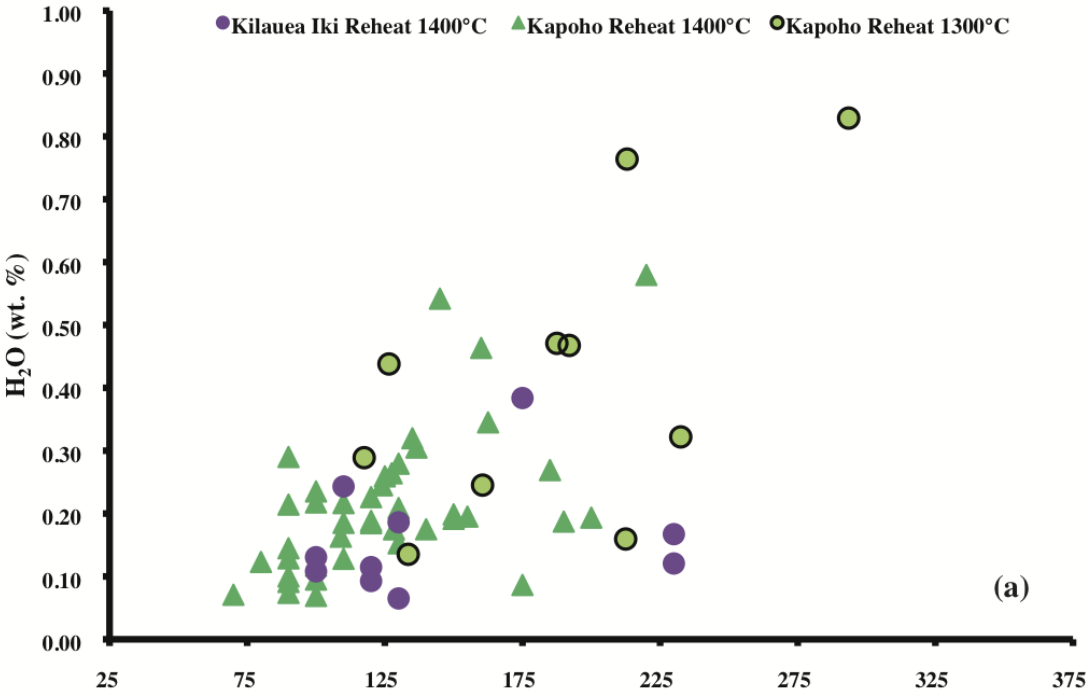
Kilauea Iki Reheat 1400°C
Kapoho Reheat 1400°C
Kapoho Reheat 1300°C
H2O (wt. %)
1.00
0.90
0.80
0.70
0.60
0.50
0.40
0.30
0.20
0.10
0.00
25
75
125
175
225
275
325
375
(a)

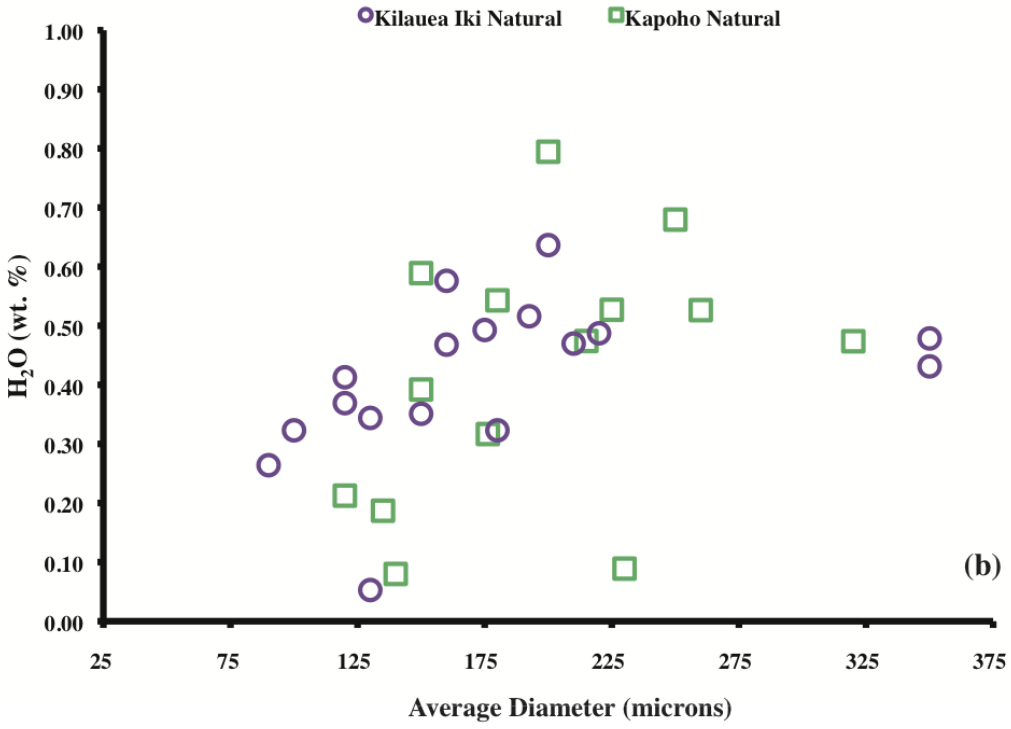
Kilauea Iki Natural
Kapoho Natural
H2O (wt. %)
1.00
0.90
0.80
0.70
0.60
0.50
0.40
0.30
0.20
0.10
0.00
25
75
125
175
225
275
325
375
(b)
Average Diameter (microns)

at 1 atm, subsequently raising the homogenization temperature of the glass. Finally, experimental reheating of melt inclusions in a 1-atm furnace at 1275°C and on the FMQ buffer showed that when melt inclusions spend less than 10 minutes in the furnace hot zone, hydrogen diffusion does not appear to take place (Hauri, 2002). Work by Cervantes et al. (2002) using a high temperature stage to redissolve shrinkage bubbles in melt inclusions from a Mauna Loa picrite also showed that hydrogen diffusive loss was minimal at temperatures up to 1420°C if the duration of reheating was short. In this work the olivine was quenched as soon as the shrinkage bubble dissolved, so melt inclusions were not exposed to high temperature longer than necessary. Most olivine in this study had to be reheated to high temperatures (in these experiments, 160°C above the estimated trapping temperature) in order to redissolve the shrinkage bubbles. Although the olivine only sit at temperature for a maximum of 15 minutes in the furnace hot zone, because of the nature of the experimental apparatus, they also have to sit in the furnace during the ramp up time from 800°C to either 1300°C or 1400°C, a process that takes approximately 40 minutes. Because of the time the olivine spent at high temperatures some hydrogen diffusion was unavoidable. However these time periods were short enough to prevent complete loss of water from the inclusion.

Reheated Melt Inclusions

Heating melt inclusions more than a hundred degrees above their original trapping temperature was required to redissolve CO_2 from the shrinkage bubble. In addition to olivine dissolution from the walls of the inclusion, which can be corrected for, as well as

the possible dissolution of Cr spinel or magnetite, the reheated melt inclusions appear to show hydrogen loss by diffusion. As H diffusive loss is accelerated at higher temperature; reheated melt inclusions that have been exposed to high temperatures should show more hydrogen diffusive loss than a naturally quenched inclusion. Like naturally quenched inclusions, when the average melt inclusion diameter is plotted against its corrected H_2O content, a weak correlation exists, amongst all eruptive suites of data (Figure 8a). There are more small reheated melt inclusions compared to the size range of naturally quenched melt inclusions, and these appear to show the greatest amount of hydrogen diffusive loss (Lloyd et al., 2012). The difference in the ramp up time between the 1300°C and 1400°C experiments is only 6-7 minutes, as the furnace ramp rate was 15°C per minute. The total time spent in the furnace when ramp up time and time olivine spent in the furnace hot zone is close to one hour. Therefore, based on previous work, it is understandable that the 1400°C experiments show more loss, because hydrogen diffusivity is T dependent, but the total amount of time at high temperature that melt inclusions experienced probably also plays a role in the reheated trend.

Based on our experimental results, I find that redissolving CO_2 with reheating experiments in a 1-atm furnace works best for relatively large (1-2mm +) olivine with high Fo content. The 1400°C experiment tended to favor the most primitive olivine population for analysis as they can withstand greater amounts of overheating without rupturing, presumably because they were originally crystallized at higher temperatures than more differentiated olivine. The 1300°C experiments appeared to have variable success, but may not have overheated the melt inclusions enough to dissolve the shrinkage bubbles. The Kap8 olivine reheated to 1300°C appear to overlap with the

natural melt inclusions in their H_2O and CO_2 contents rather than olivine reheated to 1400°C. For Kīlauea olivine-hosted melt inclusions, I conclude that the 1300°C experiments were not as effective at redissolving CO_2.

Fortunately, hydrogen loss by diffusion during the experimental reheating does not have a significant impact on using the H_2O and CO_2 contents to calculate vapor saturation pressures and crystallization depths for the olivine hosts. In Figure. 7, the H_2O-CO_2 plots, the isobars are relatively flat, showing that the low H_2O contents of both naturally quenched and experimentally reheated inclusions contribute very little to the final vapor saturation pressure. H_2O only accounts for a few tens of bars at most. Since hydrogen diffusive loss has occurred, the vapor saturation pressures calculated can be considered minimum pressures, but must be close to the original trapping pressure. Gaetani et al. (2012) remarked that hydrogen diffusive loss in melt inclusions of low H_2O magmas (as Hawaiian tholeiites would be considered) does not significantly alter the record of H_2O-CO_2 in natural inclusions, but could further enhance the loss of CO_2 to shrinkage bubbles when the hydrogen is lost. For those interested in magmatic H_2O contents more strongly than CO_2, the use of a high temperature heating stage would be the preferred technique, because the rapid heating rate of the stage would not expose the melt inclusions to high temperature for as long, and the melt inclusion can be quenched as soon as the shrinkage bubble has redissolved.

Naturally Quenched Melt Inclusions

Some naturally quenched melt inclusions from each sample appear to have also been affected to some degree by hydrogen loss by diffusion, particularly those falling

below 0.20 wt.% H_2O. When melt inclusion average diameter is plotted against the correct H_2O content of the melt inclusion, a weak correlation exists (Figure. 8b). The melt inclusion average diameter is a proxy for melt inclusion volume, and what this correlation suggests is that relatively smaller melt inclusions are more strongly affected by hydrogen diffusive loss, due to the high surface area to volume ratio (Qin et al., 1992, Lloyd et al., 2012). This evidence for hydrogen diffusive loss is somewhat surprising given that the inclusions are relatively large (>75 microns average diameter). However, this weak correlation may not be altogether unexpected because each suite of melt inclusions likely experienced different thermal histories.

The hydrogen diffusive loss experienced by Kīlauea Iki melt inclusions in this study is puzzling. The olivines were erupted in the first phase of the eruption, before drainback and extensive magma mixing took place. I would expect to see hydrogen diffusive loss in naturally quenched melt inclusions from later phases of the Kīlauea Iki eruption, because the magma erupting to the surface had the ability to exsolve most of its water, drainback, and mix with more juvenile magma in magma chamber. The juvenile magma would come in contact with the low H_2O drainbacked magma, and re-equilibration to lower H_2O could take place (Lloyd et al., 2013). Previous work (Wallace and Anderson, 1998; Sides et al., 2013) has already shown the trend of decreasing H_2O over the course of the eruption.

For Kapoho melt inclusions, it is more likely that their host magmas came in contact with low H_2O melts that were pushed into the rift zone over the course of the many drainback cycles that occurred at Kīlauea Iki (Eaton et al., 1987) or low H_2O melts that were already stored in the rift zone (Wright and Helz, 1996), since the Kapoho

eruption has a complex mixing history involving multiple components. Over the course of the Kapoho eruption, there were periods (January 29, 1960) when a lava pond appeared, inflated, and then drainbacked into the fissures, so mixing of low H_2O drained magma and juvenile magma most likely occurred there as well (Richter et al., 1966).

Olivine Crystallization Depths

The internal geometry of Kīlauea's magma plumbing system has been constrained by seismic data (Ryan, 1987a) and also summit ground deformation (Thornber, 2001; Cervelli et al, 2002). Shallow seismicity indicates ground cracking that is caused by forceful magma injections into rift zones during volcanic eruptions, and can also happen passively when the south flank slips along the décollement (Swanson et al., 1976). The summit magma chamber is present at depths of neutral buoyancy at 2-3 km, and injection of magma as dikes into the rift zone from the summit chamber occurs at a similar depth. Ryan (1987a) also suggested that a deeper part of the rift zone exists between 6-8 km, but is mostly aseismic. Clague et al. (1995) suggest that the shallow and deep portions of the rift are not physically isolated from each other but rather are interconnected by a series of almost vertical bladed dikes, allowing olivine to settle and accumulate across a large range of depths in order to form dunitic cumulate bodies. Plattner et al. (2013) have been able to model slip along Kīlauea's south flank by inserting a cumulate body into the east rift zone at 6-8 km and modeling how the gravitational instability of such a body could account for the slip rates observed at Kīlauea. While the deep rift zone may not be a frequently used pathway for magma transport, it may be important as a region where cumulates are formed. The crystallization pressures of olivine can also provide insight

into Kīlauea's magma plumbing system. The experimentally reheated melt inclusions provide information on vapor saturation pressures at the time of trapping, and can therefore be useful barometers to infer crystallization and storage depths.

Kīlauea Iki

The crystallization pressures determined for Kīlauea Iki in this study based on reheated melt inclusions agree with the estimated pressures of Anderson and Brown (1993) based on an assumed pre-eruptive bubble vol.% of 0.5 for shrinkage bubble bearing inclusions (Figure 7). In addition, Anderson and Brown (1993) measured melt inclusion CO_2 in bubble free inclusions, where no correction was needed. My results indicate that most Kīlauea Iki olivine crystallized at less than 1 kbar pressure, which corresponds to depths between 2-3 km (Figure 9). One melt inclusion has an estimated crystallization depth of ~4.5 km. Even the most primitive olivines from Kīlauea Iki (Fo86-87) do not appear to have crystallized at greater depths.

The olivine crystallization depths for reheated Kīlauea Iki olivine are consistent with previous interpretations of the Kīlauea Iki eruption (Helz, 1987; Anderson & Brown, 1993). Helz (1987) suggested that the S-1 magma ascended along a seldom used pathway through Kīlauea's magma plumbing system, ponding for some time before forcing its way through pre-existing magma and/or accumulated olivine and then erupted. This scenario would allow for a period of time which Kīlauea Iki magmas could stall shallowly and crystallize the coarse olivines that are characteristic of this eruption.

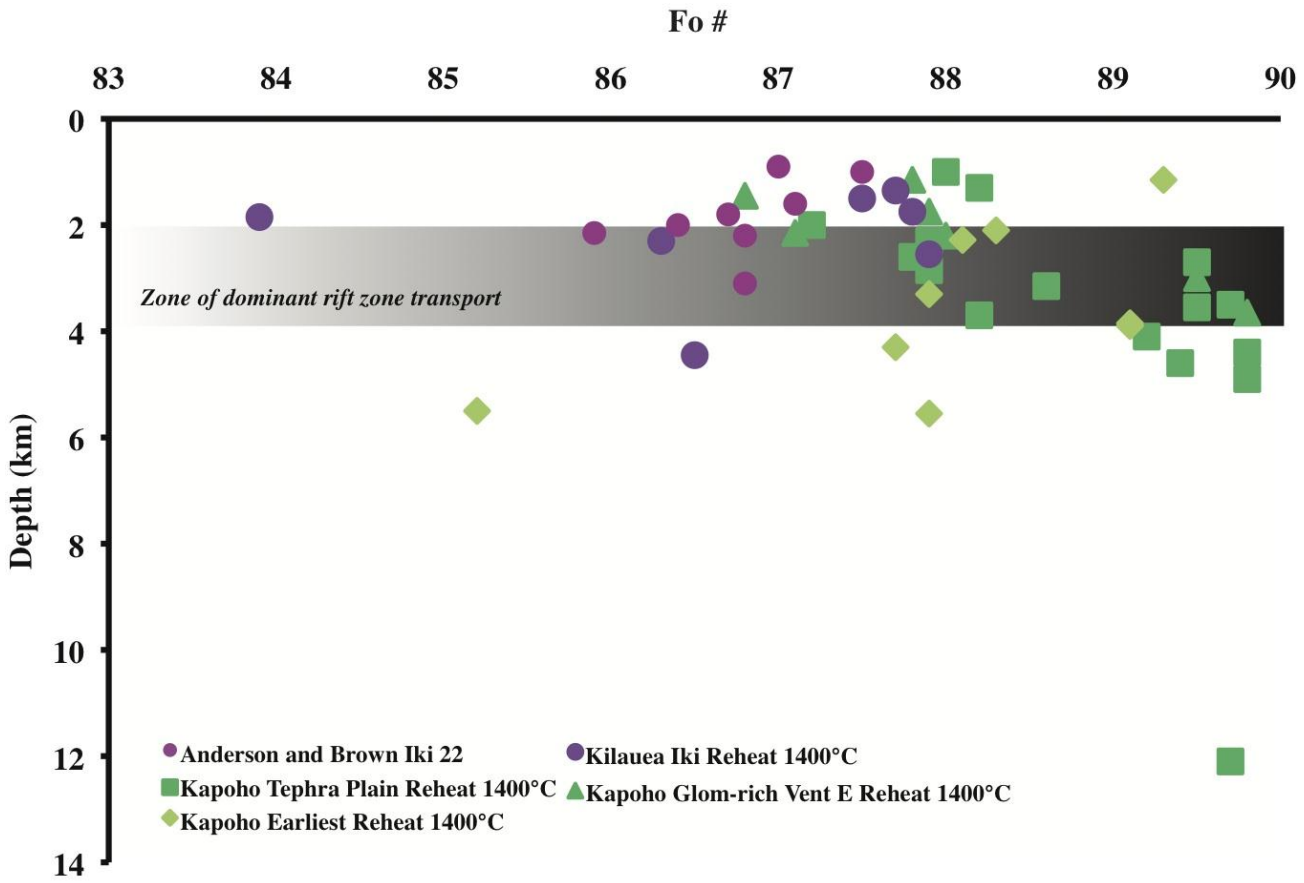

Figure 9. The forsterite content of the olivine host is plotted against the estimated crystallization depth for reheated Kīlauea Iki and Anderson and Brown (1993) bubble free Iki-22 melt inclusions and Kapoho 1400°C reheated (Kap8, Kap6, and Kap4). For Kīlauea Iki and Hiiaka, there does not appear to be any correlation between the forsterite content of the olivine host and the crystallization depth. Kapoho melt inclusions, particularly those from Kap8, suggest that primitive olivine population (Fo89) crystallized at greater depths than their more differentiated counterparts. The horizontal gray bar represents the depths of rift zone transport suggested by geophysical data.

Kapoho

The pressures for reheated melt inclusions from Kapoho suggest that some olivine crystallized at depths greater than the 2-4 km predicted by geophysical models for rift zone transport and storage of magma (Figure 9). Some Kapoho olivine crystallized at greater depths than Kīlauea Iki, with Kapoho Tephra Plain (Kap8) olivine at 1-6 km depths, Kapoho glomerocryst rich Vent E (Kap 6) at 1-5 km depth, and Kapoho Oldest Cone Complex/Pu'u Laimana Tephra (Kap4) at 2-6 km depth. One melt inclusion from Kap8 suggests a crystallization depth of ~ 16 km and thus appears anomalous. One potential explanation is that this melt inclusion may have contained a primary vapor bubble that was co-entrapped with silicate melt when it formed, causing dissolution of CO_2 during the experiment in excess of the original melt CO_2 content. The higher crystallization depths of Kapoho olivine are corroborated by Moore et al. (in prep), who measured the density of CO_2 in shrinkage bubbles in naturally quenched melt inclusions from Kīlauea Iki and Kapoho using olivine from the same samples as this study. They found that Kapoho shrinkage bubbles had a range of overlapping to higher CO_2 densities than Kīlauea Iki, with the higher densities corresponding to higher initial trapping pressures for Kapoho compared to Kīlauea Iki.

Unlike Kīlauea Iki, there does appear to be a correlation between forsterite content and crystallization depth for some primitive Kapoho olivine (Fo89.7), particularly for Kap8, which was erupted with the youngest tephra deposited by Cone Complex/Pu'u Laimana. For Kīlauea Iki, the olivine hosts had an average depth of 2.21 +/- 1.41 km and average host composition of Fo87. For the Fo89 group from Kapoho, the olivine hosts had an average depth of 3.64+/- 1 and an average host composition of Fo89.5. The

primitive nature of some olivine from Kapoho, combined with their higher crystallization pressures, indicates that their parent magma must have entered the rift system at a greater depth than normal (intermediate depths between the shallow and deep rifts) and was flushed from the rift zone following the collapse of the summit caldera, which began several days after the eruption started. Compositional comparisons between melt inclusions and matrix glass from Kīlauea Iki and these suites from Kapoho suggest that olivine erupted late in the Kapoho eruption may be the missing primitive piece of the Kīlauea Iki S-1 magma, as discussed further below.

Olivine Crystallization Pressures Across Kīlauea Volcano

A question that has arisen during the course of this study is whether the lower East Rift Zone eruptions involve magma that bypassed the summit reservoir and via the deep rift zone or the décollement (Vinet and Higgins, 2011). The submarine rift zone, which is closer to Kapoho's vent location than to Kīlauea's summit, also tends to erupt olivine-rich lavas (Clague et al., 1995). When olivine crystallization depths are plotted against their distance from Kīlauea's summit (Figure 10), it does appear that the Kapoho eruption, occurring 47 km away from the summit, erupted a population of olivine that crystallized at greater depths than those that might be predicted for the shallow rift. Many Kapoho olivine also crystallized at greater depth than those from Kīlauea Iki.

For Kapoho, olivine crystallized over a wide range of depths between the shallow and deep rift system (1-6 km), but as the histogram indicates, many Kapoho olivines crystallized at depths greater than those of the shallow rift system. The higher crystallization depth population from the Kapoho eruption belong mostly to Kap8, the

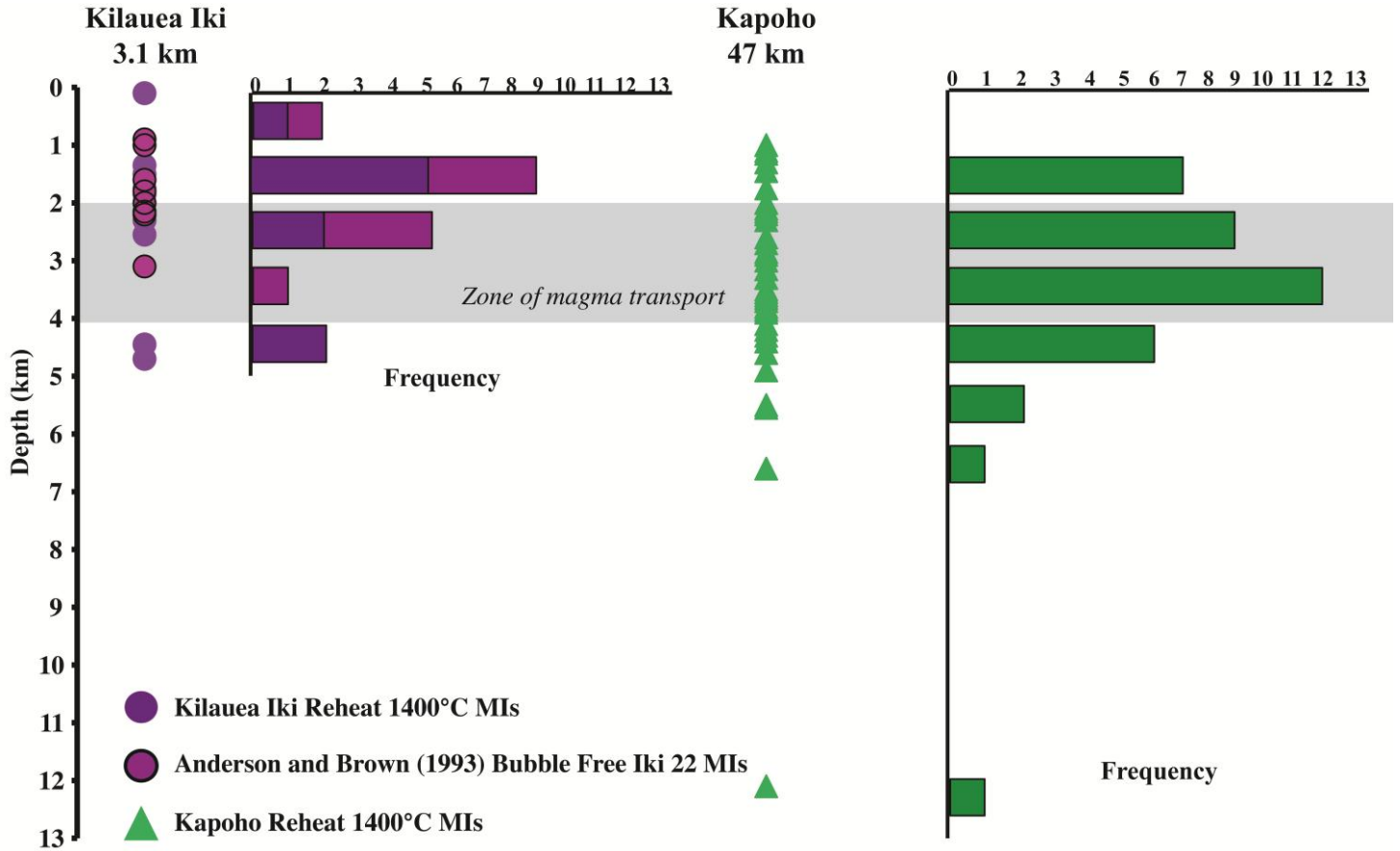

Figure 10. Olivine crystallization depths are plotted against their distance from Kīlauea's summit. Histograms appear next to the crystallization depths to show the number of olivine, which crystallized within a particular depth increment. Kīlauea Iki melt inclusions suggest that most olivine crystallization took place within the shallow summit system, between 1-3 km depth (with 2 Kīlauea Iki melt inclusions plotting between 5-6 km). The Kapoho eruption took place 47 km away from the summit, and all Kapoho eruptive suites are plotted together. Olivine crystallization depths estimated for Kapoho show 12 olivines with crystallization depths between 3-4 km, with 7 olivine-hosts crystallizing at greater depth.

youngest erupted tephra, but also includes olivine from Kap6 and Kap4. This observation suggests that some of these higher-pressure olivine were also erupted early in the eruption when multiple fissures were building the main cone complex, which became Pu'u Laimana (Kap4), as well as at the youngest tephra erupted at Vent E, as both of these deposits are older than Kap8. In this case, the lower East Rift Zone appear to flush a population of higher pressure olivine in this olivine phyric eruption, and may not be dissimilar to submarine rift eruptions that also erupt olivine-rich lavas.

Origin of Olivine: Phenocrysts or Re-Entrained Cumulate

Both Kīlauea Iki and Kapoho erupted olivine phyric tephra and lava, which are coarse in grain size. The coarse nature of the olivine suggests the crystals might be cumulate in origin and might therefore be unrelated to the magma in which they eventually erupt (Welsch et al., 2013). However, comparison of the compositions of olivine-hosted melt inclusions, bulk rock and matrix glass values can clarify the origin of olivine. If melt inclusions have compositions that are similar to matrix glass and bulk rock values, then this suggests they are phenocrysts that grew and remained entrained in the same magma. For Kīlauea Iki, a plot of CaO vs. Al_2O_3 (Figure 11a) can illustrate this point. Plotted matrix glass and bulk rock compositions were taken from Richter et al. (1966) with dates corresponding to the first phase of the Kīlauea Iki eruption. These were also plotted with matrix glass representing S-1 magma from Helz (1987). A similar plot (Figure 11b) for the olivine-hosted melt inclusions from Kapoho shows a different pattern. All Kapoho olivine-hosted melt inclusions, including restored compositions of

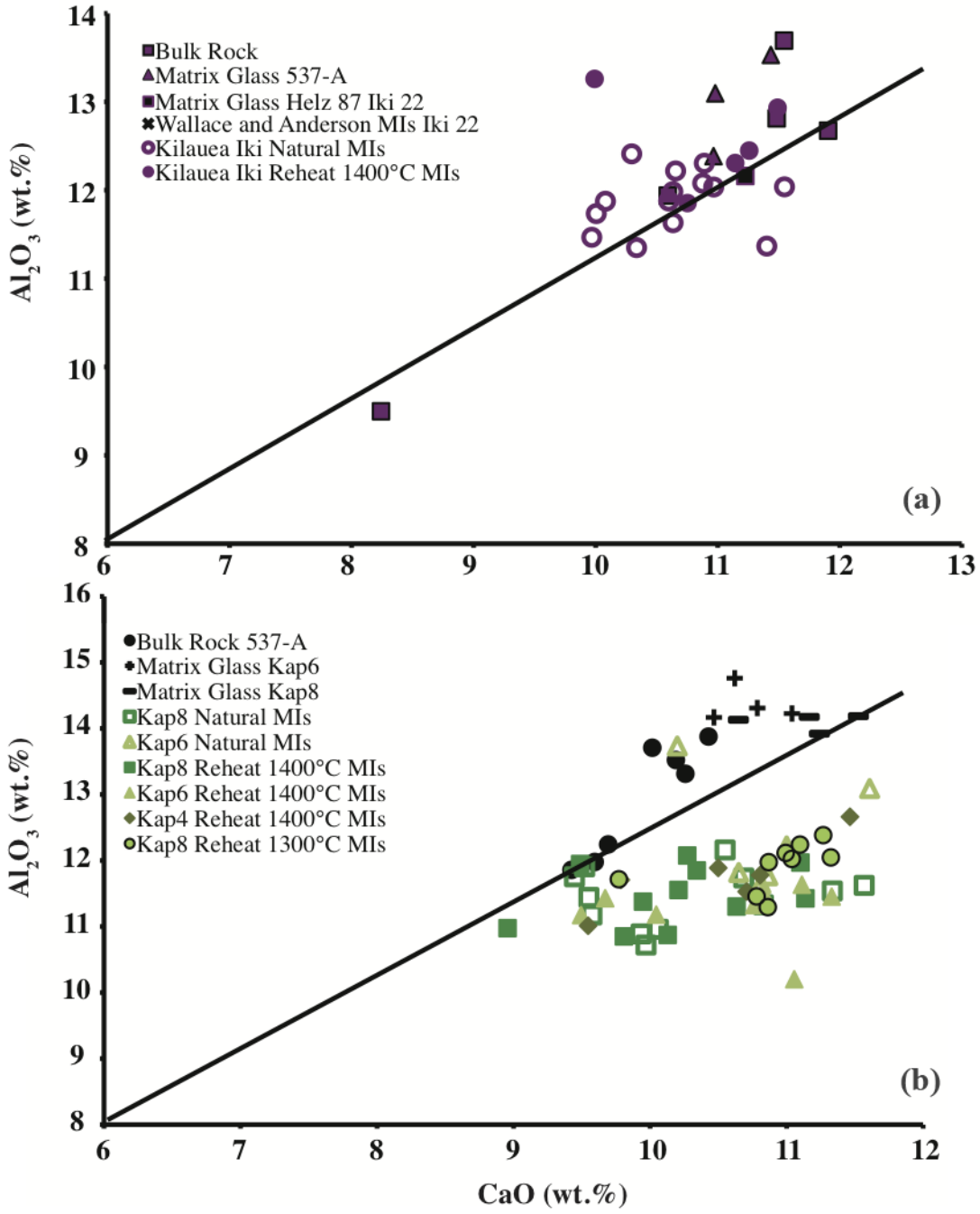

Figure 11. Melt inclusion CaO is plotted versus Al_2O_3 with the matrix glass and bulk rock of its host magma. If melt inclusions fall along the liquid line of descent defined by their host magma, than it can be assumed the olivine grew from this host magma. If melt inclusions fall away from this line, than magma mixing or entrainment of their olivine host by an unrelated magma may have occurred. (a) Kīlauea Iki melt inclusions suggest their olivine are related to their host magma. (b) Kapoho melt inclusions vary in distance from the liquid line of descent of their host magma, suggesting they are entrained cumulates or their parent magma mixed with their host magma(s).

reheated inclusions, when plotted with their matrix glass and bulk rock, lie away from the liquid line of descent predicted by their matrix glass. There are some melt inclusions that lie further away from this line than others, which may suggest magma mixing between the melt inclusions' original host magma and the magma that later entrained the olivine.

The presence of two types of magma in the Kīlauea Iki eruption is well documented (Richter et al., 1966; Wright and Fiske, 1971, Helz, 1987, Wallace and Anderson, 1998). The S-1 magma type is identifiable by its higher MgO contents (10-15 wt. %) when compared to typical summit magmas (6-7 wt. %). Appendix E reports a range of bulk rock compositions for Kilaue eruptions contemporary to 1959-1960 eruptions. Elements that are incompatible in olivine, particularly CaO and Al_2O_3, were also higher in S-1 glasses when compared to typical summit bulk rock and matrix glass compositions. Wallace and Anderson (1998) used CaO/Al_2O_3 ratios to distinguish between inclusions trapped from S-1 magma and inclusions that were trapped following eruptive drain back. CaO/Al_2O_3 is a useful ratio because it remains constant during fractional crystallization until the point of clinopyroxene saturation. Wallace and Anderson (1998) report CaO/Al_2O_3 ratios for Kīlauea Iki S-1 melt inclusions between 0.8

Figure 12 (next page). K_2O is plotted versus CaO/Al_2O_3 ratio for melt inclusions, bulk rock, and matrix glass for Kīlauea Iki (S-1 from USGS PP 537 and Helz, 1987) (a) and Kapoho (b). Kīlauea Iki naturally quenched and reheated melt inclusions plot with their bulk rock and matrix glass, suggesting that they belong along the same liquid line of descent as their host magma, and are not accumulated olivine. Kapoho naturally quenched and reheated melt inclusions do not plot with their bulk rock (USGS PP 537) and matrix glass, suggesting that they do not belong along the same liquid line of descent as their host magma. When Kapoho melt inclusions from Kap8, Kap6, and Kap4 are plotted with Kīlauea Iki melt inclusions, it suggests that some Kapoho olivine do belong with Kīlauea Iki S-1 magmas. Some melt inclusions from Kapoho are more incompatible than Kīlauea Iki melt inclusions with their olivine host, suggesting that they are more primitive.

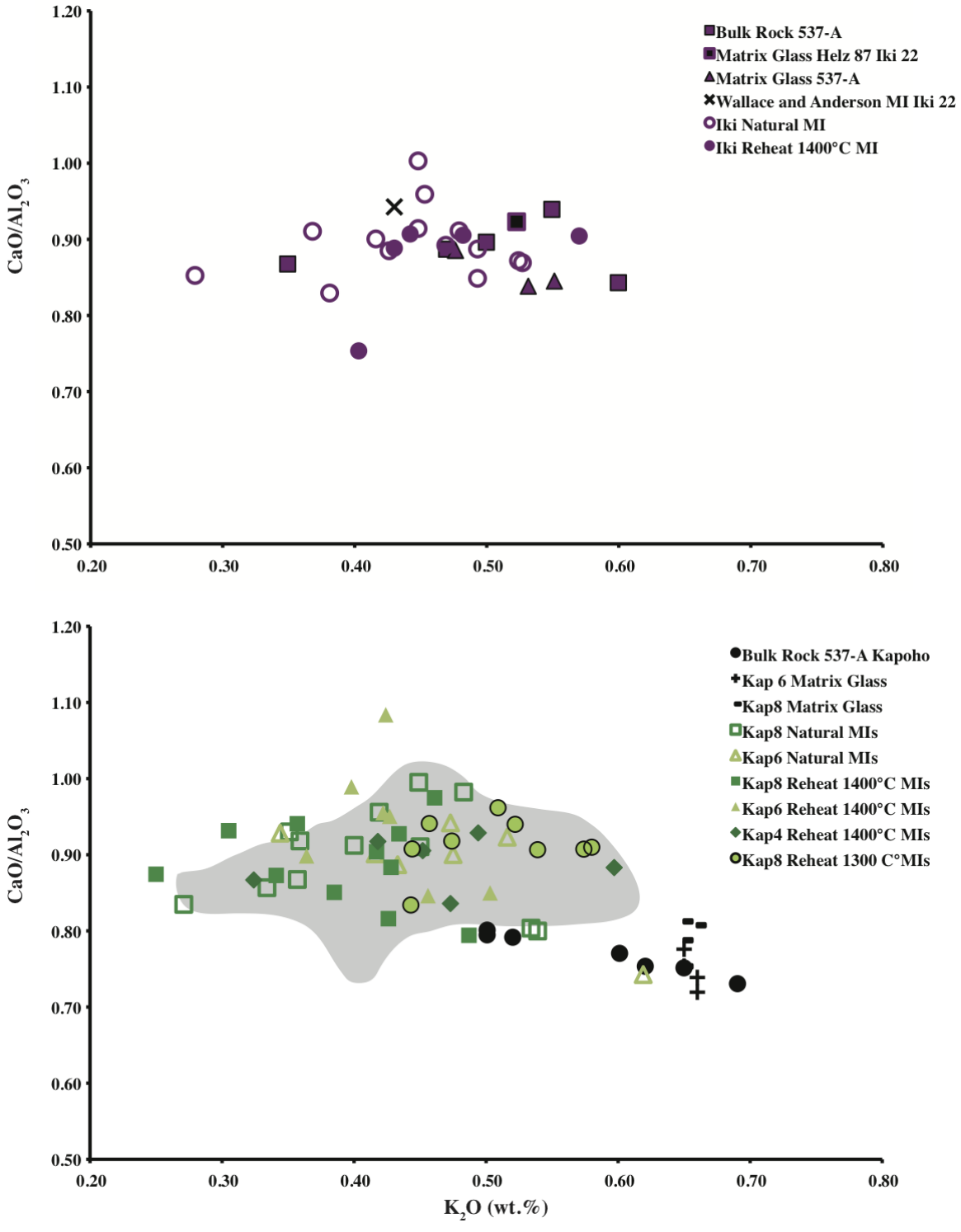
Bulk Rock 537-A
Matrix Glass Helz 87 Iki 22
Matrix Glass 537-A
Wallace and Anderson MI Iki 22
Iki Natural MI
Iki Reheat 1400°C MI
Bulk Rock 537-A Kapoho
Kap 6 Matrix Glass
Kap8 Matrix Glass
Kap8 Natural MIs
Kap6 Natural MIs
Kap8 Reheat 1400°C MIs
Kap6 Reheat 1400°C MIs
Kap4 Reheat 1400°C MIs
Kap8 Reheat 1300 C°MIs
CaO/Al2O3
K2O (wt.%)
1.20
1.10
1.00
0.90
0.80
0.70
0.60
0.50
0.20
0.30
0.40
0.50
0.60
0.70
0.80

and 1.05. Melt inclusions for this study range between 0.85 and 1.00 for the CaO/Al_2O_3 ratio, with an average of 0.90. One melt inclusion (Kil-Iki-R-1400-14) lies outside of this range, at 0.75, but appears to be more differentiated than the other melt inclusions given its lower MgO (9.9 wt. % MgO compared to the suite average of 10.7 wt. % MgO). When the CaO/Al_2O_3 ratio is plotted with another incompatible element like K_2O, it provides additional information about the interpretations used above to determine the origin of the erupted olivine (Figure 12a). By examining this plot, the same conclusions may be drawn that Kīlauea Iki olivines and their melt inclusions are related to the host S-1 magma. However, when Kapoho melt inclusions are plotted with their matrix glass and bulk rock compositions and compared to the Kīlauea Iki range (Figure 12b), the Kapoho melt inclusions are similar to Kīlauea Iki but not to their host magma. In some instances the CaO/Al_2O_3 ratios suggest the Kapoho melt inclusion compositions overlap with the Kīlauea Iki S-1 CaO/Al_2O_3 ratios, suggesting they came from the same host magma. The average MgO content for all Kapoho melt inclusions, naturally quenched and reheated, is 12.3 wt. % MgO, with an average CaO/Al_2O_3 ratio of 0.90. The average MgO for high-pressure olivine suite Kap8, is 12.8 wt. % with an average CaO/Al_2O_3 ratio of 0.90. Kapoho host matrix glass and bulk rock CaO/Al_2O_3 ratios plot between 0.75-0.85.

Based on these observations, I propose the following interpretations. It is known that Kīlauea Iki S-1 magmas were erupted late in the Kapoho eruption (Helz, 1987), following the collapse of the summit reservoir. In my work I have found a population of olivine with higher Fo content that has been found in previous studies of Kīlauea Iki or Kapoho. The olivine-hosted melt inclusions that I documented in Kapoho sample Kap8 appear to be the primitive missing piece of the S-1 component from the Kīlauea Iki

eruption. Previous studies of Kīlauea Iki found Fo86-87 olivine on average, which is not Mg-rich enough to represent the first olivine phenocrysts to crystallize from a new batch of mantle-derived magma. The melt inclusions showed greater incompatibility between the inclusion composition and the host. The olivine hosts are Fo88-89 compared to Kīlauea Iki's average olivine compositions of Fo86-87, and my results show that the Fo88-89 olivines in the Kap8 sample crystallized deeper than the Fo86-87 crystals from Kīlauea Iki S-1 magma. This is a possible indication that the most primitive Kīlauea Iki S-1 magmas were intruded into the east rift zone at a greater depth, while the rest of the S-1 magma continued to ascend and fractionate olivine and eventually intercepted stored S-2 magma northeast of the main summit reservoir. This would potentially explain why the most primitive materials erupted at Kīlauea Iki have only Fo86-87 olivine.

Interpretation of Kīlauea's Magma Plumbing System

Combining the estimated olivine crystallization pressures from reheated melt inclusions with their compositional data allows for a modified interpretation of the 1959-1960 eruptions of Kīlauea A schematic interpretation of the 1959-1960 eruption is available in Appendix F, Figures F1-F5. On August 14, 1959, deep seismicity was detected below Kīlauea's summit, at approximately 45-60 km depth. This has been interpreted as the arrival of magma into the main conduit that would eventually be erupted at Kīlauea Iki. Over the course of the three months preceding the eruption, the summit region inflated, eventually resulting in the eruption of Kīlauea Iki beginning on November 14, 1959. Eruptive fissures opened just outside of Kīlauea's main summit caldera, and it would be later interpreted that Kīlauea Iki magma had bypassed the main

summit conduit, in favor of a less used pathway, intercepting some stored magma. The strong buoyancy of the new magma, caused by the exsolution of CO_2 and formation of bubbles, propelled it through the stored magma, entraining and mixing with stored magma and accumulated olivine as it ascended (Helz, 1987). The new magma (S-1) magma was distinctive because of its higher MgO contents and CaO/Al_2O_3 ratios, which are also seen in melt inclusion compositions (Richter et al., 1966; Helz et al., 1987, Wallace and Anderson, 1998). Reheated melt inclusions from the Kīlauea Iki S-1 magma type show that olivine crystallization occurred between 2-3 km, and this is consistent with previous work on restored CO_2 in Kīlauea Iki S-1 melt inclusions by Anderson and Brown (1993), which suggested melt inclusions in Iki-22 olivine were trapped at less than 1 kbar pressure, corresponding to the same range as the melt inclusions in this study. The structure of Kīlauea Iki crater caused much of the erupted lava to drain back into the eruptive fissures and be recycled throughout the course of the eruption. By the end of the eruption, the summit region was more inflated than it had been prior to the eruption, and this over pressurization of the summit would be relieved by the subsequent rift eruption of Kapoho on the volcano's lower East Rift Zone.

The Kapoho eruption started on January 13, 1960, in the lower East Rift Zone, almost 50 km away from Kīlauea's summit. Early Kapoho lavas were differentiated, because arriving summit magmas mixed with stored rift zone magma. Like the Kīlauea Iki eruption, lava fountains at Kapoho reached spectacular heights, with some >400 m. Kīlauea's summit began to signal its collapse starting on January 17, 1960, continuing into March. Lava temperatures increased over a period of 10 days at the Kapoho vent site, which was considered to be the arrival of hotter summit magmas, following the flushing

of stored rift magmas. On February 19, 1960, the eruption was over, leaving behind a tall cone, which became known as Pu'u Laimana.

The Kapoho eruption products have been interpreted as the result of magma mixing. Stored rift magmas mixed with summit magmas, including the unusual Kīlauea Iki S-1 (Wright and Helz, 1996). However, the crystallization pressures of reheated melt inclusions from olivine erupted in tephra late in the Kapoho eruption suggest something about Kīlauea Iki S-1 magma that has not been previously recognized. The most primitive Kīlauea Iki S-1 magma may have been diverted away from the main summit system and into the East Rift Zone earlier than the rest of the S-1 magma, and at a greater depth than the typical 2-3 km suggested by seismicity. The diversion could have occurred due to the over inflation of Kīlauea's summit system, where simply no additional magma could fit, and it was redirected toward the path of least resistance, the deep rift. The stress field of Kīlauea's east rift zone is quite complex due to movement of Kīlauea's south flank seaward (Swanson, 1976). The seaward migration of the east rift zone (newer vents generally appear seaward of older features) and the curved nature of the upper east rift zone is evidence of this. Perhaps magma is occasionally diverted into the 6-8 km deep part of the rift zone, allowing for the formation of hypothesized cumulate bodies (Clague and Denlinger, 1994). The alternative interpretation is that the most primitive olivine from Kapoho formed deeper in the summit region, perhaps when the parent S-1 magma initially stalled, and that this olivine was later reentrained and carried down the rift with the remaining magma from the Kīlauea Iki eruption. However, it seems unlikely that Kīlauea Iki would have erupted olivine no more Mg-rich than Fo86-87 olivine if the most primitive S-1 component was present in a vertically integrated conduit and reservoir

system beneath Kīlauea Iki crater. Instead I favor the first interpretation where the most primitive S-1 material was intruded laterally into the deep rift, where it was stored and later forced down a deeper part of the rift to become part of the complex, mixed magmas involved in the Kapoho eruption.

Olivine erupted from Kap8, Kap6, and Kap4 did not belong on the same liquid line of descent as their matrix glass and bulk rock, suggesting that they were cumulate material that was was reentrained and flushed out of the rift over the course of the eruption. The melt inclusion compositions in the suites of Kapoho samples in this study suggest that they formed from the Kīlauea Iki S-1 magma type. Kapoho olivine hosts from this study are more primitive, Fo88-89, compared to Kīlauea Iki's Fo86-87 olivines, and many olivine from the most primitive Fo89 population crystallized at greater depths (up to 6 km) than Kīlauea Iki's 2-3 km. Kapoho melt inclusions, specifically the Fo89 population, have higher MgO than Kīlauea Iki, with an average of 14.2 wt.% MgO compared to Kīlauea Iki's 11.5 wt.% MgO. They are simply more primitive, higher-pressure olivine and their presence in Kapoho lavas cannot be explained by previous interpretations of the eruption. Lava fountains erupted during the Kapoho eruption may not have been as high as those at Kīlauea Iki (record of 580 m), but they were tall for a rift zone eruption so distant from the summit. Using the 1955 eruption for comparison, in which early vents opened very close to Kapoho's eruption site on the lower East Rift Zone, the average lava fountain height was between 15-30 m. The occasional 100-425 m tall fountains of Kapoho were tall in comparison. Kīlauea Iki S-1 magma had higher volatile contents, particularly H_2O and CO_2, and if this was a causative factor in the tall fountain heights observed during the Iki eruption, than this would help to explain the high

fountains of the Kapoho eruption as well because S-1 magma was also present, but with a complex mixture of other components. Work by Sides et al. (2013) suggests that the contrast in temperatures between stored rift zone magmas and mixing juvenile summit magmas was likely responsible for the high fountains at Kīlauea Iki and Kapoho. Sides et al. (2013) explain that rapid cooling drove exsolution of gases followed by bubble vesiculation. This great degree of bubble vesiculation and bursting at the surface was enough to trigger the high lava fountains observed during these eruptions.

CHAPTER VI

SUMMARY

Melt inclusions can be a useful tool when their limitations are understood and accounted for. Shrinkage bubbles, which form in melt inclusions during post-entrapment cooling and crystallization, can contain a significant amount of low solubility volatiles like CO_2. If melt inclusion glasses are analyzed without accounting for the CO_2 trapped in the bubble, the amount of dissolved CO_2 at the time of melt inclusion entrapment can be greatly underestimated. Calculations for vapor saturation pressure and host crystallization depth of bubble-bearing inclusions would be difficult to interpret without the ability to restore the true CO_2 in the inclusion. CO_2 in melt inclusions can be restored by overheating melt inclusions above their trapping temperature, allowing the CO_2 to dissolve back into the glass, where it can then be analyzed by FTIR or ion microprobe. Olivine dissolution that occurs during the overheating can be corrected for by knowing the range in composition for a given suite of naturally quenched melt inclusions, and by using Petrolog3.1 to restore the inclusion composition to values appropriate for equilibrium with the olivine host. The dissolved CO_2 in the inclusion at the time of trapping can then be determined, yielding a true CO_2 content for the melt inclusion. Overheating melt inclusions in a 1-atm furnace can result in hydrogen diffusive loss, but this does not impact the ability to use melt inclusions for estimating vapor saturation pressures and crystallization depths for H_2O poor magmas like those studied here because CO_2 dominates those calculations. Surprisingly, some naturally quenched inclusions from

Kīlauea also appear to show effects of hydrogen diffusive loss, which may be attributed to storage of the olivine hosts at elevated temperatures following crystallization.

Reheated melt inclusions from Kapoho suggest that olivine crystallization occurred at depths greater than the 2-3 km values that are typical for summit and rift eruptions of Kīlauea. The most primitive population of olivine at Kapoho crystallized between 3 and 6 km depth. Some olivine erupted by Kapoho may be the primitive missing piece of Kīlauea Iki S-1 magma that was not erupted at Kīlauea Iki and was instead intruded into a deeper part of the East Rift Zone.

Reheated melt inclusions from the first phase of the 1959 Kīlauea Iki eruption had primitive and olivine phyric/picrite compositions suggest that olivine crystallized at shallow depths. Olivine-hosts were not accumulated but belong along the same liquid line of descent as their host magma. Primitive magmas do not frequently bypass the main summit system, and the only historical example seems to be the Kīlauea Iki eruption. Diversion of primitive magma into deeper parts of the rift zone may help to explain how cumulate bodies form in the deep rift at 6-8 km depth. Finally, without detailed sampling of the stratrigraphy of the Kapoho eruption, this primitive population of olivine at Kapoho may not have been identified, thus emphasizing the importance of detailed fieldwork in geochemical studies of Hawaiian volcanoes.

APPENDIX A

SAMPLE DESCRIPTIONS AND FIELD COLLECTION SITES

Table A1. Kīlauea sample locations with tephra descriptions.

Kīlauea IkI	KIL_IKI	63286E	47503N	Kīlauea Iki Vent	Glassy, juvenile tephra. Collection from early, middle, and late deposit Corresponds to S-1 magma component.
1840 Littoral Cone	LITCONE S	303560E	2163067N	Lava flow	Picritic basalt from lower 1840 vents, littoral cone deposit
	LITCONE N	303488E	2163148N	Lava flow	Picritic basalt from lower 1840 vents, littoral cone deposit
Mauna Ulu	MAUNA ULU	67987E	40920N	Phase 9 Fall	Layer 1: golden pumice, Layer 2: coarse lapilli, Layer 3: medium to coarse lapilli
1960 Kapoho	Kap_SUM	306098E	2158265N	Cone	Glassy fine to medium lapilli- youngest cone complex from summit
	Kap_2	306090E	2158347N	Cone	Glassy medium to coarse lapilli with mixed spatter clasts, locally highest
	Kap_3	306104E	2158557N	Cone	Lowest glassy tephra deposited on outer flank of an early spatter rampart
	Kap_4	306104E	2158557N	Cone	Mantles spatter rampart- from earliest cone phase
	Kap_5	306307E	2158771N	Vent E	Lowest glassy tephra, well oxidized, mixed with spatter clasts
	Kap_6	306272E	2158745N	Vent E	Thin layer, highest glassy tephra, on top of a'a flow, topped by spatter
	Kap_7	307059E	2159278N	Chaotic Rafted Terrain	Fine lapilli, tephra sliding off inflated a'a flows, chaotic rafted terrain, no thicker than 7 cm
	Kap_8	306167E	2157988N	Tephra Plain	Youngest glassy tephra, 30-40 cm thick, .5-.7 cm fine lapilli, on top of transitional flow
1955 Vents	K55_1	294181E	2149889N	Vent W/Z	Fine to medium lapilli with spatter clasts, tops spatter unit, blue-grey to red-purple in color
	K55_2	294081E	2149778N	Vent Y	Flank deposit, fine to coarse grained lapilli with spatter clasts, layer of dense vegetation above, dark black
	K55_3	294489E	2150157N	Vent T	Medium to coarse lapilli, glassy, metallic black, capped by 1 m thick lava flow, 7-8 m thick unit of tephra
	K55_4	303055E	2155777N	Vent M	Glassy, metallic black tephra, medium to coarse lapilli, possible scree deposit, but difficult to tell with dense vegetation
	K55_5	303591E	2156161N	Vent E	Medium to coarse lapilli, metallic black, glassy, probably at center of fissure system with higher rampart walls to to SW and NE approximately 20 m tall.
	K55_6	297640E	2151279N	Vent S	Medium to coarse lapilli, oxidized capped by a thin non-oxidized layer

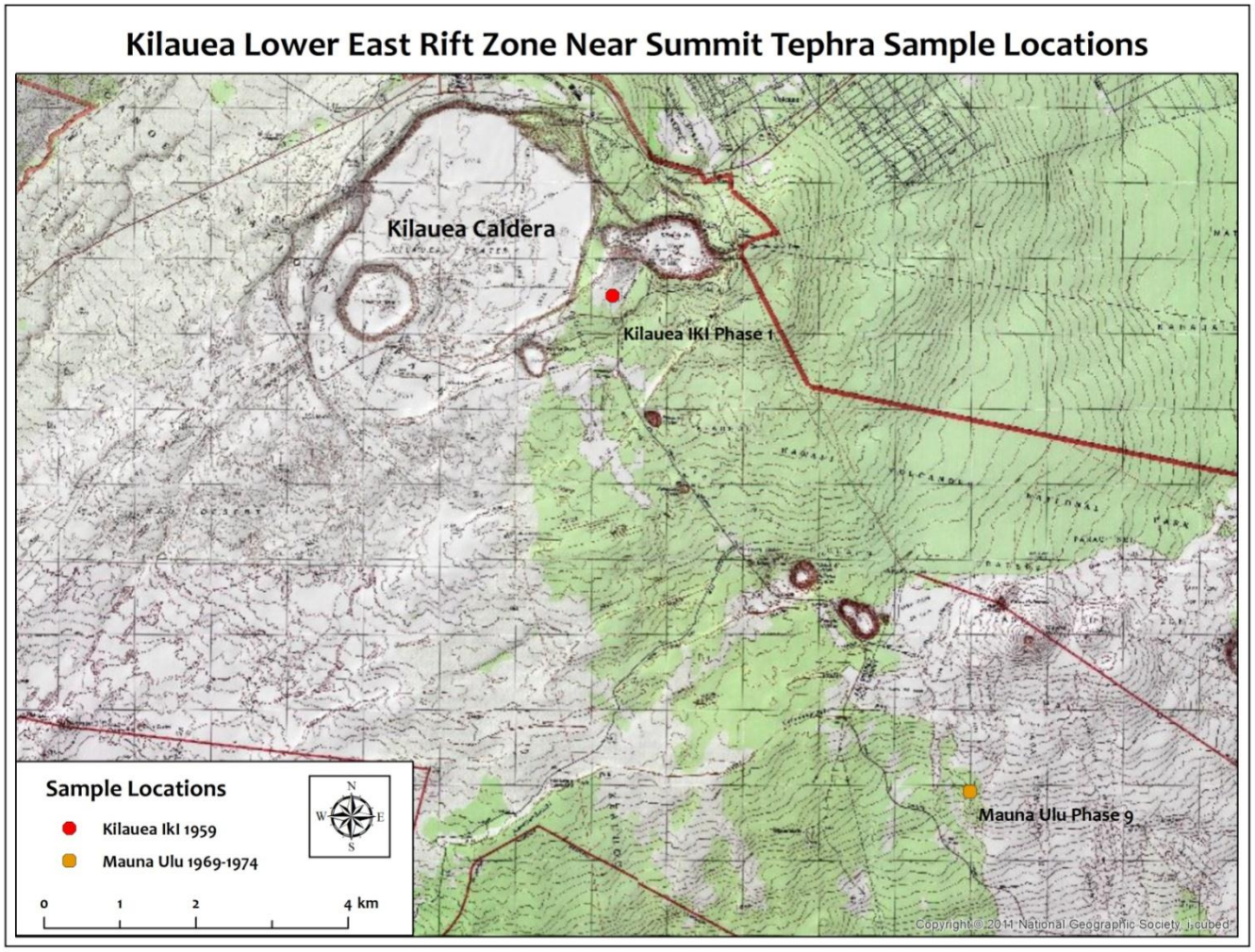

Figure A1. Near Kīlauea Summit Sample Location Sites. Sample locations for Kīlauea Iki S-1 tephra and Mauna Ulu Phase 9 tephra and golden pumice.

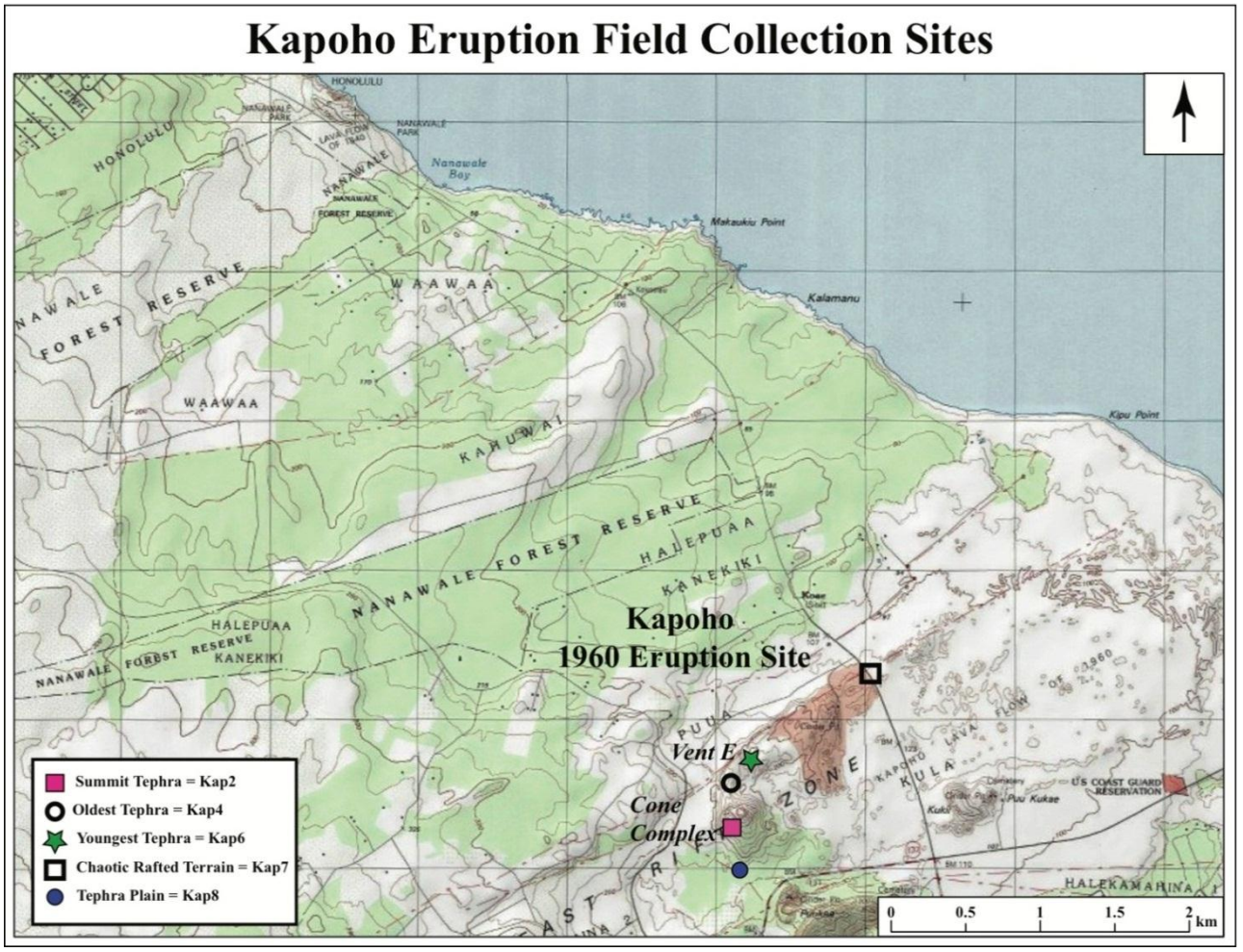

Figure A2. Sample locations on Kīlauea's lower East Rift Zone, 50 km from Kīlauea's summit. The 1960 eruption focused itself into several point sources, which developed into cones. Several samples were taken from the exposed stratigraphy of the Cone Complex and Vent E, as well as tephra samples from the "tephra plain" and "chaotic rafted terrain" described by Hazlett (1993).

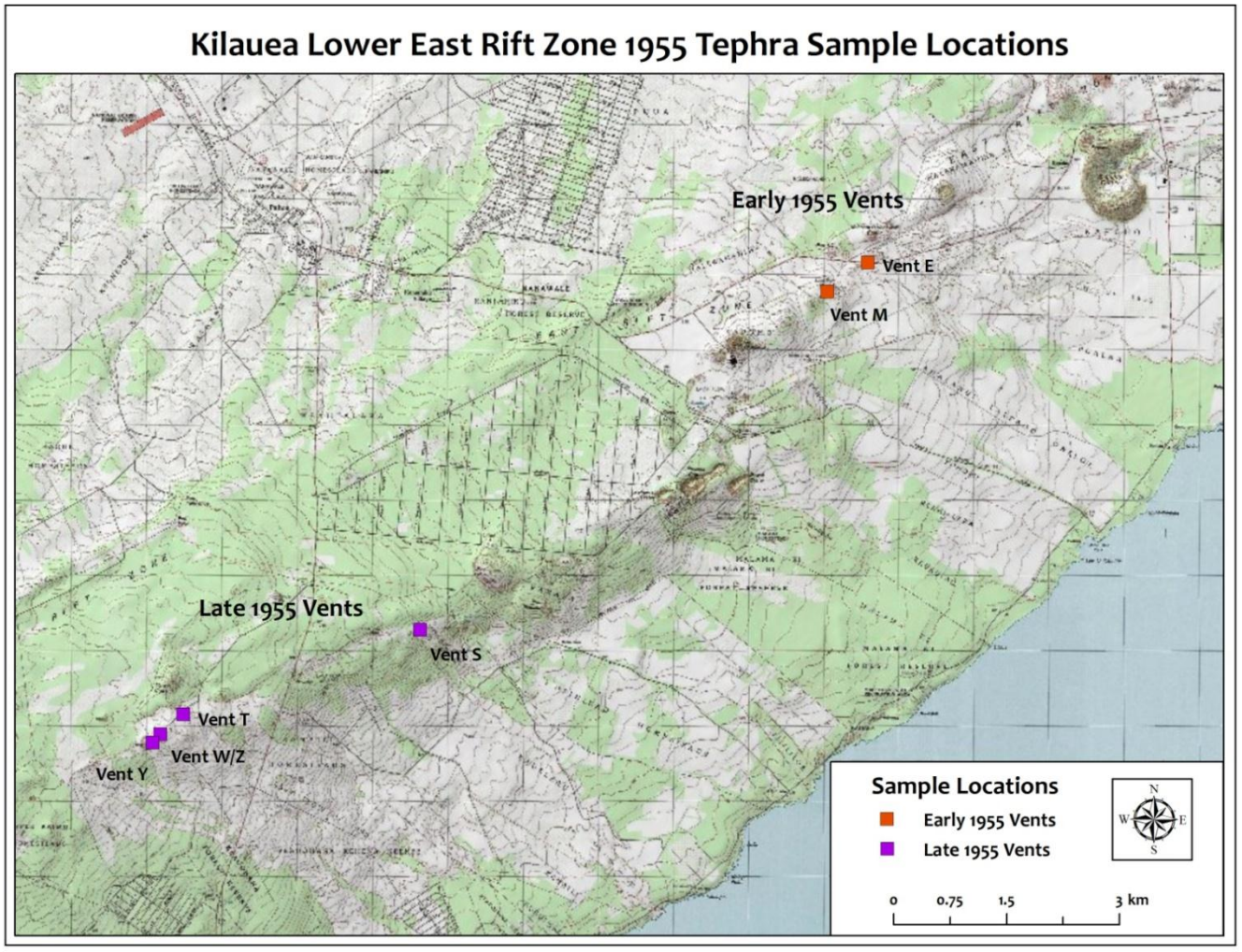

Figure A3. East Puna Lower East Rift Zone Collection Sites. 1955 early eruptive vents are located further down rift than late eruptive vents, which opened after a pause in the eruption lasting approximately two weeks.

APPENDIX B

KAPOHO ERUPTIVE SITE RELATIVE STRATIGRAPHY

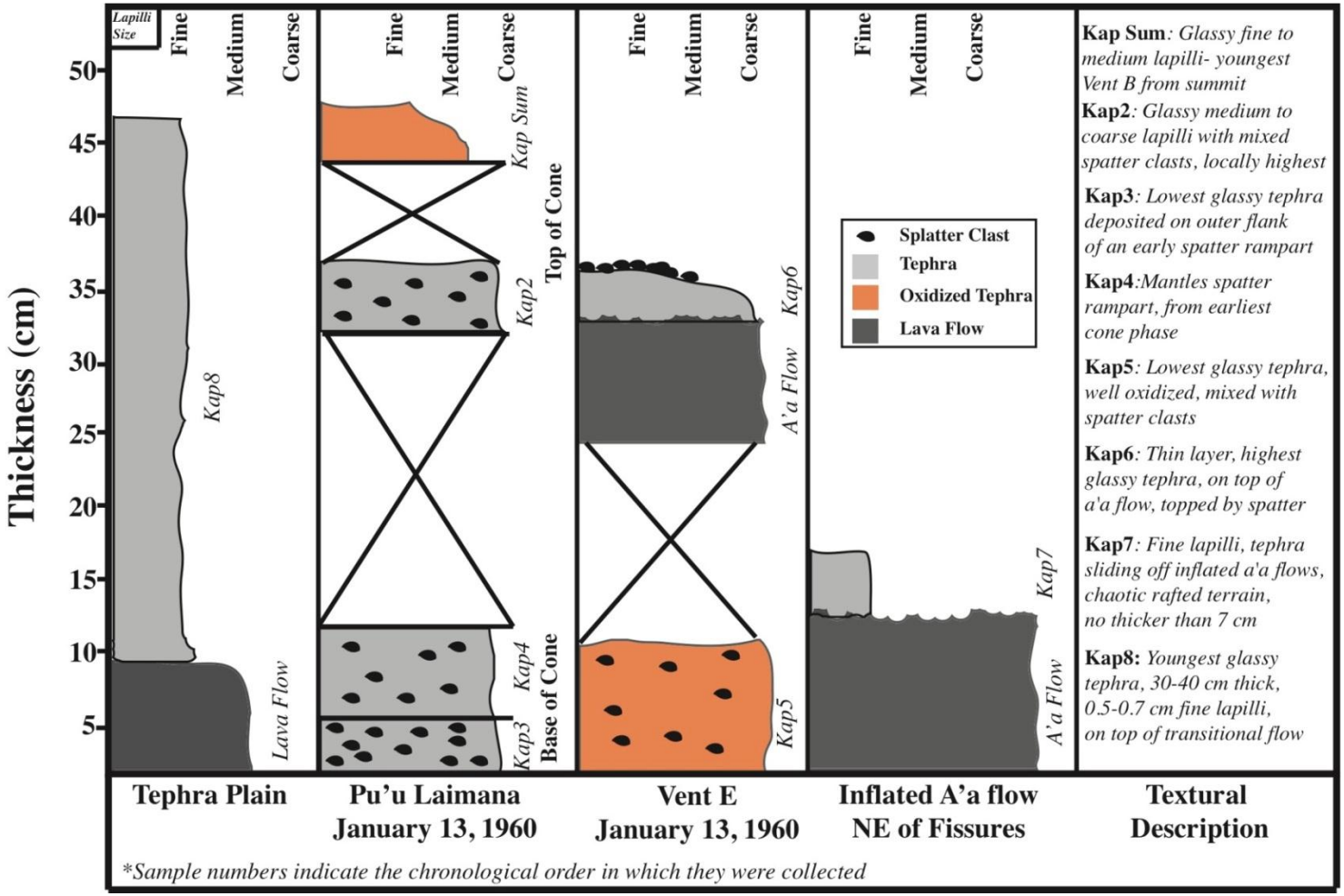

Figure B1. Kapoho tephra relative stratigraphy. The Kapoho eruption involved a series of en-echelon fissures. Some of these fissures developed into point sources, and over the course of the eruption developed a large cone complex (Pu'u Laimana). The tephra plain was downwind of the cone complex, and was deposited by high lava fountaining at the cone complex. Vent E and the inflated a'a flows were down rift of Pu'u Laimana. The inflated flows involved rafted pieces of breached cones, and were also covered with tephra. All samples collected were fine grained to coarse, glassy lapilli. Some samples have coarse spatter clasts. Some units were collected but too oxidized to actually be use (Kap Sum and Kap5).

APPENDIX C

MELT INCLUSION AND TEPHRA GLASS

MAJOR ELEMENT COMPOSITIONS

Table C1. Major Element Composition for Kīlauea Iki Melt Inclusions

	Suite: Kīlauea Iki				
	Naturally Quenched/Reheated	**Naturally Quenched**	**Naturally Quenched**	**Naturally Quenched**	**Naturally Quenched**
	Temperature (C)	**n/a**	**n/a**	**n/a**	**n/a**
	Inclusion Name	**KIL-IKI-NAT-1**	**KIL-IKI-NAT-2**	**KIL-IKI-NAT-3A**	**KIL-IKI-NAT-3B**
Raw	**SiO2**	50.43	51.15	50.63	51.45
	TiO2	2.39	2.06	2.52	2.69
	Al2O3	13.62	14.12	13.18	13.82
	FeO^T	10.02	8.43	9.71	8.17
	MnO	0.00	0.00	0.00	0.00
	MgO	7.14	6.61	7.18	7.13
	CaO	12.06	11.71	12.00	12.02
	Na2O	2.35	2.69	2.37	2.59
	K2O	0.47	0.43	0.43	0.64
	P2O5	0.28	0.28	0.28	0.37
	FeO	8.52	7.17	8.25	6.95
	Fe2O3	1.67	1.41	1.62	1.36
	$Fe2O3^T$	11.14	9.37	10.79	9.08
	Inclusion Name	**KIL-IKI-NAT-1**	**KIL-IKI-NAT-2**	**KIL-IKI-NAT-3A**	**KIL-IKI-NAT-3B**
Corrected	**SiO2**	49.70	50.31	49.56	49.47
	TiO2	2.16	1.81	2.17	2.23
	Al2O3	12.31	12.41	11.35	11.47
	Fe2O3	1.32	1.32	1.35	1.36
	FeO	10.01	10.02	10.00	9.99
	MnO	0.00	0.00	0.00	0.00
	MgO	10.80	10.85	12.59	12.54
	CaO	10.89	10.30	10.34	9.97
	Na2O	2.12	2.36	2.04	2.15
	K2O	0.43	0.38	0.37	0.53
	P2O5	0.26	0.25	0.24	0.31
	Cr2O3	0.00	0.00	0.00	0.00
	Temp Calc. Petrolog	1270	1275	1310	1313
	FO_Host	86.1	86.0	87.9	87.9
	FEO*	11.21	11.21	11.21	11.21
	FEO_Final	11.20	11.20	11.20	11.20
	Olivine Percent	-11.55	-15.44	-17.41	-20.33
	Correction Coefficient	0.89	0.86	0.85	0.82

Table C1. (continued).

	Suite: Kīlauea Iki				
	Naturally Quenched/Reheated	**Naturally Quenched**	**Naturally Quenched**	**Naturally Quenched**	**Naturally Quenched**
	Temperature (C)	**n/a**	**n/a**	**n/a**	**n/a**
	Inclusion Name	**KIL-IKI-NAT-6**	**KIL-IKI-NAT-8**	**KIL-IKI-NAT-9**	**KIL-IKI-NAT-10A**
Raw	**SiO2**	50.60	50.30	51.75	50.48
	TiO2	2.53	2.57	2.12	2.74
	Al2O3	13.97	13.64	12.59	13.85
	FeO^T	8.98	9.75	10.25	9.79
	MnO	0.00	0.00	0.15	0.14
	MgO	7.12	6.94	7.19	7.50
	CaO	12.58	11.63	12.63	12.28
	Na2O	2.16	2.38	2.52	2.34
	K2O	0.48	0.32	0.50	0.57
	P2O5	0.27	0.30	0.32	0.31
	FeO	7.63	8.29	8.71	8.32
	Fe2O3	1.50	1.63	1.71	1.63
	$Fe2O3^T$	9.98	10.84	11.39	10.88
	Inclusion Name	**KIL-IKI-NAT-6**	**KIL-IKI-NAT-8**	**KIL-IKI-NAT-9**	**KIL-IKI-NAT-10A**
Corrected	**SiO2**	49.31	49.45	50.45	48.87
	TiO2	2.19	2.21	1.91	2.37
	Al2O3	12.08	11.74	11.37	11.98
	Fe2O3	1.30	1.31	1.40	1.33
	FeO	10.03	10.03	9.94	10.01
	MnO	0.00	0.00	0.14	0.12
	MgO	11.68	12.68	10.38	11.91
	CaO	10.88	10.01	11.40	10.63
	Na2O	1.87	2.05	2.28	2.02
	K2O	0.42	0.28	0.45	0.49
	P2O5	0.24	0.25	0.29	0.27
	Cr2O3	0.00	0.00	0.00	0.00
	Temp Calc. Petrolog	1287	1311	1260	1295
	FO_Host	87.0	87.9	85.6	87.4
	FEO*	11.20	11.21	11.20	11.21
	FEO_Final	11.20	11.20	11.20	11.20
	Olivine Percent	-16.10	-18.09	-10.24	-14.77
	Correction Coefficient	0.85	0.84	0.90	0.87

Table C1. (continued).

	Suite: Kīlauea Iki				
	Naturally Quenched/ Reheated	**Naturally Quenched**	**Naturally Quenched**	**Naturally Quenched**	**Naturally Quenched**
	Temperature (C)	**n/a**	**n/a**	**n/a**	**n/a**
	Inclusion Name	**KIL-IKI-NAT-10B**	**Kil-IKI-NAT-11A**	**KIL-IKI-NAT-11B**	**Kil-IKI-NAT-11C**
Raw	**SiO2**	50.71	50.73	50.15	50.15
	TiO2	2.81	2.79	2.83	2.83
	Al2O3	13.91	13.77	13.61	13.61
	FeO^T	9.66	10.17	11.20	11.20
	MnO	0.15	0.16	0.17	0.17
	MgO	7.11	6.72	6.92	6.92
	CaO	12.41	12.55	11.87	11.87
	Na2O	2.36	2.25	2.38	2.38
	K2O	0.55	0.55	0.58	0.58
	P2O5	0.33	0.30	0.30	0.30
	FeO	8.21	8.65	9.52	9.52
	Fe2O3	1.61	1.70	1.87	1.87
	$Fe2O3^T$	10.74	11.31	12.45	12.45
	Inclusion Name	**KIL-IKI-NAT-10B**	**Kil-IKI-NAT-11A**	**KIL-IKI-NAT-11B**	**Kil-IKI-NAT-11C**
Corrected	**SiO2**	48.93	49.23	49.12	49.12
	TiO2	2.40	2.44	2.54	2.54
	Al2O3	11.88	12.04	12.22	12.22
	Fe2O3	1.33	1.33	1.34	1.34
	FeO	10.01	10.01	10.00	10.00
	MnO	0.13	0.14	0.15	0.15
	MgO	11.97	11.13	11.06	11.06
	CaO	10.60	10.97	10.66	10.66
	Na2O	2.01	1.97	2.13	2.13
	K2O	0.47	0.48	0.52	0.52
	P2O5	0.28	0.26	0.27	0.27
	Cr2O3	0.00	0.00	0.00	0.00
	Temp Calc. Petrolog	1296	1275	1277	1277
	FO_Host	87.4	86.5	86.5	86.5
	FEO*	11.21	11.21	11.20	11.20
	FEO_Final	11.20	11.20	11.20	11.20
	Olivine Percent	-16.30	-13.89	-11.32	-11.32
	Correction Coefficient	0.86	0.88	0.90	0.90

Table C1. (continued).

	Suite: Kīlauea Iki			
	Naturally Quenched/Reheated	**Naturally Quenched**	**Naturally Quenched**	**Naturally Quenched**
	Temperature (C)	**n/a**	**n/a**	**n/a**
	Inclusion Name	**KIL-IKI-NAT-13**	**KIL-IKI-NAT-14B**	**KIL-IKI-NAT-15**
Raw	**SiO2**	50.64	51.11	51.57
	TiO2	2.44	2.87	2.50
	Al2O3	12.89	14.01	13.57
	FeO^T	11.35	9.33	9.27
	MnO	0.18	0.14	0.13
	MgO	7.26	7.42	7.35
	CaO	12.36	11.89	12.41
	Na2O	2.11	2.32	2.35
	K2O	0.48	0.58	0.52
	P2O5	0.28	0.32	0.32
	FeO	9.65	7.93	7.88
	Fe2O3	1.89	1.56	1.55
	$Fe2O3^T$	12.62	10.37	10.31
	Inclusion Name	**KIL-IKI-NAT-13**	**KIL-IKI-NAT-14B**	**KIL-IKI-NAT-15**
Corrected	**SiO2**	49.94	49.16	49.63
	TiO2	2.28	2.43	2.14
	Al2O3	12.04	11.88	11.63
	Fe2O3	1.36	1.31	1.34
	FeO	10.00	10.03	10.00
	MnO	0.17	0.12	0.11
	MgO	10.00	12.26	11.77
	CaO	11.55	10.08	10.63
	Na2O	1.97	1.97	2.02
	K2O	0.45	0.49	0.45
	P2O5	0.26	0.27	0.28
	Cr2O3	0.00	0.00	0.00
	Temp Calc. Petrolog	1245.00	1303.00	1291.00
	FO_Host	85.01	87.60	87.11
	FEO*	11.21	11.21	11.20
	FEO_Final	11	11	11
	Olivine Percent	-7.1	-17.0	-15.7
	Correction Coefficient	0.94	0.85	0.86

Table C1. (continued)

	Suite: Kīlauea Iki			
	Naturally Quenched/Reheated	**Reheated**	**Reheated**	**Reheated**
	Temperature (C)	**1400**	**1400**	**1400**
	Inclusion Name	**KIL-IKI-R-2**	**KIL-IKI-R-6**	**KIL-IKI-R-8**
Raw	**SiO2**	46.14	44.80	45.10
	TiO2	1.78	1.77	1.90
	Al2O3	8.93	8.86	9.40
	FeO^T	11.92	13.01	12.56
	MnO	0.00	0.00	0.00
	MgO	20.10	19.31	18.90
	CaO	8.10	8.02	8.50
	Na2O	1.49	1.40	1.49
	K2O	0.33	0.35	0.43
	P2O5	0.20	0.20	0.23
	FeO	10.13	11.06	10.68
	Fe2O3	1.99	2.17	2.09
	$Fe2O3^T$	13.25	14.46	13.96
	Inclusion Name	**KIL-IKI-R-2**	**KIL-IKI-R-6**	**KIL-IKI-R-8**
Corrected	**SiO2**	48.64	48.21	47.68
	TiO2	2.37	2.45	2.52
	Al2O3	11.85	12.31	12.45
	Fe2O3	1.33	1.32	1.32
	FeO	10.00	10.01	10.01
	MnO	0.00	0.00	0.00
	MgO	12.38	11.86	11.93
	CaO	10.75	11.14	11.26
	Na2O	1.97	1.94	1.97
	K2O	0.44	0.48	0.57
	P2O5	0.26	0.27	0.30
	Cr2O3	0.00	0.00	0.00
	Temp Calc. Petrolog	1305.00	1293.00	1295.00
	FO_Host	87.90	87.50	87.70
	FEO*	11.19	11.19	11.20
	FEO_Final	11	11	11
	Olivine Percent	23.5	25.5	22.7
	Correction Coefficient	1.32	1.36	1.31

Table C1. (continued).

	Suite: Kīlauea Iki		
	Naturally Quenched/Reheated	**Reheated**	**Reheated**
	Temperature (C)	**1400**	**1400**
	Inclusion Name	**KIL-IKI-R-14A**	**KIL-IKI-R-15**
Raw	**SiO2**	46.76	45.58
	TiO2	1.62	1.51
	Al2O3	10.16	8.84
	FeO^T	10.52	14.98
	MnO	0.00	0.00
	MgO	19.60	17.60
	CaO	7.66	7.86
	Na2O	1.79	1.56
	K2O	0.31	0.29
	P2O5	0.19	0.27
	FeO	8.94	12.73
	Fe2O3	1.75	2.50
	$Fe2O3^T$	11.69	16.65
	Inclusion Name	**KIL-IKI-R-14A**	**KIL-IKI-R-15**
Corrected	**SiO2**	49.19	49.80
	TiO2	2.12	2.21
	Al2O3	13.26	12.93
	Fe2O3	1.27	1.36
	FeO	10.05	9.97
	MnO	0.00	0.00
	MgO	11.13	9.14
	CaO	9.99	11.49
	Na2O	2.33	2.28
	K2O	0.40	0.43
	P2O5	0.25	0.39
	Cr2O3	0.00	0.00
	Temp Calc. Petrolog	1282.00	1227.00
	FO_Host	86.50	83.90
	FEO*	11.19	11.19
	FEO_Final	11	11
	Olivine Percent	22.5	29.4
	Correction Coefficient	1.29	1.44

Table C2. Major Element Compositions for Kapoho Melt Inclusions

	Suite: Kapoho				
	Naturally Quenched /Reheated	**Naturally Quenched**	**Naturally Quenched**	**Naturally Quenched**	**Naturally Quenched**
	Temperature (C)	**n/a**	**n/a**	**n/a**	**n/a**
	Inclusion Name	**K99-9-16**	**K99-9-17**	**KAP8-NAT-8A**	**KAP8-NAT-8B**
Raw	**SiO2**	49.41	50.67	50.27	50.20
	TiO2	2.99	2.54	2.40	2.24
	Al2O3	13.63	14.37	12.08	12.17
	FeO^T	8.51	8.24	10.54	10.70
	MnO	0.13	0.12	0.13	0.14
	MgO	7.16	6.92	10.56	10.71
	CaO	13.39	12.47	11.54	11.36
	Na2O	2.29	0.00	1.96	1.99
	K2O	0.57	0.42	0.45	0.42
	P2O5	0.31	0.26	0.31	0.31
	FeO	7.23	7.01	8.96	9.10
	Fe2O3	1.42	1.37	1.76	1.78
	$Fe2O3^T$	9.45	9.16	11.71	11.90
	Inclusion Name	**K99-9-16**	**K99-9-17**	**KAP8-NAT-8A**	**KAP8-NAT-8B**
Corrected	**SiO2**	50.048	48.157	49.411	49.425
	TiO2	2.148	2.534	2.247	2.115
	Al2O3	12.16	11.539	11.33	11.491
	Fe2O3	1.092	1.362	1.34	1.334
	FeO	10.221	9.978	9.996	10.004
	MnO	0.1	0.108	0.12	0.132
	MgO	13.104	12.303	12.178	12.204
	CaO	10.549	11.335	10.83	10.726
	Na2O	0	1.94	1.836	1.879
	K2O	0.357	0.483	0.419	0.397
	P2O5	0.22	0.262	0.295	0.293
	Cr2O3	0	0	0	0
	Temp Calc. Petrolog	1288	1302	1297	1298
	FO_Host	87.3	87.99	87.5	87.5
	FEO*	11.204	11.203	11.201	11.204
	FEO_Final	11.2	11.2	11.2	11.2
	Olivine Percent	-21.78	-18.66	-5.89	-5.29
	Correction Coefficient	0.813	0.834	0.942	0.948

Table C2. (continued).

	Suite: Kapoho				
	Naturally Quenched /Reheated	**Naturally Quenched**	**Naturally Quenched**	**Naturally Quenched**	**Naturally Quenched**
	Temperature (C)	**n/a**	**n/a**	**n/a**	**n/a**
	Inclusion Name	**KAP8-NAT-9**	**Kap8-2mm-Single-1**	**Kap8-2mm-Single-3**	**Kap8-2mm-Single-4**
Raw	**SiO2**	51.84	52.47	51.28	52.72
	TiO2	2.73	2.75	3.03	2.65
	Al2O3	13.08	15.03	14.03	14.18
	FeO^T	8.88	6.86	8.04	7.89
	MnO	0.13	0.11	0.13	0.13
	MgO	7.19	6.82	7.17	6.97
	CaO	13.02	12.55	12.80	12.15
	Na2O	2.23	2.75	2.56	2.60
	K2O	0.51	0.36	0.52	0.42
	P2O5	0.41	0.30	0.46	0.28
	FeO	7.55	5.83	6.83	6.71
	Fe2O3	1.48	1.14	1.34	1.32
	$Fe2O3^T$	9.87	7.63	8.93	8.77
	Inclusion Name	**KAP8-NAT-9**	**Kap8-1mm-Single-2**	**Kap8-2mm-Single-3**	**Kap8-2mm-Single-4**
Corrected	**SiO2**	50.14	48.955	48.367	49.606
	TiO2	2.427	2.093	2.349	2.088
	Al2O3	11.624	11.442	10.889	11.175
	Fe2O3	1.377	1.345	1.383	1.351
	FeO	9.968	9.993	9.963	9.988
	MnO	0.119	0.082	0.1	0.099
	MgO	9.987	13.947	14.273	13.515
	CaO	11.568	9.552	9.934	9.574
	Na2O	1.98	2.091	1.989	2.048
	K2O	0.449	0.271	0.4	0.334
	P2O5	0.361	0.229	0.354	0.223
	Cr2O3	0	0	0	0
	Temp Calc. Petrolog	1245	1339	1345	1330
	FO_Host	85	89.02	89.4	88.59
	FEO*	11.207	11.204	11.207	11.203
	FEO_Final	11.2	11.2	11.2	11.2
	Olivine Percent	-11.37	-28.89	-26.94	-25.05
	Correction Coefficient	0.89	0.762	0.777	0.789

Table C2. (continued).

	Suite: Kapoho				
	Naturally Quenched /Reheated	**Naturally Quenched**	**Naturally Quenched**	**Naturally Quenched**	**Naturally Quenched**
	Temperature (C)	**n/a**	**n/a**	**n/a**	**n/a**
	Inclusion Name	**Kap8-2mm-Single-12**	**Kap8-2mm-single-14**	**Kap8-1mm-Single-2**	**Kap8-1mm-Single-6**
Raw	**SiO2**	51.34	51.66	50.88	52.51
	TiO2	2.90	2.66	2.95	2.78
	Al2O3	14.31	13.91	13.98	14.28
	FeO^T	9.67	8.87	10.76	7.05
	MnO	0.15	0.14	0.16	0.11
	MgO	6.56	6.85	6.54	6.64
	CaO	11.50	12.67	11.18	13.28
	Na2O	2.60	2.38	2.56	2.58
	K2O	0.65	0.53	0.63	0.47
	P2O5	0.33	0.32	0.36	0.29
	FeO	8.22	7.54	9.14	5.99
	Fe2O3	1.61	1.48	1.79	1.18
	$Fe2O3^T$	10.75	9.86	11.95	7.84
	Inclusion Name	**Kap8-2mm-Single-12**	**Kap8-2mm-single-14**	**Kap8-1mm-Single-2**	**Kap8-1mm-Single-6**
Corrected	**SiO2**	49.126	49.503	49.231	48.898
	TiO2	2.382	2.248	2.516	2.09
	Al2O3	11.754	11.736	11.904	10.72
	Fe2O3	1.328	1.337	1.321	1.397
	FeO	10.009	10.006	10.018	9.947
	MnO	0.123	0.119	0.135	0.086
	MgO	12.891	11.636	12.334	14.386
	CaO	9.446	10.686	9.521	9.97
	Na2O	2.136	2.011	2.176	1.938
	K2O	0.534	0.45	0.539	0.351
	P2O5	0.271	0.268	0.303	0.217
	Cr2O3	0	0	0	0
	Temp Calc. Petrolog	1320	1288	1309	1347
	FO_Host	88.2	86.99	87.69	89.41
	FEO*	11.204	11.209	11.207	11.204
	FEO_Final	11.2	11.2	11.2	11.2
	Olivine Percent	-20.86	-17.33	-17.12	-30.73
	Correction Coefficient	0.823	0.845	0.853	0.751

Table C2. (continued).

	Suite: Kapoho				
	Naturally Quenched /Reheated	**Naturally Quenched**	**Naturally Quenched**	**Naturally Quenched**	**Naturally Quenched**
	Temperature (C)	**n/a**	**n/a**	**n/a**	**n/a**
	Inclusion Name	**Kap8-1mm-Single-16**	**KAP6-NAT-1**	**KAP6-NAT-2**	**KAP6-NAT-3**
Raw	**SiO2**	52.19	52.11	51.22	50.97
	TiO2	2.67	2.40	2.84	2.78
	Al2O3	14.21	13.74	14.49	14.06
	FeO^T	7.32	9.05	8.30	9.31
	MnO	0.11	0.14	0.12	0.13
	MgO	7.13	6.83	6.71	6.81
	CaO	13.05	12.75	13.06	12.65
	Na2O	2.49	2.30	2.39	2.40
	K2O	0.47	0.41	0.51	0.55
	P2O5	0.38	0.26	0.37	0.33
	FeO	6.22	7.69	7.05	7.91
	Fe2O3	1.22	1.51	1.38	1.55
	$Fe2O3^T$	8.13	10.06	9.22	10.34
	Inclusion Name	**Kap8-1mm-Single-16**	**KAP6-NAT-1**	**KAP6-NAT-2**	**KAP6-NAT-3**
Corrected	**SiO2**	48.919	49.963	48.765	49.252
	TiO2	2.059	2.038	2.317	2.42
	Al2O3	10.958	11.646	11.818	12.221
	Fe2O3	1.376	1.327	1.324	1.337
	FeO	9.969	10.01	10.01	10
	MnO	0.081	0.12	0.097	0.115
	MgO	14.008	11.572	12.353	10.807
	CaO	10.061	10.811	10.649	11
	Na2O	1.919	1.949	1.948	2.09
	K2O	0.359	0.344	0.416	0.475
	P2O5	0.29	0.22	0.302	0.284
	Cr2O3	0	0	0	0
	Temp Calc. Petrolog	1338	1284	1303	1269
	FO_Host	89.09	86.8	87.79	86.19
	FEO*	11.207	11.204	11.201	11.203
	FEO_Final	11.2	11.2	11.2	11.2
	Olivine Percent	-27.4	-16.88	-21.05	-14.1
	Correction Coefficient	0.772	0.849	0.817	0.87

Table C2. (continued).

	Suite: Kapoho				
	Naturally Quenched /Reheated	**Naturally Quenched**	**Naturally Quenched**	**Naturally Quenched**	**Naturally Quenched**
	Temperature (C)	**n/a**	**n/a**	**n/a**	**n/a**
	Inclusion Name	**KAP6-NAT-4**	**KAP6-NAT-5**	**KAP6-NAT-6**	**KAP6-NAT-7**
Raw	**SiO2**	51.69	50.95	50.82	51.32
	TiO2	2.68	2.47	3.07	2.38
	Al2O3	13.55	14.14	14.03	13.76
	FeO^T	9.31	12.08	8.65	10.44
	MnO	0.14	0.16	0.11	0.15
	MgO	6.76	6.24	6.85	6.72
	CaO	12.51	10.50	13.22	12.20
	Na2O	2.47	2.40	2.34	2.29
	K2O	0.59	0.64	0.58	0.46
	P2O5	0.31	0.42	0.32	0.28
	FeO	7.91	10.27	7.35	8.87
	Fe2O3	1.55	2.01	1.44	1.74
	$Fe2O3^T$	10.34	13.43	9.61	11.60
	Inclusion Name	**KAP6-NAT-4**	**KAP6-NAT-5**	**KAP6-NAT-6**	**KAP6-NAT-7**
Corrected	**SiO2**	49.868	50.751	48.523	50.606
	TiO2	2.325	2.401	2.516	2.264
	Al2O3	11.768	13.734	11.493	13.089
	Fe2O3	1.363	1.364	1.346	1.382
	FeO	9.977	10.002	9.993	9.957
	MnO	0.121	0.153	0.093	0.142
	MgO	10.788	8.041	12.556	8.075
	CaO	10.862	10.199	10.824	11.608
	Na2O	2.147	2.329	1.919	2.179
	K2O	0.516	0.619	0.473	0.433
	P2O5	0.265	0.408	0.262	0.265
	Cr2O3	0	0	0	0
	Temp Calc. Petrolog	1270	1203	1308	1196
	FO_Host	86.1	81.62	88.08	81.82
	FEO*	11.203	11.229	11.204	11.2
	FEO_Final	11.2	11.2	11.2	11.2
	Olivine Percent	-14.21	-3.27	-20.72	-4.74
	Correction Coefficient	0.87	0.973	0.82	0.953

Table C2. (continued).

	Suite: Kapoho				
	Naturally Quenched /Reheated	**Reheated**	**Reheated**	**Reheated**	**Reheated**
	Temperature (C)	**1400**	**1400**	**1400**	**1400**
	Inclusion Name	**Kap8-R-1400-15**	**Kap8-R-1400-18**	**Kap8-R-1400-20**	**Kap8-R-1400-32**
Raw	**SiO2**	47.27	46.03	45.83	47.07
	TiO2	1.79	1.72	1.57	1.88
	Al2O3	9.14	8.61	9.19	9.73
	FeO^T	9.43	11.63	13.04	9.22
	MnO	0.13	0.16	0.19	0.12
	MgO	21.27	20.14	18.29	20.13
	CaO	8.51	8.40	8.02	8.51
	Na2O	1.61	1.37	1.45	1.63
	K2O	0.26	0.35	0.26	0.21
	P2O5	0.14	0.21	0.20	0.13
	FeO	8.02	9.88	11.08	7.84
	Fe2O3	1.57	1.94	2.17	1.54
	$Fe2O3^T$	10.48	12.92	14.49	10.25
	Inclusion Name	**Kap8-R-1400-15**	**Kap8-R-1400-18**	**Kap8-R-1400-20**	**Kap8-R-1400-32**
Corrected	**SiO2**	48.314	48.633	48.804	48.357
	TiO2	2.132	2.28	2.024	2.199
	Al2O3	10.873	11.426	11.849	11.377
	Fe2O3	1.395	1.351	1.311	1.344
	FeO	9.943	9.982	10.011	9.989
	MnO	0.158	0.218	0.247	0.135
	MgO	14.667	12.416	12.945	14.341
	CaO	10.129	11.138	10.342	9.948
	Na2O	1.913	1.816	1.863	1.902
	K2O	0.305	0.461	0.341	0.25
	P2O5	0.171	0.28	0.263	0.158
	Cr2O3	0	0	0	0
	Temp Calc. Petrolog	1352	1302	1313	1344
	FO_Host	89.7	87.9	88.2	89.4
	FEO*	11.198	11.198	11.191	11.198
	FEO_Final	11.2	11.2	11.2	11.2
	Olivine Percent	16.16	23.24	20.04	14
	Correction Coefficient	1.187	1.311	1.266	1.155

Table C2. (continued).

	Suite: Kapoho				
	Naturally Quenched /Reheated	**Reheated**	**Reheated**	**Reheated**	**Reheated**
	Temperature (C)	**1400**	**1400**	**1400**	**1400**
	Inclusion Name	**Kap8-R-1400-34**	**Kap8-R-1400-50**	**Kap8-R-1400-51**	**Kap8-R-1400-52**
Raw	**SiO2**	45.77	47.82	48.84	47.32
	TiO2	2.00	1.84	1.61	1.72
	Al2O3	9.37	9.26	8.80	9.23
	FeO^T	10.92	9.32	11.00	10.40
	MnO	0.16	0.12	0.16	0.14
	MgO	19.34	20.98	20.00	20.33
	CaO	8.69	8.37	7.18	8.68
	Na2O	1.56	1.72	1.85	1.63
	K2O	0.34	0.36	0.34	0.29
	P2O5	0.17	0.22	0.22	0.25
	FeO	9.28	7.92	9.35	8.84
	Fe2O3	1.82	1.55	1.83	1.73
	$Fe2O3^T$	12.13	10.36	12.23	11.56
	Inclusion Name	**Kap8-R-1400-34**	**Kap8-R-1400-50**	**Kap8-R-1400-51**	**Kap8-R-1400-52**
Corrected	**SiO2**	47.988	48.585	50.782	48.592
	TiO2	2.556	2.152	2.012	2.102
	Al2O3	11.969	10.85	10.975	11.303
	Fe2O3	1.336	1.399	1.372	1.367
	FeO	9.989	9.939	9.962	9.966
	MnO	0.203	0.145	0.196	0.166
	MgO	12.208	14.43	12.734	13.215
	CaO	11.101	9.808	8.956	10.633
	Na2O	1.993	2.013	2.307	1.999
	K2O	0.434	0.417	0.426	0.357
	P2O5	0.223	0.263	0.277	0.3
	Cr2O3	0	0	0	0
	Temp Calc. Petrolog	1300	1349	1319	1322
	FO_Host	87.9	89.5	87.8	88.6
	FEO*	11.191	11.198	11.197	11.196
	FEO_Final	11.2	11.2	11.2	11.2
	Olivine Percent	20.34	15.34	19.91	18.56
	Correction Coefficient	1.258	1.174	1.25	1.226

Table C2. (continued).

	Suite: Kapoho				
	Naturally Quenched /Reheated	**Reheated**	**Reheated**	**Reheated**	**Reheated**
	Temperature (C)	**1400**	**1400**	**1400**	**1400**
	Inclusion Name	**Kap8-R-1400-53**	**Kap8-R-1400-54**	**Kap8-R-1400-55**	**Kap6-R-1400-1**
Raw	**SiO2**	46.28	47.21	48.77	47.35
	TiO2	1.44	1.85	2.55	2.05
	Al2O3	8.40	9.44	11.72	10.03
	FeO^T	15.41	13.24	9.66	11.26
	MnO	0.24	0.19	0.14	0.15
	MgO	19.40	17.61	14.60	17.25
	CaO	7.14	8.34	9.31	9.58
	Na2O	1.26	1.56	2.48	1.73
	K2O	0.27	0.35	0.48	0.36
	P2O5	0.17	0.21	0.30	0.24
	FeO	13.10	11.25	8.21	9.57
	Fe2O3	2.57	2.21	1.61	1.88
	$Fe2O3^T$	17.13	14.71	10.73	12.52
	Inclusion Name	**Kap8-R-1400-53**	**Kap8-R-1400-54**	**Kap8-R-1400-55**	**Kap6-R-1400-1**
Corrected	**SiO2**	49.842	49.101	48.572	48.386
	TiO2	2.077	2.264	2.595	2.375
	Al2O3	12.076	11.554	11.947	11.633
	Fe2O3	1.283	1.327	1.351	1.354
	FeO	10.043	10.005	9.983	9.972
	MnO	0.345	0.233	0.143	0.175
	MgO	11.626	12.713	12.602	12.285
	CaO	10.272	10.208	9.488	11.112
	Na2O	1.81	1.909	2.522	2.005
	K2O	0.385	0.428	0.487	0.422
	P2O5	0.242	0.257	0.308	0.281
	Cr2O3	0	0	0	0
	Temp Calc. Petrolog	1283	1310	1320	1302
	FO_Host	86.7	88	88.2	87.9
	FEO*	11.198	11.2	11.199	11.191
	FEO_Final	11.2	11.2	11.2	11.2
	Olivine Percent	28.97	17.52	2.71	13.84
	Correction Coefficient	1.441	1.226	1.02	1.162

Table C2. (continued).

	Suite: Kapoho				
	Naturally Quenched /Reheated	**Reheated**	**Reheated**	**Reheated**	**Reheated**
	Temperature (C)	**1400**	**1400**	**1400**	**1400**
	Inclusion Name	**Kap6-R-1400-2**	**Kap6-R-1400-3**	**Kap6-R-1400-4**	**Kap6-R-1400-5**
Raw	**SiO2**	47.96	47.77	48.24	47.29
	TiO2	2.01	1.98	1.88	2.00
	Al2O3	10.26	10.62	9.48	8.83
	FeO^T	9.37	9.10	9.95	13.84
	MnO	0.13	0.13	0.13	0.16
	MgO	18.71	18.95	18.93	18.08
	CaO	9.22	8.99	9.01	7.50
	Na2O	1.78	1.77	1.77	1.67
	K2O	0.33	0.42	0.36	0.40
	P2O5	0.22	0.27	0.25	0.23
	FeO	7.97	7.73	8.46	11.77
	Fe2O3	1.56	1.52	1.66	2.31
	$Fe2O3^T$	10.41	10.11	11.06	15.38
	Inclusion Name	**Kap6-R-1400-2**	**Kap6-R-1400-3**	**Kap6-R-1400-4**	**Kap6-R-1400-5**
Corrected	**SiO2**	48.186	47.831	49.385	49.634
	TiO2	2.192	2.134	2.251	2.527
	Al2O3	11.18	11.428	11.324	11.173
	Fe2O3	1.372	1.366	1.37	1.349
	FeO	9.96	9.964	9.962	9.979
	MnO	0.147	0.145	0.159	0.205
	MgO	14.373	14.807	11.937	12.731
	CaO	10.045	9.671	10.763	9.495
	Na2O	1.941	1.908	2.121	2.115
	K2O	0.364	0.456	0.427	0.503
	P2O5	0.24	0.29	0.3	0.289
	Cr2O3	0	0	0	0
	Temp Calc. Petrolog	1346	1356	1296	1316
	FO_Host	89.5	89.8	87.4	88
	FEO*	11.195	11.193	11.195	11.192
	FEO_Final	11.2	11.2	11.2	11.2
	Olivine Percent	9.04	8.04	16.85	19.97
	Correction Coefficient	1.091	1.078	1.197	1.268

Table C2. (continued).

	Suite: Kapoho				
	Naturally Quenched /Reheated	**Reheated**	**Reheated**	**Reheated**	**Reheated**
	Temperature (C)	**1400**	**1400**	**1400**	**1400**
	Inclusion Name	**Kap6-R-1400-6**	**Kap6-R-1400-10**	**KAP4-R-1400-6**	**KAP4-R-1400-9**
Raw	**SiO2**	48.46	47.58	45.73	47.36
	TiO2	1.93	1.93	1.94	1.98
	Al2O3	8.49	9.28	9.11	9.47
	FeO^T	10.58	11.49	10.92	9.96
	MnO	0.12	0.18	0.00	0.00
	MgO	18.91	18.15	19.59	18.65
	CaO	9.20	9.18	8.04	8.21
	Na2O	1.74	1.62	1.74	1.93
	K2O	0.35	0.32	0.46	0.28
	P2O5	0.21	0.26	0.22	0.18
	FeO	8.99	9.77	9.28	8.46
	Fe2O3	1.76	1.92	1.82	1.66
	$Fe2O3^T$	11.76	12.77	12.13	11.07
	Inclusion Name	**Kap6-R-1400-6**	**Kap6-R-1400-10**	**KAP4-R-1400-6**	**KAP4-R-1400-9**
Corrected	**SiO2**	49.848	49.221	48.425	49.109
	TiO2	2.316	2.385	2.53	2.301
	Al2O3	10.201	11.453	11.888	11.012
	Fe2O3	1.435	1.364	1.361	1.379
	FeO	9.907	9.969	9.967	9.958
	MnO	0.149	0.228	0	0
	MgO	12.322	11.342	12.179	13.914
	CaO	11.056	11.33	10.499	9.546
	Na2O	2.089	1.994	2.266	2.241
	K2O	0.424	0.398	0.597	0.324
	P2O5	0.254	0.315	0.288	0.215
	Cr2O3	0	0	0	0
	Temp Calc. Petrolog	1304	1278	1307	1342
	FO_Host	87.8	86.8	87.9	89.1
	FEO*	11.198	11.196	11.192	11.199
	FEO_Final	11.2	11.2	11.2	11.2
	Olivine Percent	17.04	18.9	21.55	12.69
	Correction Coefficient	1.203	1.236	1.278	1.141

Table C2. (continued).

	Suite: Kapoho				
	Naturally Quenched /Reheated	**Reheated**	**Reheated**	**Reheated**	**Reheated**
	Temperature (C)	**1400**	**1400**	**1300**	**1300**
	Inclusion Name	**KAP4-R-1400-10**	**KAP4-R-1400-12**	**KAP4-R-1400-14**	**Kap8-R-1300-2**
Raw	**SiO2**	46.76	45.77	46.96	48.79
	TiO2	1.74	1.58	2.22	2.39
	Al2O3	9.37	8.91	10.27	10.85
	FeO^T	10.14	13.16	11.05	10.29
	MnO	0.00	0.00	0.00	0.13
	MgO	19.45	18.80	15.84	14.54
	CaO	8.60	8.07	9.54	10.44
	Na2O	1.55	1.57	1.83	1.77
	K2O	0.33	0.32	0.44	0.49
	P2O5	0.18	0.18	0.22	0.30
	FeO	8.62	11.18	9.39	8.75
	Fe2O3	1.69	2.19	1.84	1.72
	$Fe2O3^T$	11.27	14.62	12.28	11.44
	Inclusion Name	**KAP4-R-1400-10**	**KAP4-R-1400-12**	**KAP4-R-1400-14**	**Kap8-R-1300-2**
Corrected	**SiO2**	49.051	49.409	48.442	48.885
	TiO2	2.183	2.249	2.487	2.49
	Al2O3	11.778	12.662	11.529	11.294
	Fe2O3	1.328	1.347	1.357	1.35
	FeO	9.998	9.982	9.977	9.98
	MnO	0	0	0	0.139
	MgO	12.26	9.958	12.706	12.336
	CaO	10.806	11.464	10.707	10.862
	Na2O	1.947	2.224	2.056	1.846
	K2O	0.418	0.452	0.494	0.509
	P2O5	0.231	0.252	0.247	0.309
	Cr2O3	0	0	0	0
	Temp Calc. Petrolog	1301	1249	1314	1302
	FO_Host	87.7	85.2	88.3	87.8
	FEO*	11.193	11.195	11.198	11.195
	FEO_Final	11.2	11.2	11.2	11.2
	Olivine Percent	19.24	27.73	9.52	4.44
	Correction Coefficient	1.235	1.4	1.106	1.042

Table C2. (continued).

	Suite: Kapoho				
	Naturally Quenched /Reheated	**Reheated**	**Reheated**	**Reheated**	**Reheated**
	Temperature (C)	**1300**	**1300**	**1300**	**1300**
	Inclusion Name	**Kap8-R-1300-3**	**Kap8-R-1300-4**	**Kap8-R-1300-5**	**Kap8-R-1300-6**
Raw	**SiO2**	48.54	48.66	48.86	48.75
	TiO2	2.22	2.21	2.20	2.31
	Al2O3	11.50	10.91	10.75	10.89
	FeO^T	10.21	11.08	10.97	11.00
	MnO	0.16	0.16	0.15	0.16
	MgO	14.39	14.46	14.36	14.30
	CaO	10.44	9.89	10.11	9.88
	Na2O	1.84	1.89	1.89	1.93
	K2O	0.43	0.48	0.47	0.52
	P2O5	0.26	0.26	0.24	0.26
	FeO	8.68	9.42	9.33	9.35
	Fe2O3	1.70	1.85	1.83	1.83
	$Fe2O3^T$	11.35	12.32	12.19	12.22
	Inclusion Name	**Kap8-R-1300-3**	**Kap8-R-1300-4**	**Kap8-R-1300-5**	**Kap8-R-1300-6**
Corrected	**SiO2**	48.62	49.555	49.742	49.563
	TiO2	2.315	2.476	2.466	2.565
	Al2O3	11.975	12.241	12.047	12.115
	Fe2O3	1.321	1.358	1.374	1.369
	FeO	10.003	9.97	9.956	9.966
	MnO	0.164	0.175	0.164	0.182
	MgO	12.106	10.169	10.013	10.227
	CaO	10.869	11.098	11.324	10.993
	Na2O	1.917	2.124	2.12	2.151
	K2O	0.444	0.539	0.522	0.574
	P2O5	0.266	0.296	0.272	0.293
	Cr2O3	0	0	0	0
	Temp Calc. Petrolog	1297	1254	1249	1256
	FO_Host	87.6	85.4	85.2	85.5
	FEO*	11.192	11.192	11.192	11.198
	FEO_Final	11.2	11.2	11.2	11.2
	Olivine Percent	4.5	11.11	11.04	10.4
	Correction Coefficient	1.042	1.123	1.122	1.114

Table C2. (continued).

	Suite: Kapoho				
	Naturally Quenched /Reheated	**Reheated**	**Reheated**	**Reheated**	**Reheated**
	Temperature (C)	**1300**	**1300**	**1300**	**1300**
	Inclusion Name	**Kap8-R-1300-7**	**Kap8-R-1300-8**	**Kap8-R-1300-9**	**Kap8-R-1300-10**
Raw	**SiO2**	48.09	49.08	49.96	48.33
	TiO2	2.33	2.24	2.04	2.32
	Al2O3	11.59	11.00	11.50	11.04
	FeO^T	9.88	9.86	9.66	11.29
	MnO	0.15	0.14	0.14	0.16
	MgO	14.72	14.71	14.52	14.13
	CaO	10.64	10.35	9.59	10.05
	Na2O	1.87	1.91	1.92	1.90
	K2O	0.46	0.44	0.43	0.52
	P2O5	0.27	0.25	0.24	0.26
	FeO	8.40	8.38	8.21	9.60
	Fe2O3	1.65	1.64	1.61	1.88
	$Fe2O3^T$	10.98	10.96	10.73	12.55
	Inclusion Name	**Kap8-R-1300-7**	**Kap8-R-1300-8**	**Kap8-R-1300-9**	**Kap8-R-1300-10**
Corrected	**SiO2**	48.059	49.113	49.785	49.23
	TiO2	2.422	2.335	2.083	2.601
	Al2O3	12.024	11.456	11.716	12.384
	Fe2O3	1.33	1.352	1.312	1.368
	FeO	9.999	9.976	10.012	9.962
	MnO	0.161	0.149	0.139	0.174
	MgO	12.271	12.131	12.54	10.011
	CaO	11.038	10.78	9.771	11.268
	Na2O	1.945	1.99	1.956	2.129
	K2O	0.474	0.457	0.443	0.58
	P2O5	0.277	0.259	0.243	0.294
	Cr2O3	0	0	0	0
	Temp Calc. Petrolog	1301	1299	1308	1250
	FO_Host	87.9	87.6	87.7	85.3
	FEO*	11.196	11.193	11.193	11.193
	FEO_Final	11.2	11.2	11.2	11.2
	Olivine Percent	4.36	4.69	2.69	10.99
	Correction Coefficient	1.039	1.042	1.02	1.123

Table C3. Kapoho Tephra Major Element Compositions

	Kap8-T-1					
	Spot 1	**Spot 2**	**Spot 3**	**Spot 4**	**Average**	**Normalized**
SiO2	50.21	50.03	49.21	49.22	49.67	50.31
TiO2	3.21	3.08	3.03	3.14	3.11	3.16
Al2O3	14.03	14.27	14.04	13.69	14.01	14.19
FeOT	10.79	11.07	10.97	11.03	10.96	11.11
MnO	0.17	0.17	0.16	0.16	0.16	0.17
MgO	6.33	6.30	6.32	6.28	6.31	6.39
CaO	11.00	10.99	11.00	11.02	11.00	11.15
Na2O	2.35	2.39	2.42	2.46	2.40	2.43
K2O	0.64	0.64	0.63	0.67	0.65	0.65
P2O5	0.44	0.45	0.45	0.44	0.45	0.45
H2O	0.84	0.61	1.77	1.90	1.28	
TOTAL	100	100	100	100	100	100

	Kap8-T-2					
	Spot 1	**Spot 2**	**Spot 3**	**Spot 4**	**Average**	**Normalized**
SiO2	49.29	49.71	49.39	49.58	49.49	50.30
TiO2	3.14	2.92	3.04	3.11	3.05	3.10
Al2O3	14.52	13.60	13.99	13.67	13.95	14.17
FeOT	10.83	11.04	10.80	10.91	10.89	11.07
MnO	0.16	0.15	0.16	0.15	0.15	0.16
MgO	6.32	6.37	6.37	6.38	6.36	6.46
CaO	10.97	11.04	10.97	10.95	10.99	11.17
Na2O	2.37	2.32	2.47	2.51	2.42	2.46
K2O	0.64	0.62	0.63	0.65	0.63	0.65
P2O5	0.46	0.45	0.46	0.44	0.45	0.46
H2O	1.30	1.80	1.73	1.64	1.62	
TOTAL	100	100	100	100	100	100

	Kap8-T-3					
	Spot 1	**Spot 2**	**Spot 3**	**Spot 4**	**Average**	**Normalized**
SiO2	49.88	50.04	49.89	50.05	49.97	50.77
TiO2	3.13	3.18	3.02	3.10	3.11	3.16
Al2O3	13.37	14.26	13.51	13.66	13.70	13.92
FeOT	11.05	10.99	11.27	11.04	11.09	11.27
MnO	0.17	0.17	0.17	0.15	0.16	0.17
MgO	6.45	6.45	6.44	6.39	6.43	6.54
CaO	11.07	11.06	11.05	11.06	11.06	11.24
Na2O	1.79	1.83	1.78	1.82	1.80	1.83
K2O	0.66	0.65	0.64	0.65	0.65	0.66
P2O5	0.41	0.45	0.45	0.43	0.44	0.44
H2O	2.03	0.91	1.77	1.65	1.59	
TOTAL	100	100	100	100	100	100

Table C3. (continued).

	Kap8-T-4					
	Spot 1	**Spot 2**	**Spot 3**	**Spot 4**	**Average**	**Normalized**
SiO2	50.06	49.24	49.72	49.30	49.58	50.33
TiO2	2.92	3.21	3.02	2.98	3.03	3.08
Al2O3	14.08	14.40	14.03	13.18	13.92	14.13
FeOT	10.95	10.80	11.07	10.90	10.93	11.10
MnO	0.15	0.15	0.16	0.16	0.16	0.16
MgO	6.37	6.34	6.31	8.94	6.99	7.10
CaO	9.62	10.89	10.99	10.45	10.49	10.65
Na2O	2.40	2.49	2.21	2.14	2.31	2.34
K2O	0.64	0.65	0.66	0.62	0.64	0.65
P2O5	0.48	0.46	0.48	0.42	0.46	0.47
H2O	2.34	1.37	1.35	0.91	1.49	
TOTAL	100	100	100	100	100	100

	Kap6-T-1					
	Spot 1	**Spot 2**	**Spot 3**	**Spot 4**	**Average**	**Normalized**
SiO2	50.76	50.19	50.30	50.31	50.39	50.27
TiO2	3.14	3.18	3.16	3.07	3.14	3.13
Al2O3	15.62	14.52	14.87	14.18	14.80	14.76
FeOT	11.21	11.27	11.32	11.15	11.24	11.21
MnO	0.17	0.15	0.17	0.17	0.16	0.16
MgO	6.41	6.43	6.48	6.46	6.45	6.43
CaO	9.64	10.96	10.99	10.99	10.65	10.62
Na2O	2.45	2.39	2.28	2.05	2.29	2.29
K2O	0.66	0.63	0.67	0.67	0.66	0.66
P2O5	0.48	0.47	0.48	0.47	0.48	0.48
H2O	0.00	0.00	0.00	0.48	0.12	
TOTAL	100	100	100	100	100	100

	Kap6-T-2					
	Spot 1	**Spot 2**	**Spot 3**	**Spot 4**	**Average**	**Normalized**
SiO2	49.54	49.97	49.96	49.61	49.77	50.35
TiO2	2.95	3.09	3.11	2.90	3.01	3.05
Al2O3	14.33	14.22	14.00	14.03	14.14	14.31
FeOT	10.90	11.24	11.30	11.21	11.16	11.29
MnO	0.16	0.17	0.17	0.17	0.17	0.17
MgO	6.50	6.50	6.51	6.56	6.52	6.59
CaO	9.71	10.98	10.98	10.97	10.66	10.79
Na2O	2.36	2.40	2.20	2.32	2.32	2.35
K2O	0.63	0.63	0.64	0.65	0.64	0.65
P2O5	0.45	0.45	0.47	0.44	0.45	0.46
H2O	2.48	0.36	0.66	1.12	1.15	
TOTAL	100	100	100	100	100	100

Table C3. (continued).

	Kap6-T-3			
	Spot 1	**Spot 2**	**Average**	**Normalized**
SiO2	49.75	49.73	49.74	50.56
TiO2	3.20	3.12	3.16	3.21
Al2O3	13.99	13.88	13.94	14.17
FeOT	11.15	11.02	11.09	11.27
MnO	0.16	0.16	0.16	0.16
MgO	6.31	6.44	6.37	6.48
CaO	9.66	10.94	10.30	10.47
Na2O	2.51	2.57	2.54	2.58
K2O	0.66	0.63	0.64	0.66
P2O5	0.44	0.45	0.44	0.45
H2O	2	1	2	
TOTAL	100	100	100	100

	Kap6-T-4					
	Spot 1	**Spot 2**	**Spot 3**	**Spot 4**	**Average**	**Normalized**
SiO2	49.60	49.91	49.94	49.34	49.70	50.24
TiO2	3.13	3.14	3.12	3.00	3.10	3.13
Al2O3	13.85	14.07	14.18	14.20	14.07	14.23
FeOT	11.29	11.01	11.14	11.31	11.19	11.31
MnO	0.17	0.16	0.16	0.17	0.16	0.16
MgO	6.47	6.41	6.44	6.52	6.46	6.53
CaO	10.93	10.93	10.93	10.89	10.92	11.04
Na2O	2.29	2.38	2.28	2.01	2.24	2.27
K2O	0.67	0.63	0.63	0.66	0.65	0.65
P2O5	0.42	0.44	0.46	0.45	0.44	0.45
H2O	1.19	0.92	0.72	1.46	1.07	
TOTAL	100	100	100	100	100	100

APPENDIX D

MELT INCLUSION VOLATILE CONCENTRATIONS

Table D1. Kīlauea Iki Naturally Quenched Melt Inclusion Volatile Concentrations

Melt Inclusion Naturally Quenched	H_2O (wt.%)	CO_2 (ppm)	Correction Factor	H_2O corrected	CO_2 corrected	H_2O PSE	CO_2 PSE	Average Diameter (microns)	Vapor Saturation Pressure (Bars)	Depth (km)	FO	Distance from Kīlauea Summit
KIL-IKI-NAT-1	0.41	0.00	0.90	0.37	0.00	0.09	0.09	120	14	0.1	86.1	3.1
KIL-IKI-NAT-2	0.30	198.25	0.88	0.26	174.46	0.12	0.13	90	385	1.65	86.0	3.1
KIL-IKI-NAT-3	0.40	127.48	0.86	0.34	109.63	0.04	0.05	130	250	1.15	87.9	3.1
KIL-IKI-NAT-4	0.49	0.00	0.88	0.43	0.00	0.04	0.04	350	19	0.15	-	3.1
KIL-IKI-NAT-6	0.74	0.00	0.86	0.64	0.00	0.01	0.10	200	37	0.2	87.0	3.1
KIL-IKI-NAT-8	0.60	225.86	0.86	0.52	194.24	0.10	0.10	193	446	1.9	87.9	3.1
KIL-IKI-NAT-9	0.52	117.50	0.90	0.47	105.75	0.05	0.17	160	252	1.15	85.6	3.1
KIL-IKI-NAT-10A	0.56	154.01	0.87	0.49	133.99	0.05	0.07	220	314	1.4	87.4	3.1
KIL-IKI-NAT-10B	0.55	126.37	0.87	0.48	109.94	0.05	0.06	350	262	1.2	87.4	3.1
KIL-IKI-NAT-11A	0.54	101.54	0.87	0.47	88.34	0.03	0.20	210	214	1	86.5	3.1
KIL-IKI-NAT-11B	0.64	157.89	0.90	0.58	142.10	0.03	0.03	160	341	1.5	86.5	3.1
KIL-IKI-NAT-12	0.39	471.01	0.90	0.35	423.91	0.03	0.14	150	914	3.6	-	3.1
KIL-IKI-NAT-13	0.56	167.69	0.88	0.49	147.57	0.03	0.09	175	343	1.5	85.0	3.1
KIL-IKI-NAT-14A	0.38	131.42	0.85	0.32	111.71	0.04	0.11	100	253	1.15	87.6	3.1
KIL-IKI-NAT-14B	0.38	258.45	0.85	0.32	219.68	0.04	0.05	180	485	2.15	87.6	3.1
KIL-IKI-NAT-15	0.48	61.88	0.86	0.41	53.22	0.08	0.11	120	133	0.65	87.1	3.1
KIL-IKI-NAT-16	0.06	138.33	0.88	0.05	121.73	0.12	0.25	130	265	1.2	83.6	3.1
Average	0.47	143.39	0.87	0.41	125.66	0.06	0.11	179	290	1.27	86.6	3.1

Table D2. Kīlauea Iki Reheated Melt Inclusion Volatile Concentrations

Melt Inclusion Reheated	H_2O (wt.%)	CO_2 (ppm)	Correction Factor	H_2O corrected	CO_2 corrected	H_2O PSE	CO_2 PSE	Average Diameter (microns)	Vapor Saturation Pressure (Bars)	Depth (km)	FO	Distance from Kīlauea Summit
KIL-IKI-R-1400-2	0.14	214.60	1.33	0.19	285.42	0.06	0.05	130	617	2.55	87.9	3.1
KIL-IKI-R-1400-3	0.12	432.69	1.36	0.17	588.46	0.04	0.07	230	1239	4.7	-	3.1
KIL-IKI-R-1400-6A	0.08	109.72	1.39	0.11	152.51	0.08	0.08	120	332	1.5	87.5	3.1
KIL-IKI-R-1400-6B	0.07	105.30	1.39	0.09	146.36	0.07	0.14	120	319	1.5	87.5	3.1
KIL-IKI-R-1400-8	0.08	107.52	1.32	0.11	141.92	0.03	0.04	100	309	1.35	87.7	3.1
KIL-IKI-R-1400-10	0.18	0.00	1.36	0.24	0.00	0.05	0.32	110	6	0.1	-	3.1
KIL-IKI-R-1400-12	0.09	139.90	1.34	0.12	187.47	0.00	0.07	230	407	1.75	87.8	3.1
KIL-IKI-R-1400-14	0.10	425.82	1.30	0.13	553.56	0.03	0.15	100	1168	4.45	86.5	3.1
KIL-IKI-R-1400-13	0.29	183.30	1.34	0.38	245.63	0.02	0.04	175	544	2.3	86.3	3.1
KIL-IKI-R-1400-15	0.05	155.50	1.30	0.07	202.15	0.04	0.04	130	438	1.85	83.9	3.1
Average	**0.12**	**187.43**	**1.34**	**0.16**	**250.35**	**0.04**	**0.10**	**145**	**538**	**2.21**	**86.9**	**3.1**

Table D3. Kapoho (Kap8) Naturally Quenched Melt Inclusion Volatile Concentrations

Melt Inclusion Naturally Quenched	H_2O (wt.%)	CO_2 (ppm)	Correction Factor	H_2O corrected	CO_2 corrected	H_2O PSE	CO_2 PSE	Average Diameter (microns)	Vapor Saturation Pressure (Bars)	Depth (km)	FO	Distance from Kīlauea Summit
K99-9-12	0.22	288.23	0.85	0.19	245.00	0.18	0.20	135	532	2.2	89.6	47
K99-9-16	0.62	211.76	0.85	0.53	180.00	0.01	0.05	225	417	1.8	88.0	47
K99-9-17	0.25	137.36	0.85	0.21	116.76	0.05	0.09	120	259	1.2	87.3	47
Kap8-Nat-1	0.10	105.91	0.80	0.08	84.73	0.11	0.24	140	185	0.9	-	47
Kap8-Nat-2	0.49	152.17	0.80	0.39	121.74	0.14	0.14	150	280	1.25	89.7	47
Kap8-Nat-4	0.31	283.63	0.80	0.25	226.90	0.02	0.06	-	496	2.1	89.5	47
Kap8-Nat-8a	0.56	84.66	0.94	0.53	79.58	0.02	0.03	260	201	0.95	86.8	47
Kap8-Nat-8b	0.62	75.98	0.95	0.59	72.18	0.02	0.02	150	191	0.9	87.8	47
Kap8-Nat-9	0.10	143.40	0.89	0.09	127.63	0.04	0.03	230	278	1.25	86.2	47
Average	0.36	164.79	0.86	0.32	139.39	0.06	0.10	176	315	1.39	88.1	47

Table D4. Kapoho (Kap6) Naturally Quenched Melt Inclusion Volatile Concentrations

Melt Inclusion Naturally Quenched	H_2O (wt.%)	CO_2 (ppm)	Correction Factor	H_2O corrected	CO_2 corrected	H_2O PSE	CO_2 PSE	Average Diameter (microns)	Vapor Saturation Pressure (Bars)	Depth (km)	FO	Distance from Kīlauea Summit
KAP6-NAT-1	1.19	96.64	0.85	1.01	82.15	0.07	0.08	248	277	1.25	86.1	47
KAP6-NAT-2	0.58	305.64	0.82	0.47	250.62	0.05	0.06	320	561	2.3	81.6	47
KAP6-NAT-3	0.91	260.14	0.87	0.79	226.32	0.04	0.04	200	546	2.25	88.1	47
KAP6-NAT-4	0.55	232.72	0.87	0.47	202.46	0.05	0.41	215	459	1.95	81.4	47
KAP6-NAT-5	1.15	111.50	0.97	1.12	108.16	0.03	0.08	190	357	1.55	85.0	47
KAP6-NAT-6	0.66	91.10	0.82	0.54	74.70	0.03	0.09	180	191	0.9	85.0	47
KAP6-NAT-7	0.72	175.48	0.95	0.68	166.71	0.04	0.04	250	403	1.75	87.5	47
Average	0.82	181.89	0.88	0.73	158.73	0.04	0.11	229	399	1.71	85.0	47

Table D5. Kapoho (Kap8) Reheated to 1400ºC Melt Inclusion Volatile Concentrations

Melt Inclusion Reheated	H_2O (wt.%)	CO_2 (ppm)	Correction Factor	H_2O corrected	CO_2 corrected	H_2O PSE	CO_2 PSE	Average Diameter (microns)	Vapor Saturation Pressure (Bars)	Depth (km)	FO	Distance from Kīlauea Summit
Kap8-R-1400-12	0.19	392.29	1.15	0.21	451.13	0.07	0.11	90	962	3.5	89.7	47
Kap8-R-1400-13B	0.16	275.34	1.15	0.18	316.64	0.06	0.17	120	683	2.7	89.5	47
Kap8-R-1400-15	0.29	1566.06	1.19	0.35	1863.61	0.01	0.00	163	3542	12.1	89.7	47
Kap8-R-1400-20	0.15	102.68	1.29	0.19	132.46	0.19	0.21	200	291	1.3	88.2	47
Kap8-R-1400-18	0.21	189.98	1.33	0.28	252.67	0.05	0.09	130	552	2.3	87.9	47
Kap8-R-1400-22	0.15	386.53	1.23	0.19	475.43	0.18	0.04	110	1012	3.9	-	47
Kap8-R-1400-23	0.15	167.13	1.27	0.19	212.25	0.02	0.03	150	462	2	87.2	47
Kap8-R-1400-25	0.16	532.30	1.15	0.19	612.14	0.25	0.06	120	1288	4.9	89.8	47
Kap8-R-1400-28	0.16	718.71	1.23	0.20	884.02	0.04	0.05	150	1818	6.6	-	47
Kap8-R-1400-31	0.06	376.71	1.23	0.07	463.35	0.06	0.05	70	984	3.8	-	47
Kap8-R-1400-32	0.16	493.77	1.17	0.19	577.71	0.04	0.06	190	1219	4.6	89.4	47
Kap8-R-1400-34	0.10	257.23	1.28	0.13	329.25	0.07	0.07	110	708	2.85	87.9	47
Kap8-R-1400-35	0.08	432.68	1.15	0.09	497.58	0.04	0.04	100	1054	4.1	89.2	47
Kap8-R-1400-39	0.06	470.87	1.15	0.07	541.50	0.08	0.11	100	1143	4.4	89.8	47
Kap8-R-1400-40	0.06	274.12	1.23	0.07	337.17	0.12	0.13	90	723	2.9	-	47
Kap8-R-1400-41	0.10	420.89	1.23	0.12	517.70	0.05	0.06	80	1096	4.2	-	47
KAP8-1400-R-50	0.23	363.55	1.17	0.27	425.35	0.06	0.02	185	912	3.55	89.5	47
KAP8-R-1400-51	0.08	334.08	1.25	0.10	417.60	0.03	0.03	90	890	2.6	87.8	47
KAP8-R-1400-52	0.16	301.58	1.22	0.20	367.93	0.02	0.03	155	790	3.15	88.6	47
Kap8-R-1400-54	0.25	76.61	1.22	0.31	93.46	0.02	0.04	137	213	1	88.0	47
Kap8-R-1400-55	0.16	437.22	1.02	0.16	445.96	0.02	0.03	109	950	3.7	88.2	47
Average	**0.15**	**408.11**	**1.21**	**0.18**	**486.43**	**0.07**	**0.07**	**126**	**1014**	**3.82**	**88.8**	**47**

Table D6. Kapoho (Kap4) Reheated to 1400ºC Melt Inclusion Volatile Concentrations

Melt Inclusion Reheated	H_2O (wt.%)	CO_2 (ppm)	Correction Factor	H_2O corrected	CO_2 corrected	H_2O PSE	CO_2 PSE	Average Diameter (microns)	Vapor Saturation Pressure (Bars)	Depth (km)	FO	Distance from Kīlauea Summit
KAP4-R-1400-3	0.12	343.55	1.25	0.14	429.44	0.03	0.04	90	916	3.6	-	47
KAP4-R-1400-4	0.19	410.20	1.14	0.22	467.63	0.04	0.11	110	997	3.85	89.1	47
KAP4-R-1400-7	0.17	569.34	1.25	0.22	711.68	0.03	0.10	100	1486	5.55	87.9	47
KAP4-R-1400-8	0.08	101.71	1.14	0.09	115.95	0.17	0.19	90	253	1.15	89.3	47
KAP4-R-1400-9	0.18	407.24	1.16	0.21	472.40	0.04	0.07	130	1006	3.9	89.1	47
KAP4-R-1400-10	0.46	410.20	1.26	0.58	516.85	0.02	0.04	220	1122	4.3	87.7	47
KAP4-R-1400-12	0.14	560.95	1.25	0.18	701.19	0.10	0.12	140	1464	5.5	85.2	47
KAP4-R-1400-6	0.09	297.33	1.30	0.12	386.53	0.03	0.05	100	827	3.3	87.9	47
KAP4-R-1400-14	0.21	207.83	1.12	0.24	232.77	0.02	0.08	100	508	2.1	88.3	47
Average	**0.18**	**367.59**	**1.21**	**0.22**	**448.27**	**0.05**	**0.09**	**120**	**953**	**3.69**	**88.1**	**47**

Table D7. Kapoho (Kap6) Reheated to 1400ºC Melt Inclusion Volatile Concentrations

Melt Inclusion Reheated	H_2O (wt.%)	CO_2 (ppm)	Correction Factor	H_2O corrected	CO_2 corrected	H_2O PSE	CO_2 PSE	Average Diameter (microns)	Vapor Saturation Pressure (Bars)	Depth (km)	FO	Distance from Kīlauea Summit
Kap6-R-1400-1	0.25	158.04	1.16	0.29	183.33	0.04	0.04	90	405	1.75	87.9	47
Kap6-R-1400-2	0.14	317.85	1.09	0.15	346.46	0.09	0.09	130	744	3	89.5	47
Kap6-R-1400-3	0.24	404.01	1.08	0.26	436.33	0.03	0.02	125	934	3.65	89.8	47
Kap6-R-1400-4	0.19	196.63	1.19	0.23	233.99	0.03	0.04	120	510	2.15	87.1	47
Kap6-R-1400-5	0.43	183.04	1.26	0.54	230.63	0.05	0.08	145	525	2.2	88.0	47
Kap6-R-1400-6	0.22	92.98	1.20	0.26	111.58	0.20	0.00	128	253	1.15	87.8	47
Kap6-R-1400-10	0.26	123.84	1.23	0.32	152.32	0.02	0.03	135	332	1.45	86.8	47
Kap6-R-1400-11	0.11	92.85	1.17	0.13	108.63	0.02	0.09	90	247	1.1	-	47
Average	**0.23**	**196.16**	**1.17**	**0.27**	**225.41**	**0.06**	**0.05**	**120**	**494**	**2.06**	**88.1**	**47**

Table D8. Kapoho (Kap8) Reheated to 1300ºC Melt Inclusion Volatile Concentrations

Melt Inclusion Reheated	H_2O (wt.%)	CO_2 (ppm)	Correction Factor	H_2O corrected	CO_2 corrected	H_2O PSE	CO_2 PSE	Average Diameter (microns)	Vapor Saturation Pressure (Bars)	Depth (km)	FO	Distance from Kīlauea Summit
Kap8-R-1300-2	0.31	21.55	1.04	0.32	22.41	0.05	0.22	233	60	0.35	87.8	47
Kap8-R-1300-3	0.15	38.42	1.04	0.16	39.95	0.05	0.05	213	90	0.35	87.6	47
Kap8-R-1300-4	0.26	116.99	1.12	0.29	131.31	0.17	0.06	118	294	1.3	85.4	47
Kap8-R-1300-5	0.74	287.46	1.12	0.83	322.06	0.01	0.20	294	753	3.05	85.2	47
Kap8-R-1300-6	0.69	274.80	1.11	0.76	305.51	0.01	0.00	213	708	3	85.5	47
Kap8-R-1300-7	0.24	73.79	1.04	0.25	76.53	0.05	0.07	161	173	0.85	87.9	47
Kap8-R-1300-8	0.45	116.37	1.04	0.47	121.02	0.04	0.27	188	285	1.25	-	47
Kap8-R-1300-9	0.46	176.53	1.02	0.47	179.99	0.02	0.02	192	411	1.75	87.7	47
Kap8-R-1300-10	0.39	248.14	1.12	0.44	278.08	0.03	0.04	127	617	2.55	85.3	47
Kap8-R-1300-11	0.13	56.72	1.04	0.14	58.99	0.03	0.02	134	131	0.65	88.2	47
Average	**0.38**	**141.08**	**1.07**	**0.41**	**153.59**	**0.05**	**0.10**	**187**	**352**	**1.51**	**86.7**	**47**

APPENDIX E

PUBLISHED BULK ROCK COMPOSITIONS

Table E1. Chemical Analyses of the 1954 and 1955 lavas of Kīlauea (USGS Bulletin 1171, p.87)

BULK Rock	1954 - 1955											
Oxide (wt.%)	1955	1955	1955	1955	1955	1955	1955	1955	1955	1955	1954	Pre-1954 Average
SiO2	51.24	50.99	50.91	50.94	51.06	50.55	50.37	50.61	50.58	50.53	50.20	50.08
Al2O3	13.60	13.73	13.72	13.79	13.72	13.84	14.02	13.80	13.74	13.95	13.73	13.23
Fe2O3	1.87	3.39	2.65	2.16	2.44	2.98	1.88	2.66	1.97	2.56	2.65	1.89
FeO	11.19	9.36	9.87	10.25	10.34	9.32	10.07	9.31	9.95	9.40	8.80	9.62
MgO	5.12	5.42	5.64	5.57	5.44	6.19	6.75	6.61	6.57	6.33	7.20	8.13
CaO	9.03	9.38	9.58	9.57	9.46	10.10	10.39	10.28	10.27	10.28	11.56	10.94
Na2O	2.81	2.75	2.68	2.70	2.62	2.61	2.35	2.49	2.51	2.56	2.25	2.29
K2O	0.83	0.80	0.74	0.76	0.76	0.67	0.62	0.69	0.72	0.64	0.57	0.54
H2O+	0.03	0.03	0.01	0.03	0.12	0.02	0.16	0.00	0.06	0.00	0.00	-
H2O-	0.00	0.01	0.02	0.02	0.00	0.01	0.04	0.01	0.01	0.01	0.00	-
TiO2	3.74	3.57	3.60	3.70	3.65	3.31	3.09	3.12	3.22	3.23	2.72	2.67
P2O5	0.41	0.39	0.40	0.40	0.39	0.30	0.32	0.34	0.35	0.28	0.28	0.36
MnO	0.18	0.18	0.18	0.18	0.18	0.18	0.17	0.17	0.17	0.17	0.17	0.14
CO2	0.01	0.01	0.00	0.00	-	0.01	-	0.01	0.00	0.00	0.01	-
Cl	0.01	0.01	0.02	0.03	-	0.01	-	0.01	0.04	0.01	0.02	-
F	0.06	0.05	0.05	0.05	-	0.05	-	0.04	0.04	0.04	0.05	-
S	0.01	0.00	0.00	0.00	-	0.00	-	0.00	0.00	0.00	-	-
Total	100.14	100.07	100.07	100.15	100.18	100.15	100.23	100.15	100.20	99.99	100.21	99.89
minus volatiles	100.02	99.96	99.97	100.02	100.18	100.05	100.23	100.08	100.05	99.93	100.21	99.89

Table E1. (continued).

Normalized BULK Rock	1954 - 1955											
Oxide (wt.%)	**1955**	**1955**	**1955**	**1955**	**1955**	**1955**	**1955**	**1955**	**1955**	**1955**	**1954**	**Pre-1954 Average**
SiO2	51.23	51.01	50.93	50.93	50.97	50.52	50.25	50.57	50.55	50.57	50.09	50.14
Al2O3	13.60	13.74	13.72	13.79	13.70	13.83	13.99	13.79	13.73	13.96	13.70	13.24
Fe2O3	1.87	3.39	2.65	2.16	2.44	2.98	1.88	2.66	1.97	2.56	2.64	1.89
FeO	11.19	9.36	9.87	10.25	10.32	9.32	10.05	9.30	9.95	9.41	8.78	9.63
MgO	11.19	9.36	9.87	10.25	10.32	9.32	10.05	9.30	9.95	9.41	8.78	9.63
CaO	9.03	9.38	9.58	9.57	9.44	10.09	10.37	10.27	10.26	10.29	11.54	10.95
Na2O	2.81	2.75	2.68	2.70	2.62	2.61	2.34	2.49	2.51	2.56	2.25	2.29
K2O	0.83	0.80	0.74	0.76	0.76	0.67	0.62	0.69	0.72	0.64	0.57	0.54
TiO2	3.74	3.57	3.60	3.70	3.64	3.31	3.08	3.12	3.22	3.23	2.71	2.67
P2O5	0.41	0.39	0.40	0.40	0.39	0.30	0.32	0.34	0.35	0.28	0.28	0.36
MnO	0.18	0.18	0.18	0.18	0.18	0.18	0.17	0.17	0.17	0.17	0.17	0.14
FeOT	12.78	12.25	12.13	12.08	12.39	11.85	11.64	11.56	11.62	11.58	11.03	11.24

[1] 1955 column 1:Vent A erupted 2/28/5, 1955 column 2: Kii Flow erupted 3/3/55, 1955 column 3: Kaueleau flow erupted 3/14/55, 1955 column 4: Kauleau flow erupted 3/14/55, 1955 column 5: Westernmost vents, 3/20/55, 1955 column 6: Keekee flow 3/25/55, 1955 column 7: Vent T erupted 3/26/55, 1955 column 8: Kehana Flow 3/28/55, 1955 column 9: Kehena Flow 3/28/55, 1955 column 10: Basalt Flow 5/25/55, 1954 column 11: Basalt Flow floor of Kīlauea Caldera NE of Halemaumau, Column 12: Average of 15 analyses of historic basalts and olivine basalts erupted prior to 1954.

Table E2. Chemical Analyses of lavas from the 1959 Kīlauea Summit Eruption (USGS PP 537-A)

BULK Rock	**Kīlauea IKI**				
Oxide (wt. %)	S1	S2	S3	S4	S5
SiO2	49.91	50.01	49.62	48.99	46.98
Al2O3	12.69	13.70	12.82	11.95	9.52
Fe2O3	2.56	1.39	2.70	1.47	1.57
FeO	8.86	10.00	8.82	10.08	10.30
MgO	8.08	7.23	8.85	11.50	19.52
CaO	11.92	11.55	11.49	10.60	8.26
Na2O	2.13	2.30	2.11	2.05	1.52
K2O	0.55	0.60	0.50	0.47	0.35
H2O+	0.09	0.00	0.08	0.05	0.00
H2O-	0.02	0.02	0.02	0.03	0.01
TiO2	2.62	2.75	2.55	2.42	1.80
P2O5	0.25	0.28	0.26	0.23	0.18
MnO	0.17	0.17	0.18	0.18	0.17
CO2	0.01	0.00	0.02	0.02	0.02
Cl	0.02	0.02	0.01	0.02	0.01
F	0.04	0.04	0.03	0.03	0.02
Cr2O3	0.21	0.00	0.00	0.00	0.00
Total	100.13	100.06	100.06	100.09	100.23
minus volatiles and Cr2O3	99.74	99.98	99.90	99.94	100.17
Normalized BULK Rock					
SiO2	49.85	49.98	49.59	48.95	46.87
Al2O3	12.67	13.69	12.81	11.94	9.50
Fe2O3	2.56	1.39	2.70	1.47	1.57
FeO	8.85	9.99	8.81	10.07	10.28
MgO	8.07	7.23	8.84	11.49	19.48
CaO	11.90	11.54	11.48	10.59	8.24
Na2O	2.13	2.30	2.11	2.05	1.52
K2O	0.55	0.60	0.50	0.47	0.35
TiO2	2.62	2.75	2.55	2.42	1.80
P2O5	0.25	0.28	0.26	0.23	0.18
MnO	0.17	0.17	0.18	0.18	0.17
FeOT	11.02	11.18	11.11	11.32	11.61

[2] S2-S5 Cr2O3 was not measured, S1: Vent spatter from the most eastern early vent 11/14/59, S2: Vent spatter rom the most western early vent 11/14/59, S3: Lava from the main river, 1400, 11/16/59, S4: Pumice, 1500, 11/17/59, S5: Pumice, 1700, 11/18/59, this corresponds to S-1 magma component.

Table E3. Chemical Analyses of lavas of the 1960 Kapoho Flank Eruption (USGS PP 537-A)

BULK Rock	KAPOHO						
Oxide (wt.%)	**F1**	**F5**	**F7**	**F8**	**F14**	**F16**	**F20**
SiO2	50.58	50.75	50.42	49.87	49.19	48.97	49.13
Al2O3	13.88	13.70	13.51	13.29	12.24	11.84	11.96
Fe2O3	2.18	1.68	2.34	2.13	2.02	2.83	1.44
FeO	9.52	10.40	9.59	9.59	9.63	8.93	10.13
MgO	6.56	6.09	6.97	8.27	11.28	12.29	11.82
CaO	10.43	10.01	10.18	10.24	9.69	9.41	9.58
Na2O	2.58	2.71	2.59	2.41	2.25	2.09	2.19
K2O	0.65	0.69	0.62	0.60	0.52	0.50	0.50
H2O+	0.08	0.04	0.11	0.06	0.08	0.01	0.08
H2O-	0.01	0.03	0.00	0.03	0.03	0.03	0.00
TiO2	3.11	3.37	3.17	2.91	2.69	2.55	2.65
P2O5	0.35	0.36	0.34	0.33	0.28	0.26	0.27
MnO	0.18	0.18	0.18	0.18	0.18	0.18	0.18
CO2	0.02	0.02	0.01	0.02	0.00	0.02	0.00
Cl	0.02	0.02	0.02	0.02	0.01	0.02	0.01
F	0.04	0.04	0.04	0.04	0.03	0.03	0.04
Total	100.19	100.09	100.09	99.99	100.12	99.96	99.98
minus volatiles	100.02	99.94	99.91	99.82	99.97	99.85	99.85
Normalized BULK Rock							
SiO2	50.57	50.78	50.47	49.96	49.20	49.04	49.20
Al2O3	13.88	13.71	13.52	13.31	12.24	11.86	11.98
Fe2O3	2.18	1.68	2.34	2.13	2.02	2.83	1.44
FeO	9.52	10.41	9.60	9.61	9.63	8.94	10.15
MgO	6.56	6.09	6.98	8.28	11.28	12.31	11.84
CaO	10.43	10.02	10.19	10.26	9.69	9.42	9.59
Na2O	2.58	2.71	2.59	2.41	2.25	2.09	2.19
K2O	0.65	0.69	0.62	0.60	0.52	0.50	0.50
TiO2	3.11	3.37	3.17	2.92	2.69	2.55	2.65
P2O5	0.35	0.36	0.34	0.33	0.28	0.26	0.27
MnO	0.18	0.18	0.18	0.18	0.18	0.18	0.18
FeOT	11.37	11.84	11.59	11.42	11.35	11.35	11.37

[3] F1: Slab pahoehoe from an early west vent, 2010, 1/13/60, F5: Pumice 0700, 1/21/60, F7: Pumice 1900, 1/26/60, F8: Pahoehoe flow from the west side of cone, 1015, 1/29/60, F14: Aa flow to north , 2/4/60, F16: Pahoehoe, last flow east from main vent, 820, 2/12/60, F20: Pahoehoe, last flow from the west side of cone, 2/18/60.

APPENDIX F

1959-1960 ERUPTION SCHEMATIC DIAGRAMS

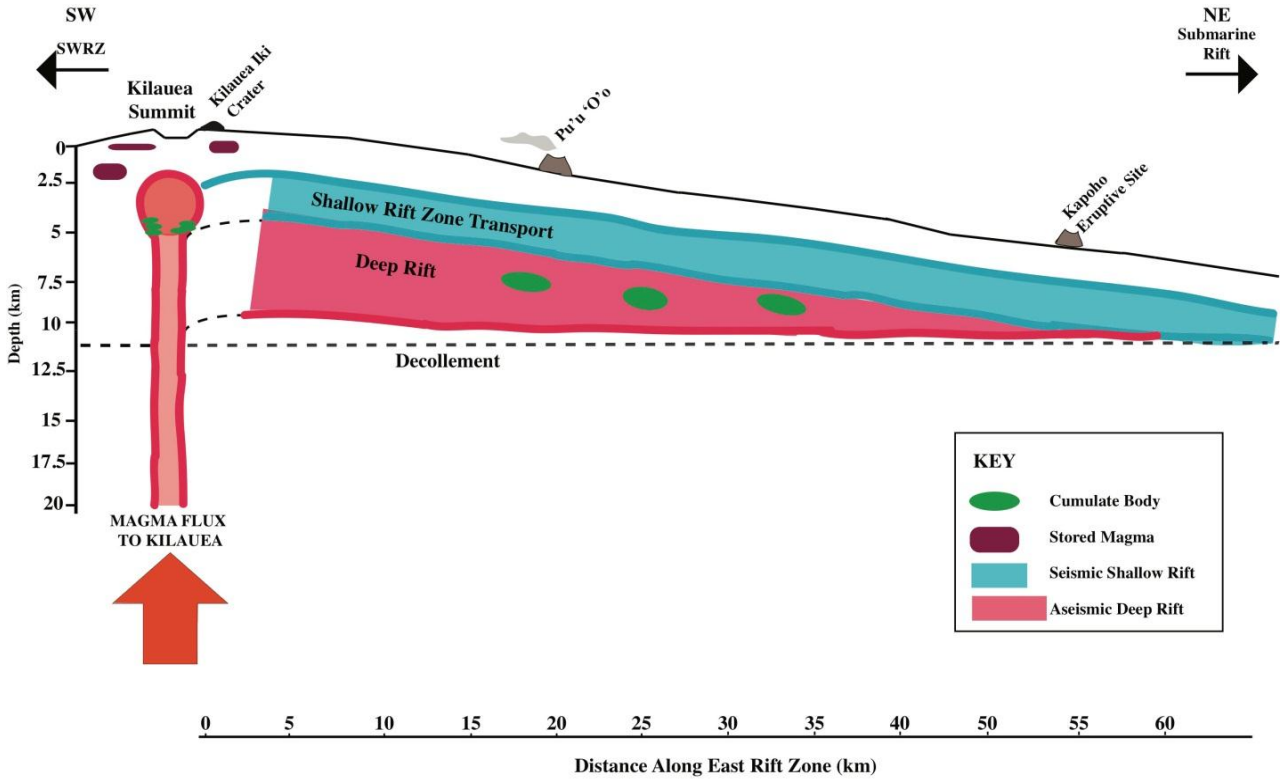

Figure F1. A cross section view through Kīlauea's magma plumbing system. Magma enters Kīlauea's magma plumbing system between 45-60 km depth and rises into the summit reservoir between 2-5 km depth, which may represent the depth of neutral buoyancy for Hawaiian magmas. Magma may then be erupted through the summit, stored, or injected laterally into the shallow rift zones. The shallow rift zone is defined seismically between 2-4 km depth. The deep rift zone is aseismic (Ryan, 1988), but is warm and may contain abundanct stored olivine cumulate bodies that make Kīlauea's south flank gravitationally unstable (Clague and Denlinger, 1994). Olivine cumulate is also stored at the base of Kīlauea's summit reservoir following the settling of coarse olivine crystals over time. These dunitic cumulates may flow out of the summit reservoir to become stored in the deep rift. The decollment represents the separation from the volcanic pile and the oceanic crust, and is the slip surface for Kīlauea's south flank movement (Ryan, 1988).

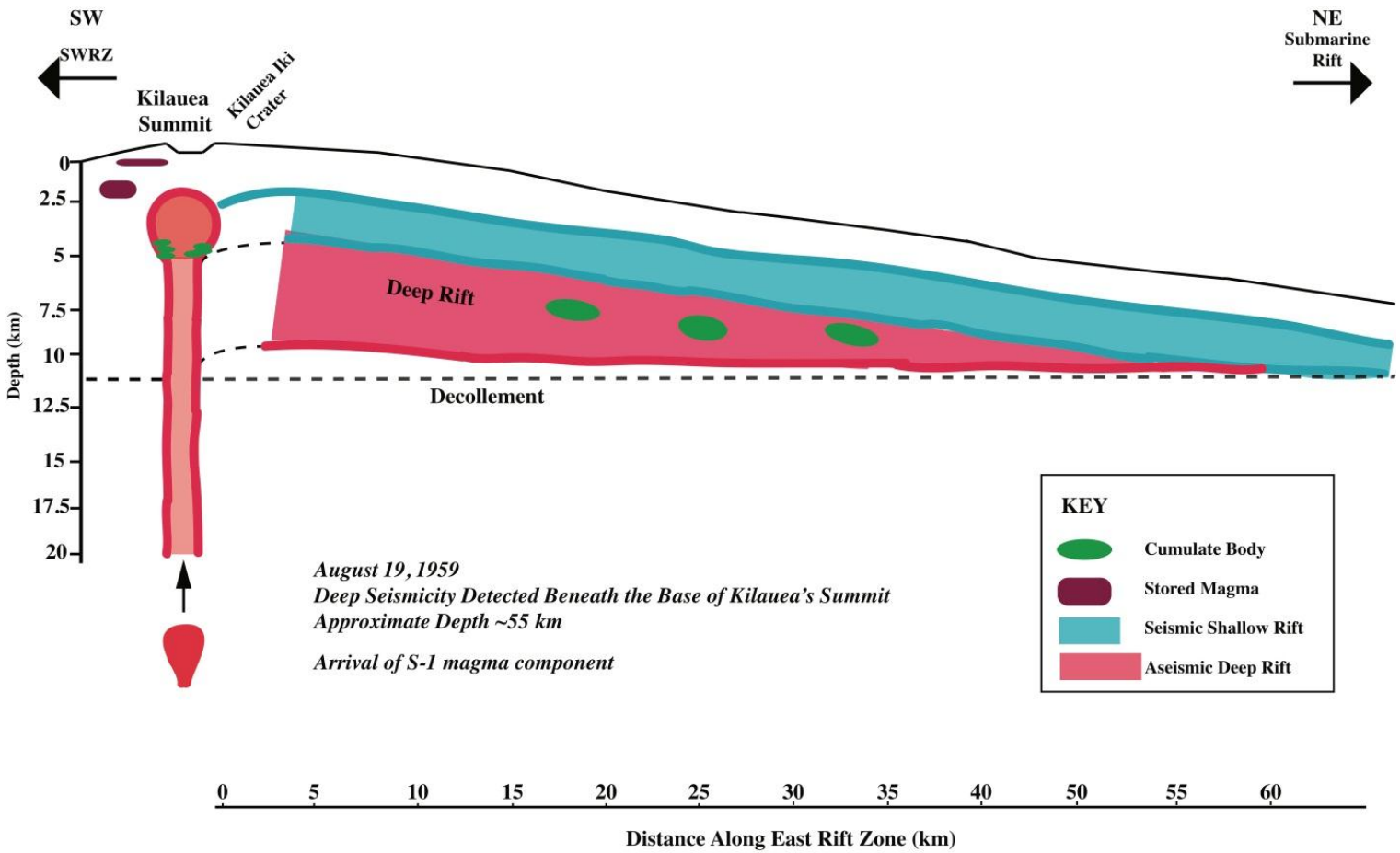

Figure F2. Eruption Precursor. In the August preceding the Kīlauea Iki eruption, deep seismicity was detected below Kīlauea's summit at approximately 55 km (Eaton et al., 1987). This signaled the arrival of the S-1 magma component into Kīlauea's conduit system.

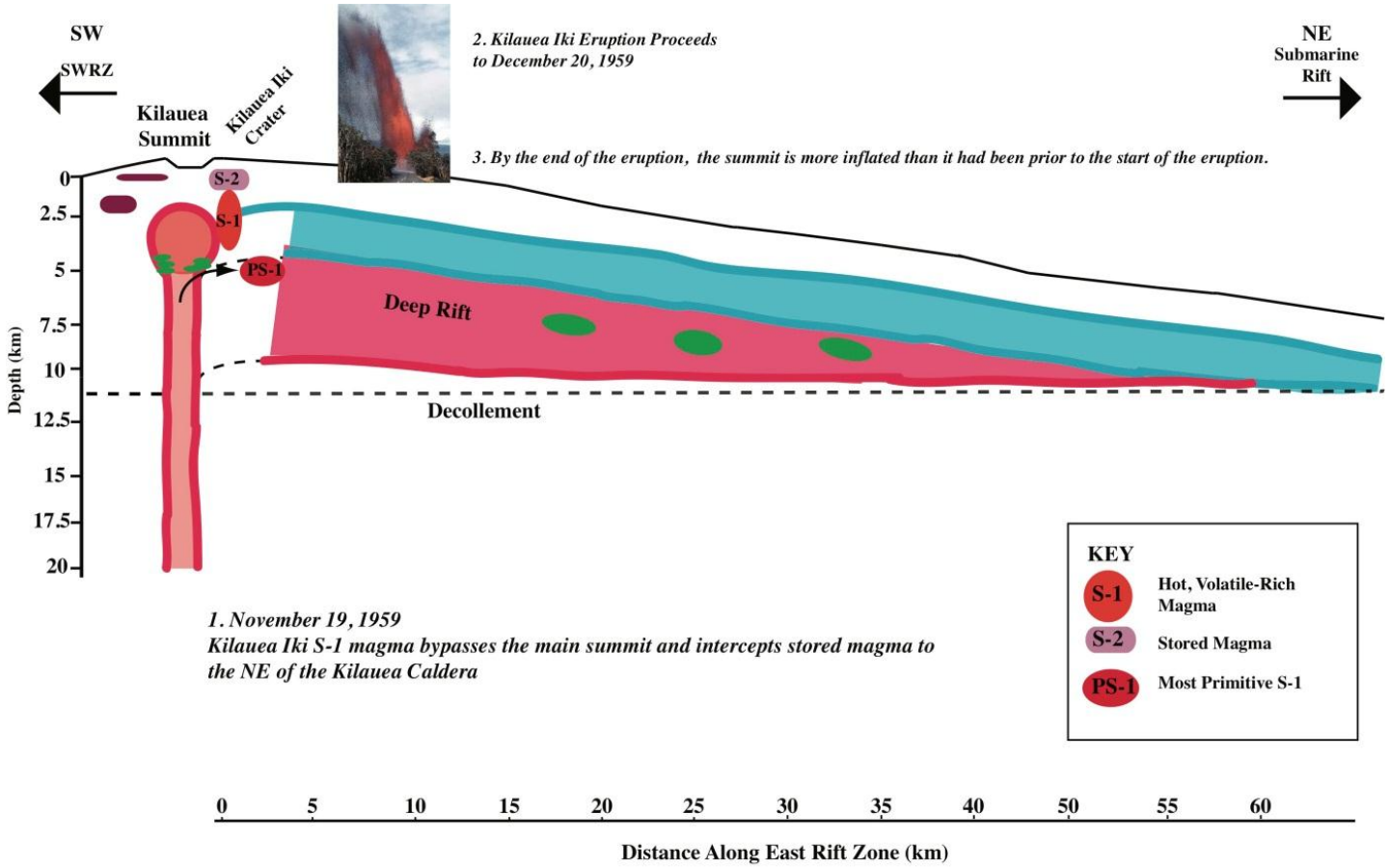

Figure F3. Kīlauea Iki eruption. Following the deep seismic activity, Kīlauea's summit reservoir began to inflate until the eruption started in Kīlauea Iki crater on November 19, 1959. The S-1 magma component intercepted stored S-2 magma to the northeast of Halemaumau. During the ascent of the S-1 magma component, the most primitive S-1 component (PS-1) may have been redirected into the rift zone due to a high magma supply rate and/or overpressurization of Kīlauea's summit reservoir. Olivine crystallization depths correspond to a depth intermediate between the shallow and deep rift system.

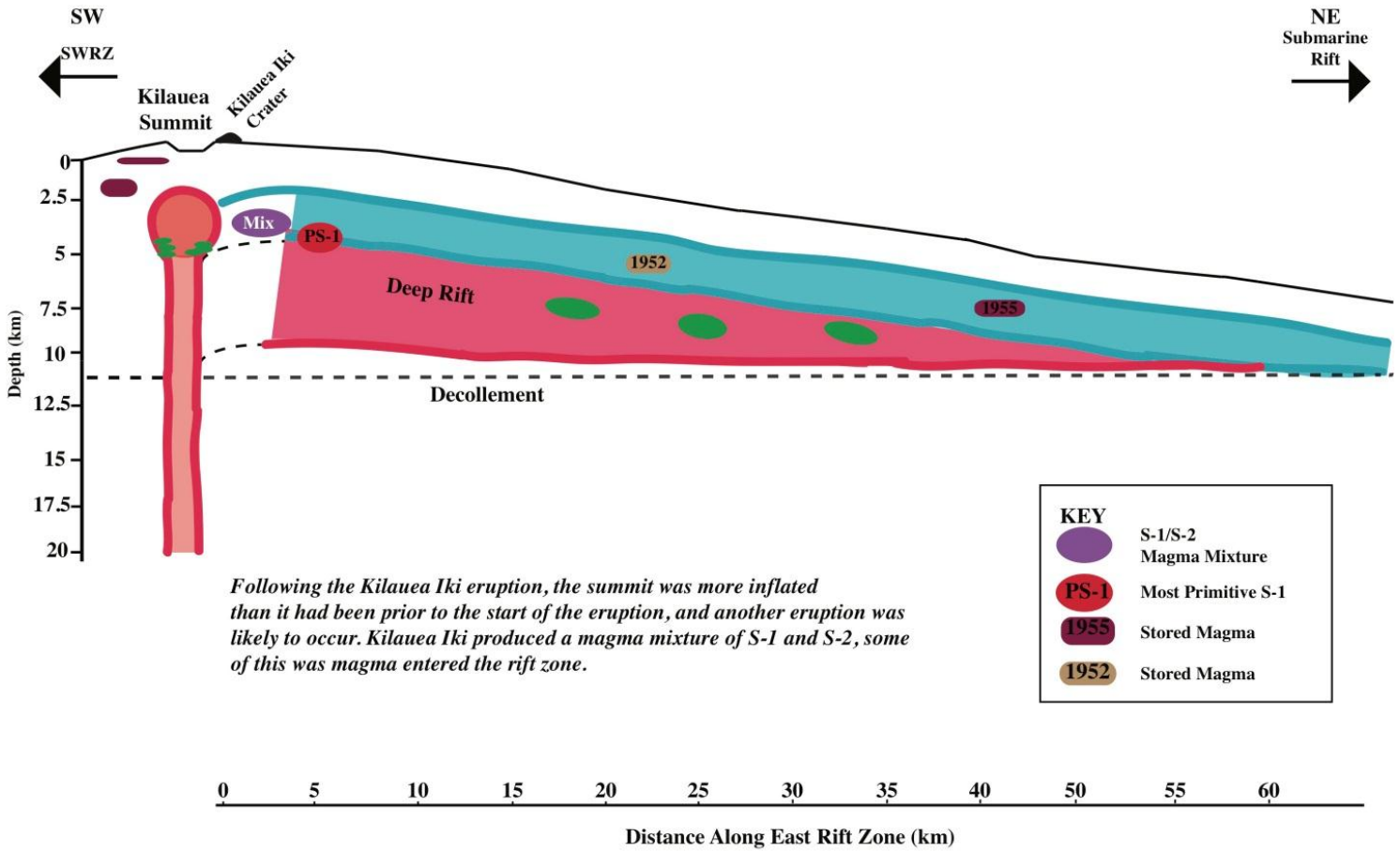

Figure F4. Quiescence before the Kapoho eruption. The Kīlauea Iki eruption ended on December 20, 1959. Kīlauea's summit was more inflated than it had been prior to the eruption, suggesting another eruption was likely to take place. Multiple stored magma components were present in the east rift zone, including a mixture of the S-1 and S-2 magma components that had been injected into the east rift zone following drainback of Kīlauea Iki's eruptive fissures. The most primitive S-1 component (PS-1) is also present in the rift zone at this time.

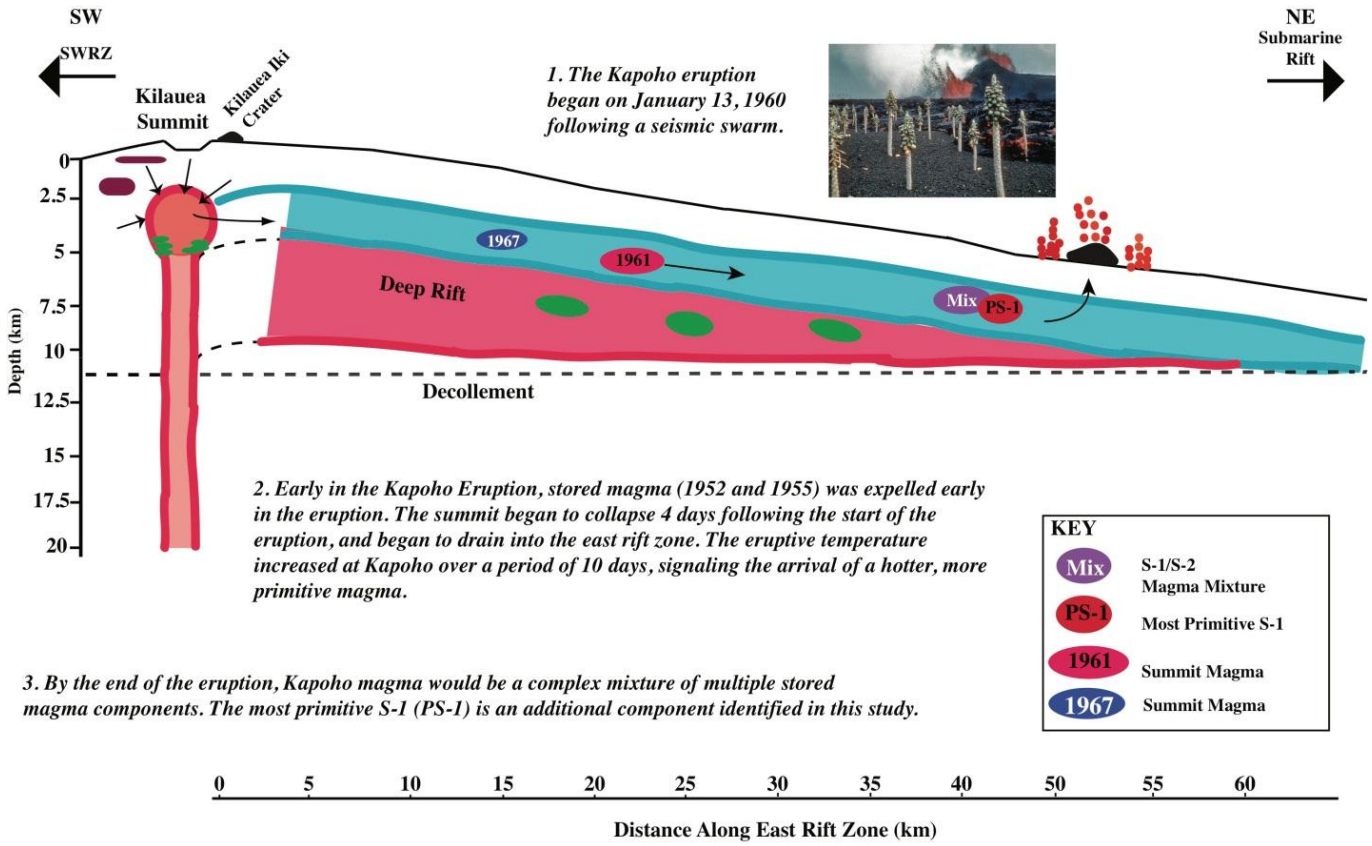

Figure F5. The Kapoho eruption begain on January 13, 1960 following a seismic swarm. The early 1960 lavas were differentiated, indicating that stored magma had been expelled from the rift zone. The eruptive temperature increased over a period of 10 days, representing the arrival of hotter, more juvenile magma. The 1960 eruption involed many mixing components including: S-1/S-2 mixture and the PS-1 magma (this study). It is not known whether the PS-1 magma traveled mostly through the deep rift and was then flushed at Kapoho or that perhaps it had moved into the shallow system closer to when it was initially redirected from Kīlauea's summit. The collapse of Kīlauea's summit introduced additional magma components that were more summit-like in composition.

REFERENCES CITED

Anderson Jr., A.T & Brown, G.G. (1993) CO_2 contents and formation pressures of some Kīlauean melt inclusions. *American Mineralogist* **78**, 794-803.

Bucholz, C.E., Gaetani, G.A., Behn, M.D., & Shimizu, N. (2013) Post-entrapment modifications of volatiles and oxygen fugacity in olivine-hosted melt inclusions. *Earth and Planetary Science Letters* **374**, 145-155.

Bureau, H., Pineau, F., Metrich, Semet, M.P. & Javoy, M. (1998a) A melt and fluid inclusion study of the gas phase at Piton de la Fournaise volcano (Reunion Island). *Chemical Geology*, **147**, 115-130.

Bureau, H., Metrich, N., Pineau, F. & Semet, M.P. (1998b) Magma-conduit interaction at Piton de la Fournaise volcano (Reunion Island): a melt and fluid inclusion study. *Journal of Volcanology and Geothermal Research* **84**, 39-60.

Cervantes, P., Kamenetsky, V. & Wallace, P. (2002) Melt Inclusion Volatile Contents, Pressures of Crystallization for Hawaiian Picrites, and the Problem of Shrinkage Bubbles. EOS, Transactions, American Geophysical Union 2002; 83: F1495-F1496.

Clague. D., Weber, W.S., & Dixon, J.E.(1991) Picritic glasses from Hawaii. *Nature* **353**, 553-556.

Clague, D. & Denlinger ,R.P. (1994) The role of olivine cumulates in destabilizing the flanks of Hawaiian volcanoes. *Bulletin of Volcanology* **56**, 425-434.

Clague, D., Moore, J.G., Dixon, J.E., & Friesen, W.B. (1995) Petrology of Submarine Lavas from Kīlauea's Puna Ridge, Hawaii. *Journal of Petrology* **36**, 299-349.

Cervelli, P., Segall, P., Amelung, F., Garbeil, H., Meertens, C., Owen, S., Miklius, & Lisowski, M., (2002) The 12 September 199 Upper East Rift Zone dike intrusion at Kīlauea Volcano, Hawaii. *Journal of Geophysical Research* **107**, ECV 3.1-3.13.

Danyushevsky, L. V., & Plechov, P. (2011) Petrolog3: Integrated software for modeling crystallization processes. *Geochemistry, Geophysics and Geosystems* **12**, 1-32.

Danushevsky, L.V., Sokolov, S., & Falloon, T.J. (2002a) Melt inlcuions in olivine phenocrysts: Using diffusive re-equilibration to determine the cooling history of a crystal, with implications for the origin of olivine-phyric volcanic rocks. *Journal of Petrology* **43**, 1651-1671.

Danyushevsky, L.V., McNeill, A.W., & Sobolev, A.V. (2002b) Experimental and petrological studies of melt inclusions in phenocrysts from mantle-derived magmas: an overview of techniques, advantages, and complications. *Chemical Geology* **183**, 5-24.

Edmonds, M., Sides, I.R., Swanson, D.A., Werner, C., Martin, R.S., Mather, T.A., Herd, R.A., Jones, R.L., Mead, M.I., Sawyer, G., Roberts, T., Sutton, A.J., & Elias, T. (2013) Magma storage, transport and degassing during the 2008-2010 summit eruption at Kīlauea Volcano, Hawaii. Geochemica et Cosmochimica Acta. p.1-39.

Eaton, J.P. & Murata, K.J. (1960) How volcanoes grow: *Science* **132**, 925-938.

Eaton, J.P., Richter, D.H., & Krivoy, H.L. (1987) Cycling of magma between the summit reservoir and Kīlauea Iki lava lake during the 1959 eruption of Kīlauea Volcano. *US Geological Survey Professional Papers* **1350**, 1307-1336.

Gaetani, G.A., O'Leary, J.A., Shimizu, N., Bucholz, C.E., & Newville, M. (2012) Rapid reequilibration of H2O and oxygen fugacity in olivine-hosted melt inclusions. *Geology* **40**, 915-918.

Garcia, M.O., Pietruzska, A.J., Rhodes, J.M. & Swanson, Kiersten (2000) Magmatic processes during the prolonged Pu`u `O`o eruption of Kīlauea Volcano, Hawaii: Journal of Petrology, v. 41: p. 967-990.

Gerlach, T.M. (1986) Exsolution of H_2O, CO_2, and S during eruptive episodes at Kīlauea Volcano, Hawaii. *Journal of Geophysical Research* **91**, 12,177-12,185.

Hauri. E. (2002) SIMS analysis of volatiles in silicate glasses,2: isotopes and abundances in Hawaiian melt inclusions. *Chemical Geology* **183**, 115-141.

Hazlett, R.W. (1993) *Roadside Geology of Kīlauea Volcano, Hawaii*. Hawaii Natural History Association.

Helz, R. (1987) Diverse olivine types in lava of the 1959 eruption of Kīlauea volcano and their eruption dynamics. *US Geological Survery Professional Papers* **1350**, 691-722.

Helz, R., & Thornber, C. (1987) Geothermometry of Kīlauea Iki lava lake, Hawaii. *Bulletin of Volcanology* **49**, 651-668.

Lloyd, A.S., Plank, T., Ruprecht, P., Hauri, E.H., Rose, W. (2013) Volatile Loss from melt inclusions of pyroclasts of differing sizes. *Contributions to Mineralogy and Petrology* 165, 129-153.

MacDonald, G.A. & Eaton, J.P. (1964) Hawaiian Volcanoes During 1955. *US Geological Survey Bulletin* **1171**, p. 1-169

Massare, D., Metrich, N. & Clocchiatti, R.(2002) High temperature experiments on silicate melt inclusions in olivine at 1 atm: inference on temperatures of homogenization and H2O concentrations. Chemical Geology **183**, 87-98.

Metrich, N. & Wallace, PJ. (2008) Volatile abundances in basaltic magmas and their degassing paths tracked by melt inclusions. *Reviews in Mineralogy and Geochemistry* **69**, 363-402.

Moore, L., Tuohy, R., Gazel, E., Lloyd, A., Esposito, R., Wallace, P., Plank, T. & Bodnar, R.J. Bubbles matter: An assessment of the contribution of vapor bubbles to melt inclusion volatile budgets. (in prep) *American Mineralogist.*

Newman, S., & Lowenstern, J.B., 2002, VolatileCalc: a silicate melt-H2O-CO2 solution model written in Visual Basic for Excel: *Computers and Geosciences* **28**, 597-604.

Plattner, C., Amelung, F., Baker, S., Govers, R. & Poland, M. (2013) The role of viscous magma mush spreading in volcanic flank motion at Kīlauea Volcano, Hawaii. *Journal of Geophysical Research* **118**, 1-14.

Poland, M.P., Miklius, A., Sutton, A.J., Thornber, C.R. (2012) A mantle-driven surge in magma supply to Kīlauea Volcano during 2003-2007. *Nature Geoscience* **5**, 295-300.

Qin, Z, Lu, F., & Anderson, A T. (1992) Diffusive reequilibration of melt and fluid inclusions. *American Mineralogist*, **77**, 565-576.

Rhodes, J.M. & Vollinger, M.J. (2005) Ferric/ferrous ratios in 1984 Mauna Loa lavas: a contribution to understanding the oxidation state of Hawaiian magmas. *Contributions to Mineralogy and Petrology* **149**, 666-674.

Richter, D.H., Eaton, J.P., Murata, K.J., Ault, W.U., Krivoy, H.L.(1966) Chronological narrative of the 1959-60 Eruption of Kīlauea volcano, Hawai'i. *US Geological Survey Professional Papers* **537-D**,1-73.

Riker, J. (2005) The 1859 Eruption of Mauna Loa Volcano, Hawai'i: Controls on the development of long lava channels. Master's Thesis. University of Oregon. p. 117-127

Rowe, M.C., Nielsen, R.L. & Kent, A.J.R. (2006) Anomalously high Fe contents in rehomogenized olivine-hosted melt inclusions from oxidized magmas. *American Mineralogist* **91**, 82-91.

Ryan. M.P., Koyanagi, R.Y. & Fiske, R.S. (1981) Modeling the 3-dimensional structure of macroscopic magma transport systems- Applications to Kīlauea Volcano, Hawaii. *Journal of Geophysical Research* **86**, 7,111-7,129.

Ryan, M.P. (1987) Elasticity and Contractancy of Hawaiian Olivine Tholeiite and its Role n the Stability and Structural Evolution of Subcaldera Magma Reservoirs and Rift Systems. *US Geological Survey Professional Papers* **1350**, 1395-1447.

Ryan, M. (1988) The Mechanics and Three-Dimensional Internal Structure of Active Magmatic Systems, Kīlauea Volcano, Hawaii. *Journal of Geophysical Research* **93**, 4213-4248.

Sides, I., Edmonds, M., Maclennan, J., Houghton, B.,& Swanson, D. (in press) Magma mixing and high fountaining during the 1959 Kīlauea Iki eruption, Hawaii. *Earth and Planetary Science Letters*.

Swanson, D.A., Duffield, W.A. & Fiske, R.S.(1976) Displacement of the South Flank of Kīlauea Volcano: The Result of Forceful Intrusion of Magma into Rift Zones. *US Geological Survey, Professional Papers* **963**, 1-38.

Swanson, D.A., personal communication, December 5, 2013

Thornber, C.R. (2001) Olivine-liquid relations of lava erupted by Kīlauea volcano from 1994 to 1998: Implications for shallow magmatic processes associated with the ongoing east-rift-zone eruption, *Canadian Mineralogist.* **39**, 239-266.

Tilling, R.I. & Dvorak, J.J. (1993) Anatomy of a basaltic volcano. *Nature* **363**, 125-132.

Vigouroux, N., William-Jones. A.E., Wallace, P., & Staudacher, T. (2009) The November 2002 eruption of Piton de la Fournaise, Reunion: tracking the thermal evolution of magma using melt inclusions. *Bulletin of Volcanology* **71**, 1077-1089.

Vinet, N. & Higgins, M.D. (2010) Magma solidification processes beneath Kīlauea Volcano, Hawaii: a quantitative textural and geochemical study of the 1969-1974 Mauna Ulu lavas: *Journal of Petrology* **51**,1297-1332.

Wallace, P. & Anderson, A.T. (1998) Effects of eruption and lava drainback on the H_2O contents of basaltic magmas at Kīlauea Volcano. *Bulletin of Volcanology*, **59,** 327-344.

Welsch, B. , Faure, F., Famin, V., Baronnet, A., & Bachelery, P. (2013). Dendritic crystallization: A Single Process for all the Textures of Olivine in Basalts. *Journal of Petrology* **54**, 539-574.

Wright, T.L. & Fiske, R. (1971) Origin of the Differentiated and Hybrid Lavas of Kīlauea Volcano, Hawaii. *Journal of Petrology* **12**, 1-65.

Wright, T.L. & Helz, R. (1996) Differentiation and magma mixing on Kīlauea's east rift zone: A further look at the eruptions of 1955 and 1960. Part. II. The 1960 lavas. *Bulletin of Volcanology* **57**, 602-630.

Wright, T.L. & Klein, F.W. (2006) Deep Magma Transport at Kīlauea Volcano. Lithos **87**, 50-79

Wysoczanski R, Tani K (2006) Spectroscopic FTIR imaging of water species in silicic volcanic glasses and melt inclusions: An example from the Izu-Bonin arc. *Journal of Volcanology and Geothermal Research* **156**, 302-314.